A distributed modular self-reconfiguring robotic platform based on simplified electro-permanent magnets

Li Zhu

THÈSE

En vue de l'obtention du

DOCTORAT DE L'UNIVERSITÉ DE TOULOUSE

Délivré par : *l'Université Toulouse 3 Paul Sabatier (UT3 Paul Sabatier)*

Présentée et soutenue le *Vendredi 16 février 2018* **par :**

LI ZHU

A distributed modular self-reconfiguring robotic platform based on simplified electro-permanent magnets

JURY

Nadine Le Fort Piat	Professeur Université de Bourgogne, Franche-Comté	France
Julien Bourgeois	Professeur Université de Bourgogne, Franche-Comté	France
Patrick Danes	Professeur Université de Toulouse III Paul Sabatier	France
Didier El Baz	Chargé de Recherche CNRS, LAAS-CNRS	France

École doctorale et spécialité :

MITT : Domaine STIC : Réseaux, Télécoms, Systèmes et Architecture

Unité de Recherche :

Laboratoire d'Analyse et d'Architecture des Systèmes - CNRS

Directeur(s) de Thèse :

DIDIER EL BAZ, LAAS-CNRS, Toulouse, France

et *HUANGSHENG NING, Professeur Université des Sciences et Technologies de Pékin, Chine*

Rapporteurs :

NADINE LE FORT PIAT, Professeur Université de Bourgogne Franche-Comté, France

et *DANGXIAO WANG, Professeur Université Beihang, Chine*

Acknowledgments

I would like to take this chance to express my sincere thanks to the people who have guided and helped me to accomplish my thesis, as well as to the people who have supported me and shared the pleasant time during my PhD study. Because of you, I could have learned a lot of things in the professional area and got so many shining memories.

First of all, I would like to thank the head of LAAS-CNRS, Liviu Nicu, for permitting me to do my research work in such a wonderful lab. LAAS is the best lab I've ever worked in, it has first-class equipment, good working environment and friendly atmosphere. The researchers and staff of LAAS are also very kind, like Philippe Owezarski the head of the networks and communication department, he supports me to continue my work after PhD; Marie-Agnès Bellieres who always helps me with patient.

Then I would like to thank the people work in the Paul Sabatier University and the doctoral school MITT. Isabelle Izarie and Agnès Requis helps to do the inscriptions every year. Martine labruyere helps me a lot to paper the files for PhD defense and explain the rules to us kindly.

I wish to give my deepest gratitude to my supervisor, Didier El Baz for his excellent guidance, caring and encouragements. He not only taught me vast knowledge, but also showed me the correct way of working, always be rigorous, be active and be patient. His advice on both research and on my career, is invaluable. Except for the research work, he is more like my father in France, he always takes care of me, thinks about my family and helps me solve the problem of my daily life. I'm not a person who is good at expressing, when Didier helps me, I always say "thank you" to him, but I always think these two words are too far from the meaning I want to express.

I would also like to say a heartfelt thank you to my co-supervisor Huansheng Ning for all the helps and supports that he provided. I've known him for many years, each time I need to make big decisions or face problems, he always be my side and helps me to make the right decisions.

Many thanks also to my committee members for their interest in my work. Thanks to the reporters, Nadine Le Fort Piat and Dangxiao Wang, for their precious advice and feedback that were helpful to ameliorate my current work. Thanks to the examiners, Julien Bourgeois and Patrick Danes, they are experts in my area, their attendance of my PhD defense supervises me to review my work repeatedly.

Regards and gratitude go out to my colleges and friends at LAAS. Thanks to Li Zheng for finding a nice apartment before I arrive France and also her help during my stay in here. Thanks to Lunde Chen for not only helping me with daily problems but also my research work, his unique insights on the subject also inspire me from time to time. Thanks to Bilal Fakih for giving me advise on many things, helping me to translate some materials, and all the enjoyable moments we spent together. Thanks to my college Bastien Plazolles and other PhD students for bringing me so many happy and wonderful moments, they are Rui Wang, Min Zhu, Zukun Qu and so on.

Lastly, I would like to give my most gratitude to my parents; they always stand by my side and give me the strongest support. I would like to specially acknowledge my wife Huilan Luo who just give birth to our lovely son. She suffered a lot, and nearly didn’t sleep in these days. Now, it’s a really challenging period for us, we will certainly overcome the difficulties just as ever.

I am so grateful for living in the lovely city-Toulouse, and so luck to meet so many nice persons. To anyone that I may have forgotten. I apologize and thank you as well.

Abstract

Specialty: NETWORKS, TELECOM, SYSTEM AND ARCHITECTURE

Family name: ZHU

Given name: Li

Thesis delivered at: LAAS, UPS Toulouse

Title: A distributed modular self-reconfiguring robotic platform based on simplified electro-permanent magnets

A distributed modular self-reconfiguring robotic (MSRR) system is composed of many repeated basic modules with certain functions of motion, perception, and actuation. They can adapt to environment and goals by connecting and disconnecting to achieve the desired configuration and shape. MSRRs often contain two hardware systems: one is for actuation (motion), another one is for connection. At present time many institutions work on MSRRs; structural design, miniaturization, energy saving, control algorithms have been the focus of research in this area. However, only a few of them work on both the hardware and the corresponding algorithms. This thesis describes the design, fabrication, experimental results, distributed algorithm, and simulator of a MSRR platform. Via theoretical calculation and numerical simulation, we present the simplified electro-permanent (SEP) magnet which can change the magnetic field direction and does not require energy consumption while connected. A new concept of linear motor based on SEP is proposed. Then we construct DILI, a cubical MSRR, the length of each module is 1.5cm. DILI module can slide on a flat surface; the maximum speed can reach 20mm/s. With the new actuator, DILI can achieve the functions of motion and connection with only one system inside. Finally, a distributed algorithm is proposed in order to build a smart conveyor, and a simulator is designed that permits one to perform distributed simulations, test and validate distributed algorithms.

Keywords: Distributed computing, Modular robot, Smart System

Résumé

Spécialité : RESEAUX, TELECOM, SYSTEME ET ARCHITECTURE

Nom : ZHU

Prénom : Li

Thèse effectuée au : LAAS, UPS Toulouse

Titre de la thèse en français : Plate-forme robotique distribuée et auto-reconfigurable basée sur un aimant électro-permanent simplifié

Un système robotique distribué et reconfigurable (MSRR) est composé de plusieurs modules ayant certaines fonctions de mouvement, de perception et d’action. Ils peuvent s'adapter à l'environnement et aux objectifs en se connectant et en se déconnectant pour obtenir la configuration et la forme désirées. Les MSRR contiennent souvent deux systèmes : l'un constitué d’actionneurs pour le mouvement, l'autre pour la connexion. A l'heure actuelle, de nombreuses institutions travaillent sur les MSRR ; la conception, la miniaturisation, l'économie d'énergie, les algorithmes de contrôle ont fait l'objet de recherches dans ce domaine. Cependant, il existe peu d’études conjointes sur le matériel et les algorithmes correspondants.

Cette thèse décrit la conception, la fabrication, les résultats expérimentaux, l’algorithmique distribuée et un simulateur d'une plate-forme MSRR. En nous appuyant sur le calcul et la simulation numérique, nous présentons un aimant électro-permanent simplifié (SEP) qui ne consomme pas d'énergie lorsque le module est connecté à un autre module. Un nouveau concept de moteur linéaire basé sur les SEP est également proposé. Ensuite, nous présentons DILI, un MSRR cubique, de longueur 1,5cm. Le module DILI peut coulisser sur une surface plane, la vitesse maximale pouvant atteindre 20mm/s. Avec le nouvel actionneur, DILI peut réaliser les fonctions de mouvement et de connexion. Un module DILI peut se connecter avec quatre autres modules. Enfin, un algorithme distribué est proposé et un simulateur est conçu pour permettre de simuler le système distribué, de tester et valider les algorithmes distribués.

Mots-clés : Calcul distribué, Robot modulaire, Système intelligent

Content

Table of content vii

List of Figures vii

List of Tables. xi

Chapter I. General Introduction 1

I.1. Context 1

I.2. Contributions 3

I.3. Manuscript Organization 4

References in Chapter I 7

Chapter II. Related Work 9

II.1. The Smart Surface and Smart Blocks Projects 9

II.2. Modular Reconfigurable Robots (MRR) 10

II.2.1. Applications of MRR 11

II.2.2. MRRs from 1988 to 2017 13

II.3. Classification and State of the Art 18

II.3.1. Classification via actuation mechanism 19

II.3.2. Classification via connection mechanism 20

II.4. Methods for Miniaturization 24

II.4.1. Method 1: modules without actuation system 24

II.4.2. Method 2: substitution of the actuation system for an affiliate system 26

II.4.3. Method 3: multi-system multiplexing 27

II.5. Distributed Algorithms and Simulators for MSRR 28

II.6. Cellular Automata Theory Applied to MSRR 30

II.6.1. Cellular automata 30

II.6.2. Applications to MSRR 31

II.7. Conclusion 34

References in Chapter II 35

Chapter III. New Concept of Linear Motor..45

III.1. Introduction 45

III.2. Electro-Permanent (EP) magnet 45

III.2.1. Magnetic Materials 45

III.2.2. Electro-Permanent (EP) Magnet 46

III.3. Analysis of Magnetic Field in the Solenoid 49

III.4. Linear Motor Based on Simplified Electro-Permanent (SEP) Magnets.. 53

III.4.1. Principle of Simplified Electro-Permanent (SEP) magnet 53

III.4.2. Motion and connection mechanisms 54

III.4.3. Enhanced magnetic field 57

III.5. Fabrication of a SEP Magnet and Tests 57

III.6. Conclusion.. 58

References in Chapter III 59

Chapter IV. Design and Numerical Simulation of Simplified Electro-Permanent Magnet………… 61

IV.1. Introduction 61

IV.2. Hysteresis Loop.. 61

IV.3. Jiles-Atherton Model.. 63

IV.4. Numerical Simulation with COMSOL Multiphysics 66

IV.4.1. Model 66

IV.4.2. Physical parameters.. 68

IV.4.3. Mesh.. 69

IV.4.4. Study and model calibration.. 70

IV.5. Simulation Results.. 77

IV.5.1. Effect of the number of coil turns 77

IV.5.2. Effect of the pulse intensity.. 78

IV.5.3. Effect of the coverage area of coil 79
IV.5.4. Effect of the diameter of copper wire 80
IV.6. Conclusion 81
References in Chapter IV 82
Chapter V. Hardware Design: Circuit and Structure 84
V.1. Introduction 84
V.2. Pulse Signal Generation Circuit 85
V.2.1. Capacitance pulse discharge 85
V.2.2. H-bridges for controlling the magnetization direction 87
V.2.3. Dead-time in H-bridges 89
V.2.4. Drawbacks of dead-time 90
V.2.5. Dead-time controllable H-bridge 91
V.3. Microcontroller and Circuit 93
V.4. Structure of DILI Robot 95
V.5. Motion and Connection Principle of DILI Robot 99
V.6. Experiments 100
V.6.1. Speed test 101
V.6.2. Holding force test 102
V.6.3. Vertical force test 104
V.7. Conclusion 105
References in Chapter V 105
Chapter VI. Distributed Algorithms and Simulation Software for DILI Robot System 106
VI.1. Introduction 106
VI.2. Capabilities of DILI Module 107
VI.2.1. Elementary motion 107
VI.2.2. Extended motion capabilities of DILI module 108
VI.2.3. Push capability 109

VI.2.4. Pull capability 111

VI.2.5. Combined push and pull 111

VI.2.6. Carry capability 112

VI.2.7. Tests of DILI module 112

VI.3. Distributed Algorithm 113

VI.3.1. Basic principle of the distributed algorithm 114

VI.3.2. Details 115

VI.3.3. Step 1: distributed election 116

VI.3.4. Step 2: definition of square domain centered at the selected module 117

VI.4. Simulator of Smart Modules (SSM) 120

VI.4.1. Interface 121

VI.4.2. Usage of SSM 122

VI.4.3. Results 124

VI.5. Conclusion 126

References in Chapter VI 127

Chapter VII. Conclusion and Perspectives 128

VII.1. Conclusion 128

VII.2. Perspectives 129

List of publications and demos 131

List of Figures

Figure I-1 Thesis structure 6

Figure II-1 A rescue application by M-TRAN 11

Figure II-2 Catoms scanning a complex environment...12

Figure II-3 Two MRRs for education 13

Figure II-4 Some examples of modular robot architectures 18

Figure II-5 Several classifications of MRRs 19

Figure II-6 Mechanical connections and their real applications...22

Figure II-7 Trend of the connection methods 23

Figure II-8 Some MRRs without actuation system 26

Figure II-9 Automatic Modular Assembly System...27

Figure II-10 Two prototypes of Catoms modular robot system 28

Figure II-11 Example of simulation of reconfiguration for cubical MSRR. 29

Figure II-12 Different cellular automata neighborhoods...31

Figure II-13 Rules for eastward locomotion with obstacles...32

Figure II-14 Four snapshots of a simulation...32

Figure II-15 Boing 747 in CAD 33

Figure III-1 Principle of Electro-permanent (EP) magnet...47

Figure III-2 EP magnets in a Ara (Google modular phone) module 48

Figure III-3 EP magnets on Robot Pebbles (MIT) 48

Figure III-4 Structure of solenoid...50

Figure III-5 The principle of SEP...53

Figure III-6 Motion mechanism of new linear motor........54

Figure III-7 Status of magnetic filed of SEP magnets in motion........55

Figure III-8 Circular motion, NdFeB is the rotor........56

Figure III-9 Circular motion, SEP is the rotor........56

Figure III-10 Possibilities of motion........56

Figure III-11 Principle of enhanced magnetic field........57

Figure III-12 Alnico5 magnet reversely magnetized........58

Figure IV-1 Hysteresis loop........63

Figure IV-2 2D domain of the numerical simulation including Alnico5, coil and surrounding air........67

Figure IV-3 Three views at SEP magnet model........67

Figure IV-4 Mapped mesh of Alnico5 and copper coil........69

Figure IV-5 Meshed model........70

Figure IV-6 Calibrated hysteresis loop by COMSOL........71

Figure IV-7 Relationship of the coil current intensity I (unit is 10 A) and internal average magnetic field B_z in function of the time (s).........72

Figure IV-8 3D magnetic flux density view........72

Figure IV-9 Magnetic flux density (in Tesla) at four representative times for sinusoidal excitation.........73

Figure IV-10 Positive pulse signal: rect1........74

Figure IV-11 Positive pulse signal: rect2........74

Figure IV-12 The complete pulse signal: pw1........75

Figure IV-13 B-H curve of the pulse signal........76

Figure IV-14 Relationship between internal average magnetic field B_z and the coil current intensity I (pulse case, unit is 10A)........76

Figure IV-15 Anti-magnetic field in Alnico5........77

Figure IV-16 Effect of number of coil turns 78

Figure IV-17 Effect of pulse peak 78

Figure IV-18 Effect of the coverage area of coil 79

Figure IV-19 Effect of the diameter of copper wire 80

Figure V-1 Schematic diagram of capacitance pulse discharge 85

Figure V-2 Waveforms of the three states of the capacitance pulse discharge 87

Figure V-3 Principle of H-bridge 88

Figure V-4 Scheme of H-bridge circuit 89

Figure V-5 Timing diagram showing the effect of dead-time 91

Figure V-6 Dead-time controllable semi-H-bridge 92

Figure V-7 Half-bridge multiplex design 92

Figure V-8 Circuit of the main board 94

Figure V-9 PCB and the real main board for controlling our robot 94

Figure V-10 Bridge circuit board 95

Figure V-11 Structure of DILI robot 96

Figure V-12 Details of big holes on DILI for SEP magnets 97

Figure V-13 Details of small holes on DILI for NdFeB magnets 97

Figure V-14 Real DILI module 98

Figure V-15 Relative positions of two DILI modules for working purpose 99

Figure V-16 Status of SEP magnets in one complete movement process 100

Figure V-17 Speed test 102

Figure V-18 Holding force test with pulse signal 103

Figure V-19 Holding force test with sinusoidal signal 104

Figure V-20 Static vertical force test 104

Figure VI-1 Structure of centralized and distributed control 107

Figure VI-2 Elementary motion of DILI module 108

Figure VI-3 Elementary motion of DILI module without expansion capability 108

Figure VI-4 Three extended motion capability of DILI module 109

Figure VI-5 Push function providing the possibility of expansion 110

Figure VI-6 Turning strategy 110

Figure VI-7 Pull capability providing contraction 111

Figure VI-8 Push and pull cooperative capability 112

Figure VI-9 Tests on the loading capacity of DILI module 113

Figure VI-10 Deformation diagram 114

Figure VI-11 Steps of the distributed algorithm 115

Figure VI-12 Module motion coordinate system 115

Figure VI-13 Position of module and associated Presence Matrix 118

Figure VI-14 Tree of possible motions 119

Figure VI-15 Four areas of the graphics interface 122

Figure VI-16 Setting the Input (occupied by module 3), Output and initial shape 123

Figure VI-17 Modules (in green) in the domain around the elected module 124

Figure VI-18 Simulation results of the shortest path problem 124

Figure VI-19 Complete solution of the shortest path problem via distributed algorithm displayed with SSM simulator 125

Figure VI-20 Initial shape 126

List of Tables

stable mode -1 Modular robots characterized by their connection and actuation 14

Table II-2 Qualitative comparison of several connection methods for MRRs 23

Table II-3 Some simulators of modular robotic systems 30

Table III-1 Residual magnetism and coercivity of NdFeB and Alnico5 46

Table IV-1 Global parameters for simulation with COMSOL 68

Table IV-2 Mesh data 70

Table IV-3 Definition of positive pulse signal: rect1 73

Table IV-4 Definition of positive pulse signal: rect2 74

Table IV-5 Definition of the complete pulse signal: pw1 75

Table IV-6 AWG wire sizes 81

Table V-1 Status of switches of H-bridge 88

Table V-2 Capacitance parameters of two MOSFET 90

Table V-3 Key features of STM32F103 microcontroller 93

Table V-4 Speed test on different surfaces 101

Chapter I. General Introduction

This chapter presents the context of this study and significance of this thesis as well as the research work that has been done. This thesis was carried out in the Distributed Computing and Asynchronism (CDA) team of the Laboratory for Analysis and Architecture of Systems of National Center for Scientific Research (LAAS-CNRS), Toulouse, France with the funding of Chinese Ministry of Education.

I.1. Context

The first two industrial revolutions aimed essentially at increasing human productivity thanks to mechanization and use of steam engines (1760-1840) or electric motors (1860-1950). The third industrial revolution featured systematization and faster management thanks to automatic data processing via computers (1960-2010). Those three revolutions have changed the very nature of our societies, the way people work, live, communicate as well as organize themselves. The fourth industrial revolution that aims at the fusion of physical, digital world and the Internet (starting 2010) also promises important changes in the way people work and live. This revolution may lead to dramatic changes in the operation of companies and the factory of the future leading to more automatization, the cooperation of robotics systems and workers, flexibility and better adaptation to client's demand.

Factory of the future will feature more efficient assembly lines like reconfigurable systems that can adapt to new goals or faulty situations in real time. This will lead to distributed, sustainable and economic robotic systems, like smart conveyors, which are an important part of the industry. Conveyors are usually designed as monolithic entities solving one problem at a time. They lack the flexibility to goals and environmental changes as well as robustness to failures that occur at small scale. To solve the problems, self-reconfigurable distributed modular robot systems are potential solutions, which are also new trends in robotics. The Smart Surface [1-3] and Smart Blocks [4-6] projects are two examples in this domain. The Smart Surface project gave rise to a unique concept of modular smart conveyor with distributed intelligence. The Smart Blocks project aimed at conveying and positioning fragile micro-parts by means of a dynamically reconfigurable distributed system consisting of modules with

Micro Electro Mechanical Systems (MEMS) that can move. This thesis is an extension of the Smart Blocks project, which aimed at building a distributed Modular Self-Reconfiguring Robotic (MSRR) system.

Since the year 1954, the world's first industrial robot UNIMATE invented by George Devol [7], the application of robot is no longer confined to workshop lines, factories. It has been used in hospitals, military industry, science and technology museums, entertainment venues, automobiles, textiles and homes and other places [8]. With the rapid development of science and technology, people have higher requirements for the automation and intelligence of robotics. Sometimes in order to take full advantage of resources, a robot is used to achieve different tasks, which requires the robot to quickly change its configuration to meet the requirements. Unfortunately, the mechanical structure of each robot limits what it can do. In addition, due to the risk that people may incur, more and more robots are applied in uncertain environments. However, in this kind of environment, it is difficult to determine the task of the robot in advance, and its working environment also has unpredictable conditions. Traditional robots are not capable of doing this because of their poor ability to adapt to changing circumstances and tasks. In view of the above problems, the researchers have put forward the theory of Modular Reconfigurable Robots (MRR) and modular self-reconfigurable robots (MSRR), which can also be called as modular self-reconfiguring robotic systems.

MRRs can change their shape and position by reorganizing the position and connection of the modules in the system. In a MRR system, a damaged module does not affect the overall normal operation; it can be replaced by other modules. Since the invention of the first MRR, more than one hundred kinds of MRRs have been invented.

MSRRs may have many applications. For example, they can be produced for the educational purpose. They can be used in smart manufacturing (like smart conveyors for drug manufacturing or tiny systems, e.g. clockwork manufacturing) or smart robots that evolve on difficult terrain. They can be used for programmable matter, e.g. furniture, tools, artworks.

So far, MRR systems are used in the lab as demonstrators or prototypes or in the education area. When designing a MRR, several principles need to be considered, for instance, the module should have a spatial symmetry that satisfies the motion requirements; the module should have sufficient freedom and drive capability (actuation); there must be a reliable connection between the modules; the moving parts in the module must be able to be individually controlled; the modules should have data processing and communication capability.

On what concerns software aspect, MRRs are difficult to control. The control algorithm needs to match the structure of the modules, as the number of modules increases; the complexity of the algorithm also increases.

This thesis firstly presents a new type of actuator for distributed modular self-reconfiguring robotic (MSRR) systems. This actuator is based on simplified electro-permanent magnets, which can change its magnetic field direction and provide holding force without continuous power supply. A series of simulations have been made to figure out the impact of different parameters on the design of actuator.

Based on this actuator, we construct a new modular self-reconfigurable robot system. We call this cube-shaped modular robot system DILI, the length of each module is 1.5 cm. DILI can slide on a flat surface; the maximum speed can reach 20mm/s. With the new actuator, DILI can achieve the functions of both actuation (motion) system and connection system with only one system inside. A DILI module can connect with four other modules. The independent motion of a module also meets the rules of cellular automata.

Finally, a distributed algorithm and a simulator are designed for DILI. DILI is more like a platform, because of its structural and kinematic advantages; people can study complex robot design and algorithms based on it.

I.2. Contributions

This thesis completed the design and fabrication of a distributed modular self-reconfiguring robotic system. This system is a platform which presents the advantage of being easy to manufacture. The main work includes actuator design, actuator simulation, circuit design, modular robot structure design, conception of distributed algorithm, simulation software design.

In particular, the following work was done:

• Formalization of the new concept of simplified electro-permanent (SEP) magnet, which can change its polarity by a pulse current.

• Accurate design of the SEP magnet model with COMSOL Multiphysics and series of numerical simulations to observe the effects of different parameters. The numerical simulation results play a guidance role in designing and validating SEP magnet. Some laws of making SEP have also been summarized.

• The conception of a new type of linear motor (actuator), based on SEP magnet, and characterization of its performance. This linear motor can achieve both motion and connection with only one system; there is no energy consumption when modules are connected.

• Development of a dead-time controllable pulse circuit for the SEP magnet, and experimental verification.

• Construction of a new modular self-reconfigurable robot system: DILI, which can have 2D motion (four directions).

• Study of the performance of DILI robotic system through a series of experiments.

•Design of three capabilities of motion related to a possible load of a module, and proof of feasibility via experiments.

• Proposal of a distributed algorithm for controlling the motion of modules.

• Development of a simulation software for DILI modular robotic system that permits one to test and validate distributed algorithm.

I.3. Manuscript Organization

The structure of this thesis is shown in Figure I-1, details are presented as follows:

• **Chapter II** is a brief presentation of modular robot systems in state of the art. We then present a summary of the actuation and connection mechanisms and miniaturization methods of MRRs.

• **Chapter III** presents the theoretical design of a linear motor based on Simplified Electro-permanent (SEP) magnet. This new linear motor can achieve both motion and connection with only one system.

• **Chapter IV** puts forward a series of numerical simulations of SEP magnet. These simulation results play a guidance role in designing and validating SEP magnet.

• **Chapter V** concentrates on the hardware design and fabrication of the circuit and the structure of DILI module. Experiments on real DILI modules are also given in this chapter.

• **Chapter VI** begins with the capabilities of DILI module. Afterwards, it presents a distributed algorithm for DILI. Finally, a simulator is presented, which allows people to test and validate distributed algorithms.

• **Chapter VII** summarizes the thesis, exposes the remaining questions to be addressed, and gives an outline of the subsequent work enabled by my research.

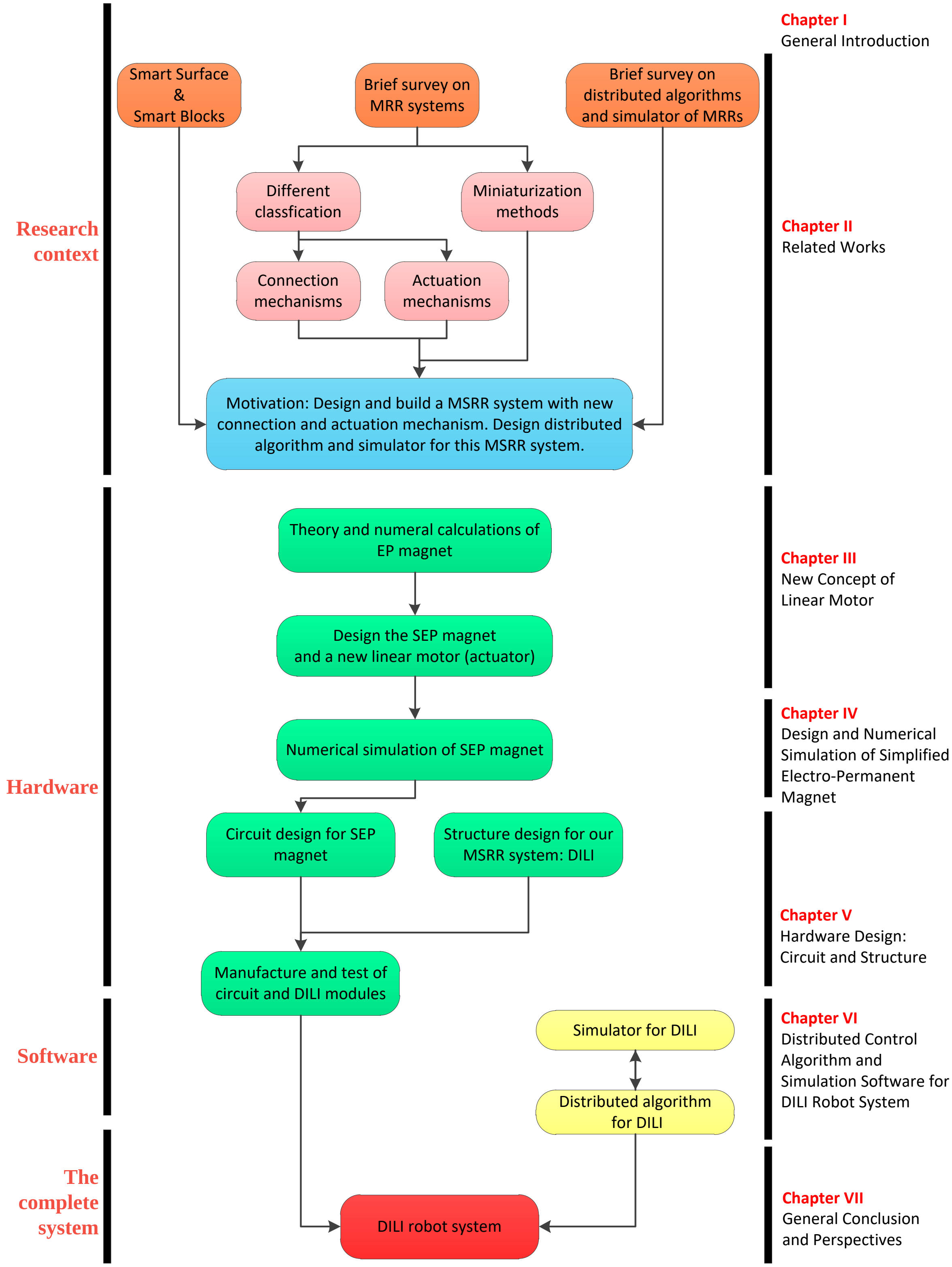

MRR: Modular Reconfiguring robotic
MSRR: Modular Self-Reconfiguring robotic
EP magnet: Electro-Permanent magnet
SEP magnet: Simplified Electro-Permanent magnet

Figure I-1 Thesis structure

References in Chapter I

[1] Matignon L, Laurent G J, Le Fort-Piat N, and Chapuis, Y. A. Designing decentralized controllers for distributed-air-jet mems-based micromanipulators by reinforcement learning [J]. Journal of intelligent & robotic systems, 2010, 59(2): 145-166.

[2] El Baz, D., Boyer, V., Bourgeois, J., Dedu, E., and Boutoustous, K. Distributed part differentiation in a smart surface [J]. Mechatronics, 2012, 22(5): 522-530.

[3] Delettre A, Laurent G J, and Le Fort-Piat N. A new contactless conveyor system for handling clean and delicate products using induced air flows [C]. Intelligent Robots and Systems (IROS), 2010 IEEE/RSJ International Conference on. IEEE, 2010: 2351-2356.

[4] El Baz D, Piranda B, Bourgeois J. A distributed algorithm for a reconfigurable modular surface [C] Parallel & Distributed Processing Symposium Workshops (IPDPSW), 2014 IEEE International. IEEE, 2014: 1591-1598.

[5] Delettre A, Laurent G J, Haddab Y, and Le Fort-Piat, N. Robust control of a planar manipulator for flexible and contactless handling [J]. Mechatronics, 2012, 22(6): 852-861.

[6] Dahroug B, Laurent G J, Guelpa V, and Le Fort-Piat, N. Design, modeling and control of a modular contactless wafer handling system [C]. Robotics and Automation (ICRA), 2015 IEEE International Conference on. IEEE, 2015: 976-981.

[7] Nof, Shimon Y. Handbook of Industrial Robotics (2nd ed.) [M]. John Wiley & Sons. 1999: pp. 3–5.

[8] Siciliano, Bruno, and Oussama Khatib. Springer handbook of robotics [M]. Springer, 2016.

Chapter II. Related Work

In this chapter, we would like to present the general context, state of the art and proposed methodology of this thesis, which can help to clarify the current states, locate the PhD thesis in the correct context and have a global view of our work.

The purpose of this thesis is to build a modular self-reconfigurable robot system; the work is related to structure design, the actuation system, the connection system, miniaturization, distributed algorithm, and simulator. In the following sections, we present state of the art in these areas.

Section II.1 describes the background and the previous works. In Section II.2, we study some characteristics of modular robots; details on 121 modular robot systems are presented in this subsection. Section II.3 concentrates on two classifications of robotic systems; they are based on actuation mechanism and connection mechanism, respectively. Section II.4 deals with several methods for miniaturization, which is one of the challenges of modular self-reconfiguring robotic systems. Section II.5 concentrates on distributed algorithms and simulators for modular self-reconfiguring robotic systems. Section II.6 introduces the cellular automata and its application in modular self-reconfiguring robotics. Conclusions of this thesis are given in Section II.7.

II.1. The Smart Surface and Smart Blocks Projects

This work is an extension of the Smart Surface [1-4] and Smart Blocks [5-7] projects, which were funded by the French National Agency of Research (ANR) and that federated three French research laboratories and Japanese laboratory. The Smart Surface project gave rise to a unique concept of the modular smart conveyor with distributed intelligence which was essentially a static device. The Smart Blocks project aimed at conveying and positioning fragile micro-parts by means of a dynamically reconfigurable distributed system consisting of modules with Micro Electro Mechanical Systems (MEMS) that can move. It combined new results in microtechnology, control theory, and computer science to create a modular self-reconfiguring conveyor based on a contact-free technology. This conveyor is composed of centimeter-size blocks, called smart blocks that can connect in order to form a conveying surface. Each block also includes a MEMS actuator array in the upper face in order to move the objects.

II.2. Modular Reconfigurable Robots (MRR)

Nowadays, robotic systems have become an indispensable part of the human production process; many current human activities have been replaced by robots. In general, these robots are designed for specific-use according to the environment and mission requirements. At the beginning of the design, they are assigned a specific mission that is difficult to adapt to changes in the environment and goal.

It is a huge investment for redeveloping robots, and it takes a lot of time. In addition, people cannot accurately predict some of the working conditions in advance, and therefore a kind of robot which can change its own structure based on the environment and tasks is required. Thus, some principles which originally belonged to software engineerings like reusability and reconfiguration have been used in robotic hardware research. With the developing of electronic, MEMS and microsensor technologies, the processors, actuators, and sensors have become smaller and smaller. The control, actuation, connection and communication systems can be integrated into a single module. Then, with further researches, the initial simple Modular Robots gradually developed into Modular Reconfigurable Robots (MRR). MRR is composed of a large number of repeated basic modules with certain functions of motion, perception, and actuation. They can adapt to environment and goals by connecting and disconnecting to achieve the desired configuration and shape. For example, worm-like robots can pass through narrow holes, can cross the rugged terrain by transforming into quadruped robots, and also can form a ring-shaped configuration in a planar environment to achieve high-speed rolling motion [8]. Compared with traditional robots, MRR has the following characteristics: versatility, adaptively, extensibility, robustness, redundancy and low cost. According to the reconfiguration process, MRR can also be divided into Modular Manual Reconfigurable Robots (MMRR) and Modular Self-Reconfigurable Robots (MSRR). The former class requires manual participation. The biggest advantage of the MSRR is the adaptability, that is, MSRR can change their own configuration based on the environment, and achieve goal changes without external interference [9, 10].

The MRR concept can be traced back to the late 1980's; it was first introduced by Toshio Fukuda at the Science University of Tokyo with the name CEBOT (an abbreviation for 'cellular robotic system') [11]. The size of CEBOT is 18x9x5cm; the weight is about 1.1kg. After more than 30 years of development, more than one hundred MRRs have been developed, they are different in shape and size, some weight a few kilograms (3D Unit is 7kg [12], ModReD is 3.17kg [13]), and some only weight a few grams (Pebbles is 4g [14], Tribolon is 3.7g [15,16]).

II.2.1. Applications of MRR

MRR has been studied in a number of areas, such as bionic, adaptive toolset, drug-delivery, inspection, rescue, exploration (satellite), mapping, and education and so on [17]. Figure II-1 gives an example of rescue application by M-TRAN [18]. M-TRAN can change its shape to achieve some tasks, such as locomotion in terrain through a four-legged gait, locomotion among debris through flow, supporting a beam, and to shelter survivors. Figure II-2 shows the Catoms [19] (in green, purple and blue). The Catoms collaboratively explore an unknown physical environment and inform a "macro" user through a data sink. Since groups of moving Catoms are able to share the map of the environment while transmitting it to the sink, a fast and detailed exploration of an unknown environment is facilitated [20].

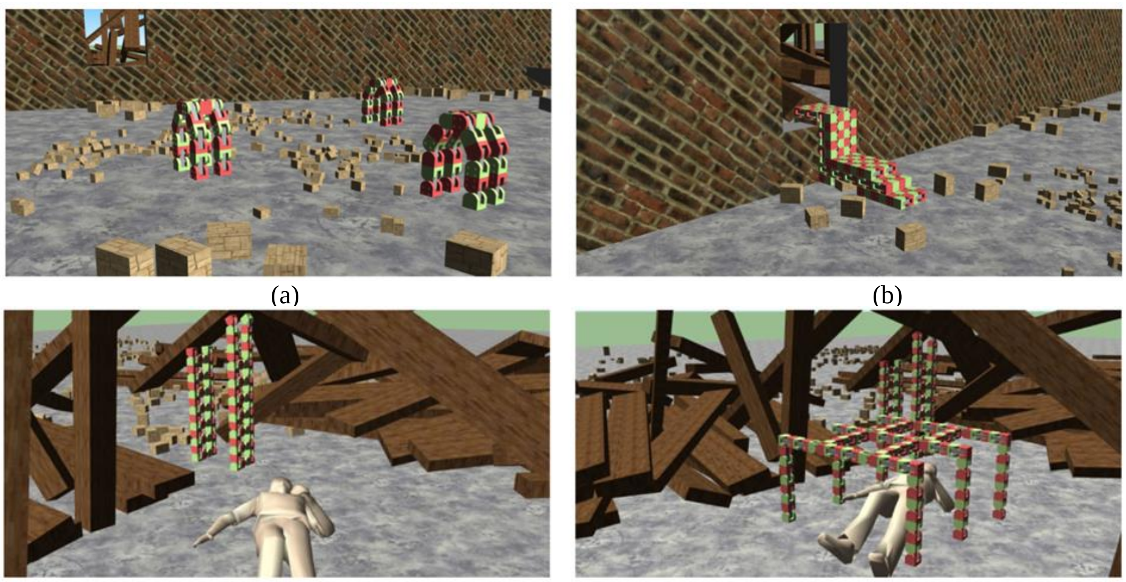

(a) (b) (c) (d)

Figure II-1 A rescue application by M-TRAN: (a) Locomotion in terrain through a four-legged Gait; (b) Locomotion among debris through flow; (c) Supporting a beam; (d) Shape formation to shelter survivors.

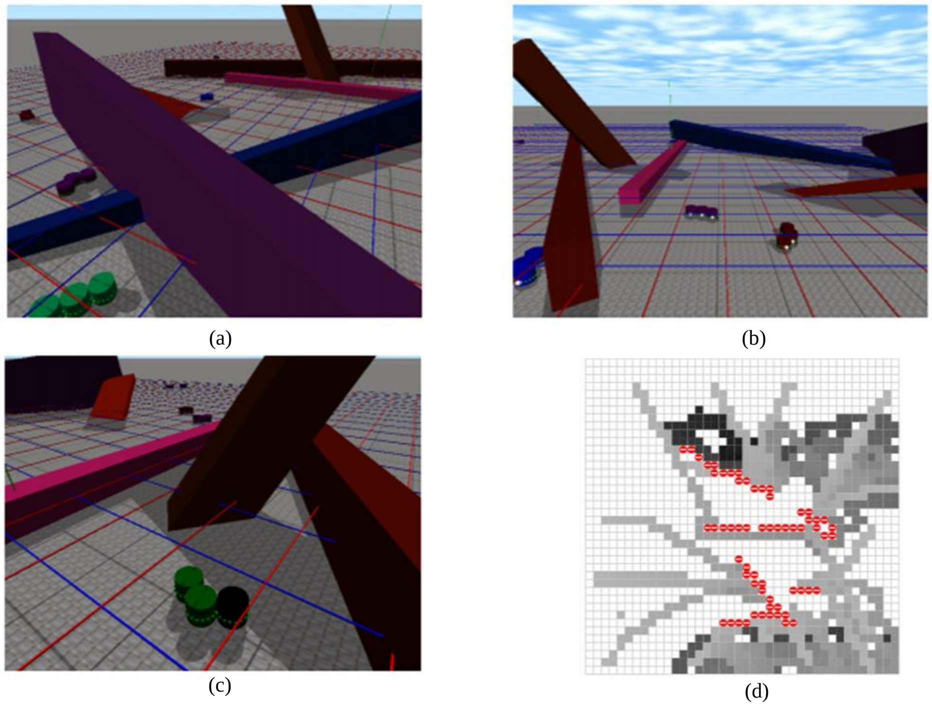

Figure II-2 Catoms scanning a complex environment: (a) Snapshot of the environment (rear view); (b) Snapshot of the environment (front view); (c) Example of a Catom escaping a cavity trap with backtrack; (d) Map overview at tick 14940.

In the field of education, two MRRs have been successfully commercialized: Cellrobot [21] and Cubelets [22] (see Figure II-3).

Cellrobot. Cellrobot is a spherical shaped MSRR that consists of two kinds of modules, one called "Heart" whose diameter is 88mm another one called "Cell" whose diameter is 80mm. Each module has eight joint faces which can be connected to each other through a simple twist movement. The joints will snap together for secure attachment. Cellrobot allows one Heart unit to be connected up to 20 Cells, including wheels and vision devices; each individual cell has a full 360-degree rotation. People can program and control Cellrobot through a smartphone.

Cubelets. Cubelets is a cubical shaped MSRR, which is designed for kids age 8 and up. Cubelets modules connect to each other through permanent magnets, these modules can be divided into three categories based on their functions:

- Sense blocks, this type of module is equipped with sensors for temperature, light, etc.;
- Think blocks, this type of module handles the information collected by the perceptual modules, which determines how the robot responds;
- Action blocks, this type of module is equipped with a motor or speaker and other devices.

Action modules receive instructions from the thinking modules and then respond. People also can program Cubelets via a computer.

(a)

(b)
Figure II-3 Two MRRs for education: Cellrobot (a), Cubelets (b)

II.2.2. MRRs from 1988 to 2017

We present now MRR. We counted 121 types of MRRs. Table II-1 gives details on these MRRs, the information about connection mechanism, actuation mechanism, architecture, shape, and Degree Of Freedom (DOF) is also given here. Sometimes we present several versions of some MRRs when they had an important revolution.

Table II-1 Modular robots characterized by their connection and actuation

Year	*Modular robot*	*Connection Mechanism*		*Actuation*	*Architecture*	*Shape*	*DOF*	*Ref.*
		Categories	*Subdivision*					
1988	CEBOT I	Mechanical	Latch	SMA	Chain	Cuboid	3D	[21]
1988	CMU RMMS	Mechanical	Key & Lock	Motor	Truss	Heterotype	2D	[23]
1990	CEBOT II	Mechanical	Latch	DC motor	Chain	Cuboid	3D	[24]
1993	Polypod	Mechanical	Latch	Manual	Chain	Cubical	3D	[25]
1994	Fracta	Magnet	Electro-magnet	Current	Lattice	Triangular	2D	[26]
1994	Metamorphic I	Mechanical	Key & Lock	Motor	Lattice	Hexagon	2D	[27]
1994	Ganryu	Mechanical	Gripper	Motor	Lattice	Heterotype	3D	[28]
1996	Metamorphic II	Mechanical	Key & Lock	DC motor	Chain	Square	2D	[29, 30]
1996	Tetrobot	Mechanical	Latch	Manual	Hybrid	Cylindrical	3D	[31]
1998	3D unit	Mechanical	Hooks	DC motor	Lattice	Cubical	3D	[12]
1998	3D-Fractum	Mechanical	Hooks	Motor	Lattice	Cubical	3D	[32]
1998	Molecule	Magnet	Electro-magnet	Current	Lattice	Cuboid	3D	[33]
1998	Vertical	Mechanical	Key & Lock	Servo motor	Lattice	Cubical	2D	[34]
1999	ACM-R1	Mechanical	Latch	Manual	Chain	Rectangle	2D	[35]
1999	CONRO	Mechanical	Latch	SMA	Chain	Cuboid	3D	[36]
1999	I-Cube	Mechanical	Key & Lock	Servo motor	Lattice	Cubical	3D	[37]
1999	Micro-robot	Other	Pneumatic	Servo motor	Chain	Heterotype	3D	[38]
1999	Miniaturized	Mechanical	Key & Lock	SMA	Lattice	Cubical	2D	[39]
2000	Crystalline	Mechanical	Key & Lock	DC motor	Lattice	Cuboid	2D	[40]
2000	M-TRAN I	Magnet	Permanent magnet	SMA	Hybrid	Semicylnd	3D	[18]
2000	Microunit I	Mechanical	Latch	SMA	Lattice	Cubical	2D	[41]
2000	ACM-R2	Mechanical	Latch	Manual	Chain	Rectangle	3D	[42]
2000	Proteo	Mechanical	Latch	Manual	Hybrid	Cubical	3D	[43, 44]
2000	PolyBot I	Mechanical	Latch	Manual	Chain	Cubical	3D	[45]
2001	ACM-R3	Mechanical	Latch	Manual	Chain	Rectangle	3D	[46]
2002	Microunit II	Mechanical	Latch	SMA	Lattice	Cubical	3D	[47]
2002	PolyBot II, III	Mechanical	Latch	SMA	Chain	Cubical	3D	[48]
2002	Pneumatic Cellular	Other	Pneumatic	Pneumatic	Lattice	Cubical	2D	[49]
2002	TeleCube	Magnet	Permanent magnet	SMA	Lattice	Cubical	3D	[50]
2002	Millibot	Mechanical	Latch	SMA	Chain	Elliptical	2D	[51]
2002	Uni-Rover	Mechanical	Gripper	Servo motor	Chain	Cylinder	3D	[52]
2003	M-TRAN II	Magnet	Permanent magnet	SMA	Hybrid	Cylindrical	3D	[53, 54]
2003	CHOBIE	Mechanical	Latch	Motor	Lattice	Cylindrical	3D	[55]

Table II-1 Continue

Year	*Modular robot*	*Connection Mechanism*		*Actuation*	*Architecture*	*Shape*	*DOF*	*Ref.*
		Categories	*Subdivision*					
2003	Gear-Type units	Magnet	Permanent magnet	---	Free form	Cylindrical	2D	[56]
2003	Swarm-Bot	Mechanical	Gripper	Motor	Hybrid	Cylindrical	3D	[57, 58]
2004	ATRON	Mechanical	Hooks	DC motor	Lattice	Octagonal	3D	[59]
2004	Claytronics	Magnet	Electro-magnet	Electro-magnet	Free form	Cylindrical	2D	[60, 61]
2004	HitMSR	Magnet	Permanent magnet	Motor	Lattice	Cubical	3D	[62]
2004	Neubot	Magnet	Permanent magnet	Motor	---	---	---	[63]
2004	Random Parts	Mechanical	Latch	Motor	Lattice	Cubical	2D	[64]
2004	Stochastic 2D	Magnet	Electro-magnet	Random movement	Lattice	Cubical	2D	[65]
2005	Y1	Mechanical	Latch	Servo motor	Chain	Heterotype	3D	[66]
2005	Stochastic 3D	Magnet	Electro-magnet	Random movement	Lattice	Cubical	3D	[67]
2005	Catoms	Other	Electro-magnet	Voltage	Free form	Cylindrical	2D	[19]
2005	HYDRON	---	----	----	Lattice	Spherical	2D	[68]
2005	Molecube	Magnet	Electro-magnet	Current	Hybrid	Cubical	3D	[69]
2005	Microrobot	Mechanical	Latch	SMA	Chain	Cylindrical	3D	[70]
2005	Programmable parts	Magnet	Permanent magnet	DC motor	Lattice	Triangular	2D	[71]
2005	Superbot	Mechanical	Latch	Manual	Hybrid	Cuboid	3D	[72, 73]
2005	Slimebot	Other	Velcro	Pneumatic	Free form	Cylindrical	2D	[74,75]
2006	AMAS	Mechanical	Hooks	Servo motor	Hybrid	Cubical	3D	[76]
2006	Deformatron	Mechanical	Latch	Servo motor	Hybrid	Cubical	3D	[77]
2006	MEMS	Other	Electrode	Voltage	Free form	L shaped	2D	[78]
2006	ORTHO-BOT	Mechanical	Latch	Manual	Truss	Heterotype	3D	[79]
2006	Yamor	Other	Velcro	Manual	Chain	Semicylnd.	3D	[80]
2007	AMOEBA-I	Mechanical	Latch	Manual	Chain	Cuboid	3D	[81, 82]
2007	CHOBIE II	Mechanical	Latch	Motor	Lattice	Cylindrical	3D	[83]
2007	CkBot	Magnet	Permanent magnet	Manual	Hybrid	Cubical	3D	[84]
2007	Miche	Magnet	Permanent magnet	Motor	Lattice	Cubical	3D	[85]
2007	ROBMAT	Mechanical	Latch	Motor	Hybrid	Cuboid	3D	[86]
2007	Shady 3D	Mechanical	Gripper	Servo motor	Hybrid	Cuboid	3D	[87]
2007	TETwalker	Mechanical	Latch	Manual	Truss	Heterotype	3D	[88]
2007	Tribolon	Magnet	Permanent magnet	Current	Lattice	Triangular	2D	[15,16]
2007	X-bot	Magnet	Permanent magnet	SMA	Lattice	Cubical	2D	[89]
2008	M-TRAN III	Mechanical	Hooks	DC motor	Hybrid	Semicylnd	3D	[90]
2008	Em-cube	Magnet	Electro-magnet	Current	Lattice	Cubical	2D	[91]

Table II-1 Continue

Year	Modular robot	Connection Mechanism		Actuation	Architecture	Shape	DOF	Ref.
		Categories	Subdivision					
2008	JL-1	Mechanical	Latch	DC motor	Chain	Trapezoid	3D	[92]
2008	GZ-I	Mechanical	Latch	Manual	Chain	Cubical	3D	[93]
2008	Morpho	Mechanical	Latch	Manual	Truss	Cubical	3D	[94]
2008	Odin	Mechanical	Latch	Manual	Truss	Cylindrical	3D	[95]
2008	SYMBRION	Mechanical	Latch	Motor	Hybrid	Cylindrical	3D	[96]
2009	Hinge	Mechanical	Threads	Manual	Truss	Cylindrical	3D	[97]
2009	Raupi	Mechanical	Gripper	Servo motor	Hybrid	Cylindrical	3D	[98]
2009	Roombots	Mechanical	Hooks	Manual	Hybrid	Cuboidal	3D	[99]
2010	Factory Floor	Mechanical	Gripper	Manual	Truss	Cylindrical	3D	[100]
2010	JL-2	Mechanical	Gripper	DC motor	Chain	Trapezoid	3D	[101]
2010	iMobot	Mechanical	Latch	Manual	Hybrid	Cuboid	3D	[102]
2010	Modular-Expanding	Mechanical	Threads	Manual	Chain	Cylindrical	3D	[103]
2010	Mod-Leg	Mechanical	Latch	Servo motor	Chain	Cylindrical	3D	[104]
2010	Responsive Truss	Mechanical	Key & Lock	Manual	Truss	Cylindrical	3D	[105]
2010	Sambot	Mechanical	Hooks	Servo motor	Lattice	Cubical	3D	[106]
2010	Single-material	Mechanical	Latch	Random movement	Lattice	Cubical	3D	[107]
2010	Pebbles	Magnet	Electro-permanent	Random movement	Lattice	Cubical	2D	[14]
2010	Stochastic fluidic	Other	Binder material	Manual	Lattice	Cubical	3D	[108]
2010	M^3	Mechanical	Hooks	DC motor	Hybrid	L shaped	3D	[109]
2010	Thor	Mechanical	Gripper	DC motor	Chain	Cuboid	3D	[110]
2010	UBot	Mechanical	Hooks	DC motor	Hybrid	Cubical	3D	[111]
2010	Vaccubes	Other	Pneumatic	Manual	Hybrid	Cubical	3D	[112]
2011	Steering	Mechanical	Latch	---	Chain	Cuboid	2D	[113]
2011	Blinky blocks	Magnet	Permanent magnet	Manual	Lattice	Cubical	3D	[114]
2011	Anibot	Mechanical	Latch	Heat	Chian	Cuboid	2D	[115]
2011	Cross-ball	Magnet	Electro-magnet	Motor	Lattice	Spherical	3D	[116]
2011	Cubelets	Magnet	Permanent magnet	Manual	Lattice	Cubical	3D	[22]
2011	Heterogeneous	Mechanical	Latch	Motor	Chain	Cubical	3D	[117]
2011	HitMSR II	Mechanical	Hooks	Servo motor	Chain	Cubical	3D	[118]
2011	M-Cubes	Mechanical	Latch	DC motor	Lattice	Cubical	3D	[119]
2011	M-Lattice	Mechanical	Latch	Servo motor	Lattice	Triangular	2D	[120]
2011	HexBot	Magnet	Electro-magnet	DC motor	Lattice	Hexagonal	3D	[121]
2011	SMART	Mechanical	Hooks	Motor	Lattice	Cubical	3D	[122]

Table II-1 Continue

Year	*Modular robot*	*Connection Mechanism*		*Actuation*	*Architecture*	*Shape*	*DOF*	*Ref.*
		Categories	*Subdivision*					
2011	X-Cell	Magnet	Electro-magnet	Motor	Lattice	Cubical	2D	[123]
2012	ModRED	Mechanical	Latch	Motor	Chain	Cuboid	3D	[13]
2012	M^3Express	Mechanical	Latch	SMA & servo	Hybrid	L shaped	3D	[124]
2012	Neurobot	Mechanical	Latch	DC motor	Hybrid	Cubical	3D	[125]
2012	Smart Blocks	Magnet	Electro-permanent	Electro-permanent magnet	Lattice	Cubical	3D	[5,6]
2012	SMORES	Magnet	Permanent magnet	DC motor	Hybrid	Cubical	3D	[126]
2012	Transmote	Mechanical	Key & Lock	Manual	Chain	Cubical	3D	[127]
2013	M-blocks 2D	Magnet	Permanent magnet	Electro-permanent magnet	Lattice	Cubical	2D	[128]
2013	USS	Mechanical	Latch	Servo motor	Chain	Cubical	3D	[129]
2013	Fable	Magnet	Permanent magnet	Manual	Chain	Cylindrical	3D	[130]
2014	Petro	Mechanical	Latch	Manual	Lattice	Tetrahedral	3D	[131]
2014	Cellrobot	Mechanical	Latch	Manual	Chain	Spherical	3D	[21]
2014	Soldercubes	Other	Binder material	Current	Hybrid	Cubical	3D	[132]
2015	M-blocks 3D	Magnet	Permanent magnet	Electro-permanent magnet	Lattice	Cubical	3D	[133]
2016	Trimobot	Mechanical	Hooks	DC motor	Hybrid	Hexagonal	3D	[134]
2016	HyMod	Mechanical	Latch	Manual	Lattice	Cubical	3D	[135]
2016	MHP	Mechanical	Latch	Pump	Lattice	Cubical	3D	[136]
2016	Diamobot	Mechanical	Latch	Manual	Hybrid	Cubical	3D	[137]
2016	Larva-Bot	Mechanical	Hooks	Servo motor	Lattice	Cubical	3D	[138]
2016	Pitch-pitch	Mechanical	Hooks	Servo motor	Chain	Cubical	3D	[139]
2017	EMeRGE	Magnet	Permanent magnet	Manual	Lattice	Cubical	2D	[140]
2017	HexaMob	Mechanical	Latch	Motor	Chain	Rectangle	2D	[141]

II.3. Classification and State of the Art

MRR can be classified into various categories and subcategories, among which the widely accepted classifications are based on architecture, scale, locomotion, and structure. The categories based on architecture are the primary and best-known classifications. Murata and Kurokawa [8] studied the architecture of modular robots and formally classified their architecture into the *chain, lattice*, *hybrid*, and *truss*. Some examples of these architectures are shown in Figure II-4, which could give people an intuitive vision. Then, Gilpin and Rus [142] introduced *free-form* architecture in order to cover a few unique systems that do not fit into conventional architectures.

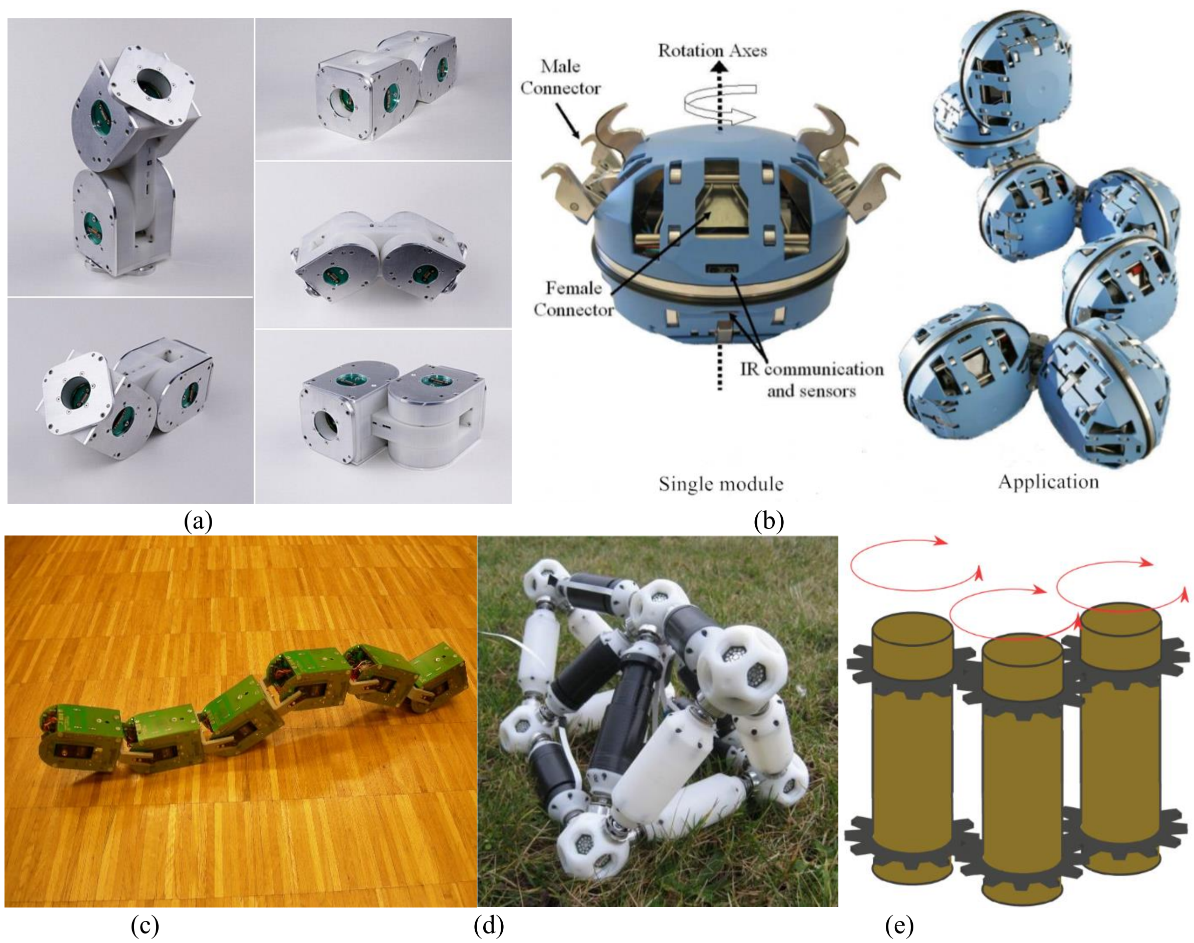

Figure II-4 Some examples of modular robot architectures: (a) iMobot (hybrid) [102], (b) ATRON (lattice) [59], (c) YaMoR (chain) [80], (d) Odin (truss) [95], (e) Gear-Type Units (free-form) [56]

According to structure, MRR can be classified into *linear*, *spatial*, and *planar*. In linear structure, there is no cross, no corner in the structure when modules connect to each other. This structure is mainly used in some snake-shaped or warm-shaped modular robots, such as ACM [35]. The plane structure is a kind of modular robots that can only move in the plane, such as Fracta [26]. Spatial structure means that the modular robots can move in three-dimensions, such as Tetrobot [31], TeleCube [50], M-TRAN [18] and SuperBot [72, 73].

On what concerns aspects related to composition, actuation and connection are two main systems of a MRR. Therefore, we classified the MRR according to these two properties, as shown in Figure II-5. Details will be given in the following two sub-sections.

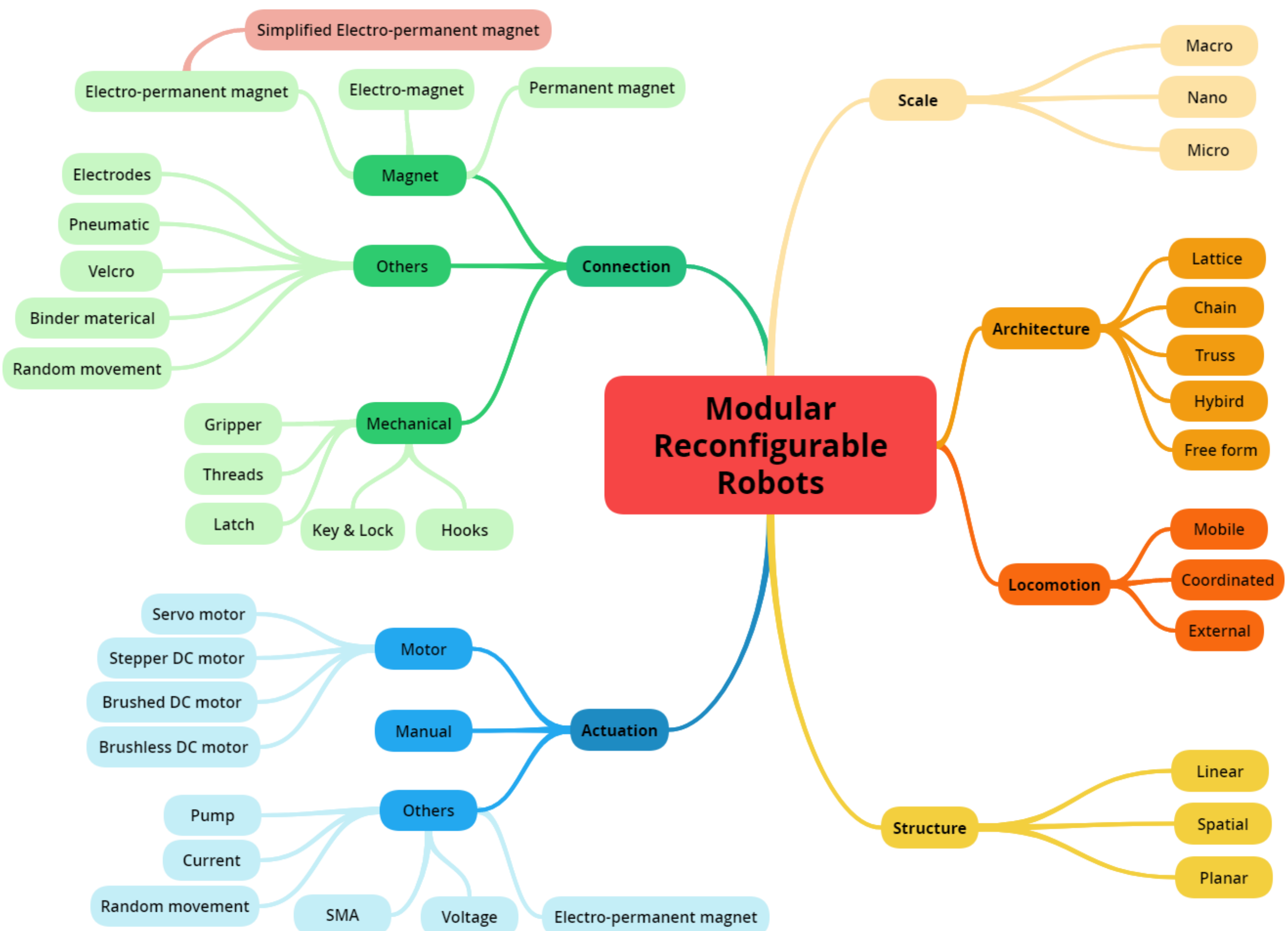

Figure II-5 Several classifications of MRRs

II.3.1. Classification via actuation mechanism

In this section, the actuation attribute refers only to the actuation and transmission mechanisms embedded in modules to enable gait locomotion, self-reconfiguration, self-assembly. Typically, actuators occupy more than 50% of the volume and weight of modules. We also note that actuation systems constitute major obstacles in downsizing modules [89].

When classifying MSRR based on actuation, we introduce the following classes: *motor, manual* and *others* (see Figure II-5). We detail now the different classes.

Motor

From the invention of modular robots to the present, the motor has been the most widely used actuation system. Furthermore, motor can also be subcategorized into brushless direct current (BLDC) motor like Telecube [50], PolyBot [45, 48], and Odin [95], brushed DC (BDC) motors like SMART [122], M3Express [124], and Roombots [99], stepper DC (SDC) motors like X-Cell [123] and ModRed [13], servo motor like CKBot [84].

Manual

In order to reduce the complexity of the controller and docking interfaces, some modular robots are sometimes assembled manually from an ensemble of different modules and connectors. They require human intervention at the time when reshaping of the morphology is desired. Since such kind of modular robots does not have to consider a complex actuation process, they are mainly designed to work with fixed topologies rather than for self-reconfiguration.

We stress that, even if this kind of modular robots is assembled manually, then they still may have the moving possibilities, GZ-I [93] is one example of modular chain robots with a manual configuration that can also achieve movement by cooperation.

Others

In addition to the motor and manual, with the development of materials science, sensor technology, there have been some interesting ways of actuation. Such as Shape Memory Alloy (SMA), pump, current, random movement, voltage and electro-permanent magnet.

II.3.2. Classification via connection mechanism

Connectors play a crucial role in modular robotics since they provide a key function between modules. Based on Connection mechanism, MRR can be categorized into *mechanical*, *magnet*, *others* (see Figure II-5).

Mechanical

Mechanical can be subcategorized into the *latch*, *gripper*, *key & lock*, *hooks,* and *treads* (examples are shown in Figure II-6). These methods have a big advantage of stability and can provide strong connecting force; but they also have some drawbacks, such as the complexity of structure and response time is relatively long. These drawbacks limit their application in robots, especially at a small scale.

Magnet

Magnet connection methods contain the *permanent magnet* (Miche [85]), *electro-magnet* (Hexbot [121]), and *Electro-Permanent (EP) magnet* (Pebbles [14]). Permanent magnets can provide a tight connection between modules, but they require manual intervention which is contrary to the idea of autonomous robots. Electro-magnet is easy to control and act fast; however, the limit is that it requires a continuous power supply. EP magnet can also act fast and does not need continuous power supply during working, which is a new concept of connector for modular robots.

Others

Mechanical and magnet can be seen as the traditional connection methods. Some new methods have been used in recent years. In Stochastic Fluidic Robot system, Tolley et al. present a novel reversible module connection mechanism using a low melting point alloy which is soldered to a fluid environment [107]. Meanwhile, other methods such as *Velcro* (Simebot [74]), *binder material* (Soldecubes [132]), *random movement* (single-material [107]), *pneumatic* (Vaccubes [112]), *electrodes* (MEMS [78], where MEMS is here the name of a robot) have also been used in MRR. We summaries them into *others* due to the limited applications.

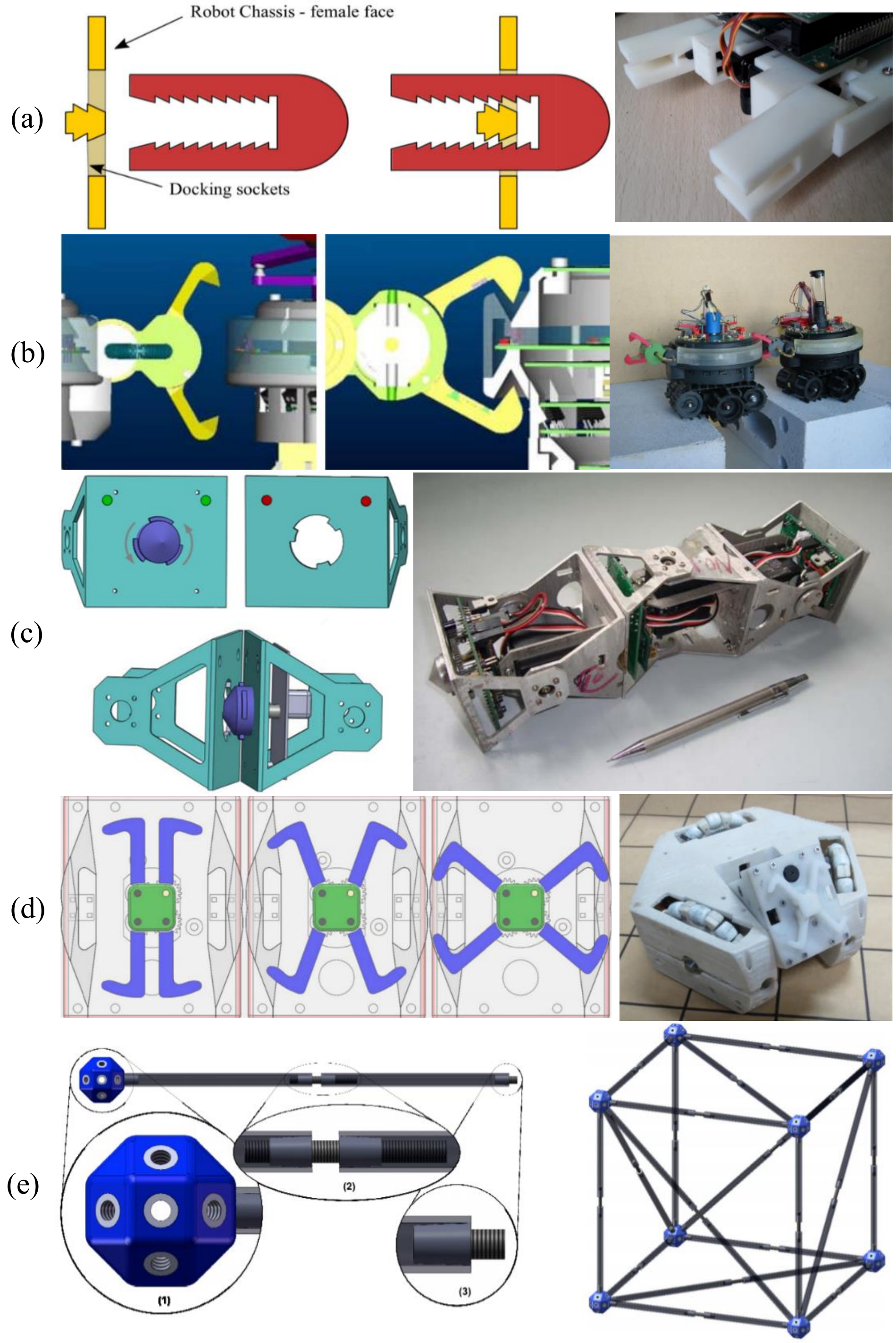

Figure II-6 Mechanical connections (shown in the left of each subfigure) and their real applications (shown in the right of each subfigure): (a) HexaMob (latch) [141], (b) SWARM-BOT (gripper), (c) Transmote (key&lock), (d) Trimobot (hooks), (e) Hinge (threads)

A qualitative comparison of several main connection methods for MRR can be seen in Table II-2. This table can provide a reference for choosing the connection method.

Table II-2 Qualitative comparison of several connection methods for MRRs

Methods	*Size and Weight*	*Strength*	*Switching Time*	*Power required for*	*Manufacturability*
Latch	medium	high	1-10 s	disconnect	difficult
Gripper	large	high	1-10 s	connect & disconnect	difficult
Key & Lock	large	high	1-10s	connect & disconnect	difficult
Permanent magnet	small	high	-	None	simple
Electromagnets	small	medium	<1 s	connect	simple
Electro-permanent magnets	small	small	<1 s	disconnect	difficult
Hydraulic	large	high	>10 s	connect & disconnect	difficult
Pneumatic	large	high	>10 s	connect & disconnect	difficult
Electrodes	small	small	<1 s	connect	difficult
Velcro	small	medium	-	None	simple
Binder material-based	small	high	-	None	simple

Through the analysis of Table II-1, we get the trend of the development of connection methods from the year 1988 to 2017 (see also Figure II-7). Obviously, mechanical is the most widely used connection method, the ratio of magnet systems is increasing.

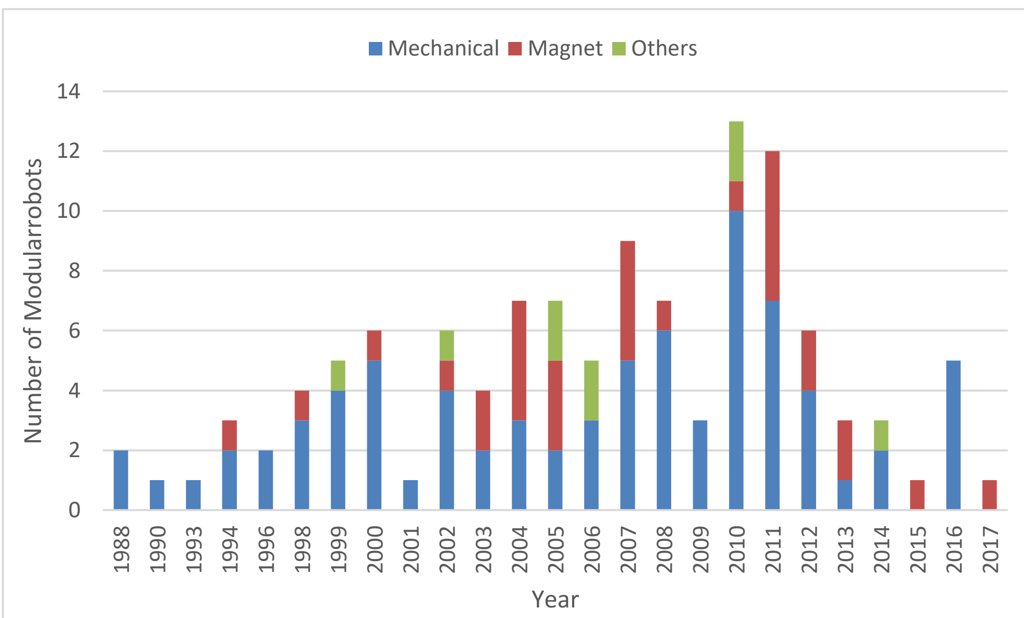

Figure II-7 Trend of the connection methods

II.4. Methods for Miniaturization

At present, most MRRs are in the research stage; they are rarely used in practical applications. One of the grand challenges of self-reconfiguring modular robotics is the assembly of a functional system from tens or hundreds of components. However, only systems comprised of small numbers of modules have been demonstrated. Miniaturization is one of the main reasons that stop MRR to be actually applied. One approach to scaling to large numbers of modules is to simplify module design by relieving the modules of the typical power, control, and actuation requirements necessary for locomotion like fluidic manipulation [107]. Scientists have made many attempts on this aspect. Therefore, some interesting design appears. There are three main methods for miniaturization.

II.4.1. Method 1: modules without actuation system

Since actuators occupy more than 50% of the volume and weight of modules, people developed some MRRs without actuation system. These MRRs are mainly used to study the communication between modules or control algorithms.

Miche. The Miche robots [85] (see Figure II-8 a) were invented by Kyle Gilpin, Keith Kotay, Daniela Rus at MIT. Miche robots are a set of robots that consists of 28 1.8-inch autonomous cube-shaped robots which are able to connect to and communicate with their immediate neighbors. Modules can disengage their magnetic couplings and fall away under the influence of gravity. Miche robots starting from an amorphous arrangement can be assembled into arbitrary shapes and then commanded to self-disassemble in an organized manner to form complex 3D shapes. When assembled into a structure, the modules form a system that can be virtually sculpted using a computer interface via a distributed process.

In addition to gravity, random movements are also often used for modular combinations as in the following examples:

Pebbles. The Pebbles [14] (see Figure II-8 b) is also developed by Kyle Gilpin and Daniela Rus's team at MIT. With the assistance of external stochastic force which comes from a vibration table, Pebbles is capable of self-assembling into a uniform structure from a loose collection of disjoint modules. During the random movement, once a module meets with another one as desired, they will connect to each other via electro-permanent magnets. Pebbles system forms an initial uniform grid of modules, and then subtracts the unnecessary modules until the goal structure is obtained.

Single-material. Michael T. Tolley and Hod Lipson at Cornell University [107] developed the Single-material system; it is composed of 15 mm scaled cubic modules which are made by 3D printing material. Single-material can assemble 3D target structures stochastically within a 1.3 litter assembly tank by manipulating the fluid flow at an active assembly substrate using external valving. The modules connect to each other by a mechanical structure and do not have any electronic equipment or power supply (see Figure II-8 c).

Stochastic 2D and 3D. P.J. White et al. also from Cornell University [65, 67] presented several modular robot systems in both 2D and 3D, all these robot systems do not have actuation system. The 2D system (see Figure II-8 d) has two prototype units, a square-shaped unit which uses electromagnets for connection and a triangle-shaped unit which use swivelling permanent magnets instead. The modules were shuffled randomly on an oscillating air table, when two modules collide properly, they bond one to another via the magnets, and release from each other if the configuration is not desired. The 3D system (see Figure II-8 e) uses electromagnets for connection, like Single-material robot, Stochastic 3D also moves thanks to the random fluid.

For the above modular robot systems, there are obvious drawbacks, they take time to reach the desired configuration, and they have a low success rate for configuration.

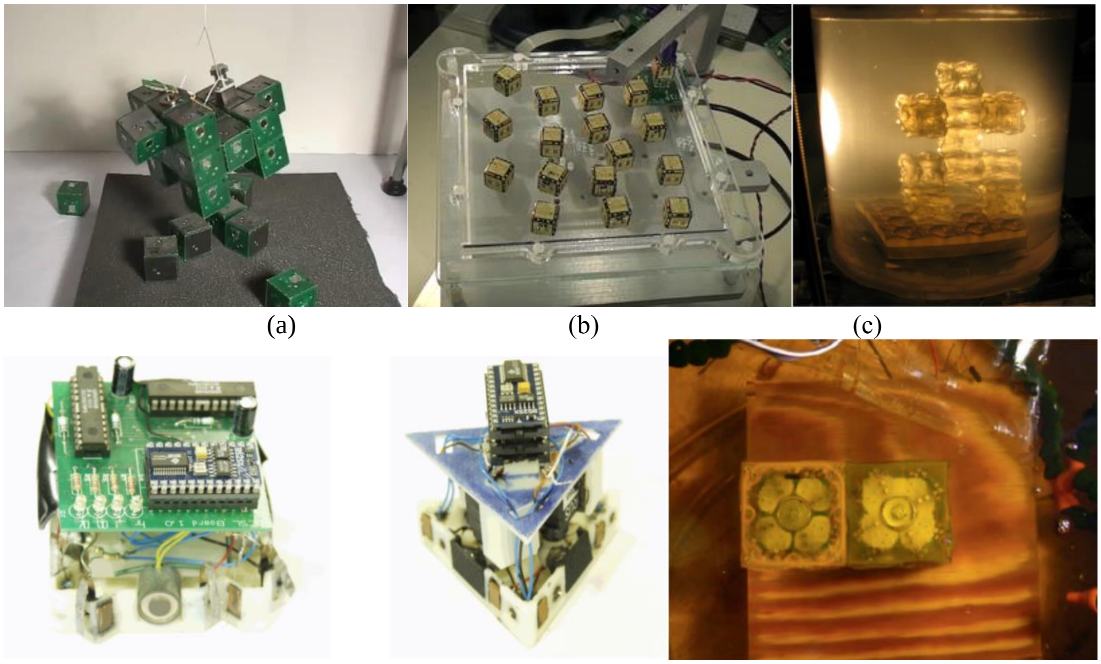

(a) (b) (c)

(d) (e)

Figure II-8 Some MRRs without actuation system: (a) Miche, (b) Pebbles, (c) Single-material, (d) Two prototype of Stochastic 2D units, (e) Stochastic 3D

II.4.2. Method 2: substitution of the actuation system for an affiliate system

Automatic Modular Assembly System (AMAS). Yuzuru Terada and Satoshi Murata at Tokyo Institute of Technology [76, 143] developed AMAS to simplify construction work by introducing modularity into both structural components and means of assembly. AMAS is mainly composed of cubical modules; the modules can connect to each other by mechanical hooks on their surface. The AMAS modules do not contain actuation system. Thus, an affiliated system whose name is assembler robot was introduced (see Figure II-9). The assembler robot with four degrees of freedom can walk on the modules by using an inchworm motion, repeating connection and disconnection actions. The assembler robot can carry a module with its hand (L shaped part). Thus, the assembler robot can construct nearly any structure by combining basic assembly actions.

Obviously, the limitation of this method is that it requires complex control algorithm.

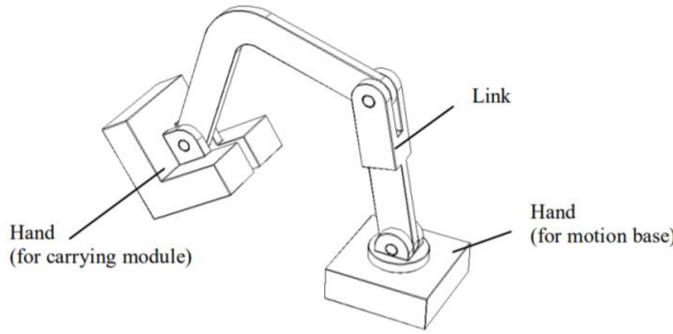

(a) Assembler robot

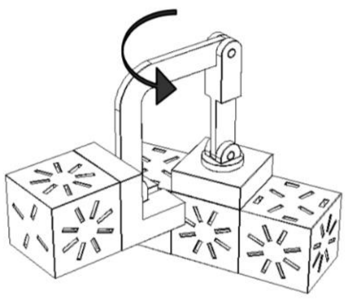

(b) Rotation

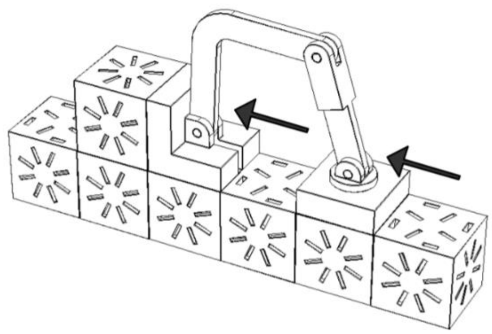

(c) Inchworm motion

Figure II-9 Automatic Modular Assembly System

II.4.3. Method 3: multi-system multiplexing

Catoms. Catoms robot [19] provides a good idea about miniaturization of robots. Catoms belong to Claytronics project carried out by Goldstein et al. at Carnegie Mellon University. Catoms is a series of cylindrical-shaped modular robots which had eight versions; the Planar Catom V8 is the newest one. The architecture of Catoms is free-form. The novel feature of Catoms is their ability to reconfigure (move) relative to one another without classical actuation methods presented in subsection II.3.1. Electromagnets are arranged around the robots, by controlling the state of electromagnets, a module can move and connect to other modules. Thus, one system can achieve both actuation and connection (see Figure II-10). This method is innovative; it can save size and weight. The drawbacks of Catoms are: the electro-magnets need a continuous power supply, and their cylindrical structure makes the movement tricky.

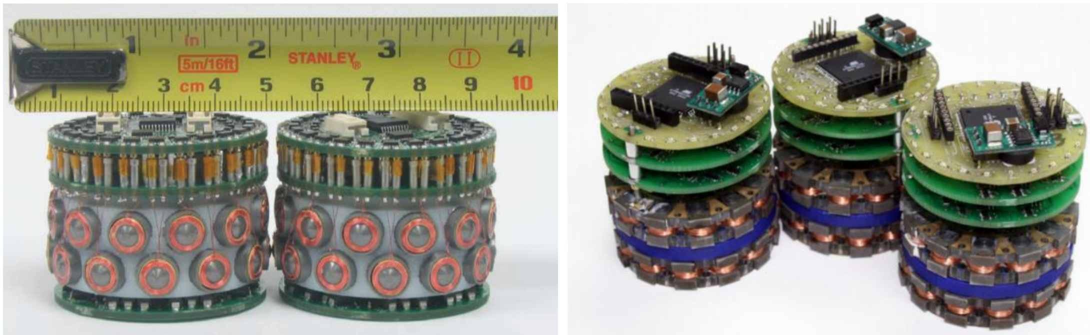

Figure II-10 Two prototypes of Catoms modular robot system

II.5. Distributed Algorithms and Simulators for MSRR

In this subsection, we deal with the different aspects related to control, distributed algorithm, software, and simulator of the reconfigurable modular robot. The reassembly process of MSRR has proven to be difficult to control because it involves the control of a distributed system with many mechanically coupled modules connected in time-varying ways [144]. Thus, a variety of distributed algorithms for MSRR has been developed.

In order to facilitate the task of programming ATRON, U. P. Schultz [145] presented a concept of distributed control diffusion: distributed queries are used to identify modules that play a specific role in the robot, and behaviours that implement specific control strategies are diffused throughout the robot based on these role assignments. Kamimura et al. developed both centralized and decentralized control method for M-TRANN III [90]. W M Shen et al. have presented a biologically inspired approach to distributed collaboration between the physically coupled modules for CONRO. This approach was used to accomplish global effects such as locomotion and reconfiguration [146]. Miao et al. [147] proposed a distributed algorithm for enveloping an object inside a hexagonal lattice environment based on local communications among neighboring modules and between modules and the lattice node containing a target object.

Julien Bourgeois's team contributed a lot on distributed self-reconfiguration algorithm for cylindrical modular robots, such as Catoms. In 2014, they proposed a flexible distributed algorithm allowing the reorganization of a set of modular micro-robots into the desired target shape. Since their algorithm does not need an explicit description of the final shape, it shows a great flexibility concerning the range of target shapes [148]. In 2016, they proposed a parallel, asynchronous and fully decentralized distributed algorithm to self-reconfigure robots from an initial configuration to a goal one. They also evaluated their algorithm at the millimetre-scale, which indicates that the number of communications, the number of movements and the execution time of their algorithm is highly predictable [149].

El Baz at LAAS-CNRS developed a distributed algorithm based on distributed election for establishing quickly a smart conveyor made of smart modules. This research work was done in the framework of the ANR Smart Block project [6].

Robert Fitch et al. present both centralized and decentralized algorithms for cubical MSRR, which plans module trajectories through the volume of the structure. They define free space by an arbitrarily-shaped bounding region. This addresses the important problem of reconfiguration among obstacles, and reconfiguration over a rigid surface [150]. By using this algorithm, they successfully simulated a transformation from a chair to a table (see Figure II-11).

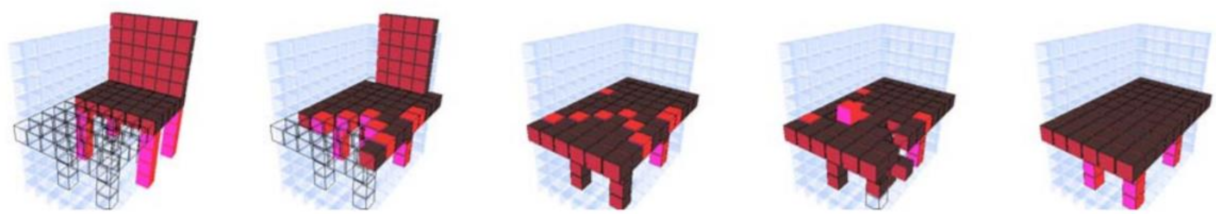

Figure II-11 Example of simulation of reconfiguration for cubical MSRR

Meanwhile, many simulators for MRRs have been developed, such as Adam [151], Webots [152], OpenMR [153] (see Table II-3). These simulators allow people to create virtual environments for MRR, such as robots work on the surface of water [154], under the water [155] or on an air surface [156]. Simulators also allow people to visualize and debug in real-time, for example, VisibleSim permits one to test and visualize distributed algorithms in a 3D environment. As a consequence, simulators can not only facilitate the development of efficient algorithms but also can inspire hardware designers with innovative features [17].

Table II-3 Some simulators of modular robotic systems

Simulator	*Simulated Modules*	*Operating System*	*Programing Language*	*Graphic Engine*	*Dynamic Engine*
M-TRAN	M-TRAN	Windows, Linux	C++	OpenGL, GLUT, MUI	Vortex, ODE
Adam	Hinge-like modules	Windows, Linux, Mac OS	C++	GULT	ODE
Webots	YaMor, RoomBots M-TRAN	Windows, Linux, Mac OS	C++, Java, Python, Matlab	OpenGL	ODE
DPRsim	Catom	Linux	C++	OpenGL, Gtk2lib	ODE
USSR	ATRON, Odin M-TRAN	Windows, Linux,	Java, C	JME	PhysX
CubeInterface	Molecube	Windows	C++	Ogre3D	AGEIA, PhysX
Symbricator3D	SYMBRON, Replicator	Linux	C++	Delta-3D, Game Manager	ODE
OpenMR	Y1, ATRON	Windows, Linux	C++, Python	OpenGL	ODE
ReMod3D	M-TRAN	Windows, Linux	C++	OpenGL	Physx
Micromult	Heterogeneous Chain modules	Windows	C++	OpenGL	ODE
VisibleSime	Smart blocks Blinky blocks	Linux	C++	OpenGL	ODE

II.6. Cellular Automata Theory Applied to MSRR

This subsection deals with a different approach based on cellular automata. We note that during the distributed control process of MSRR, the modules in the system could behave independently; in particular, motion plans can be made in parallel. In that case, the regular overall macro motion of the whole system results from the combination of local and concurrent module motions. Cellular automata have simple rules but can achieve complex movement, which can also provide a good reference for the distributed control of MSRR.

II.6.1. Cellular automata

Cellular automata (CA, single: cellular automaton) were introduced by Von Neumann in the 1940s; CA are discrete models studied in computability theory, mathematics, physics, complexity science, theoretical biology and microstructure modelling. CA are finite-state machines whereby each cell decides upon its next state based on its current state and the state of its neighboring cells [157]. The two most common types of neighborhoods are the Von Neumann neighborhood (each cell has four neighbors) and the Moore neighborhood (each cell has eight neighbors), which is shown in Figure II-12.

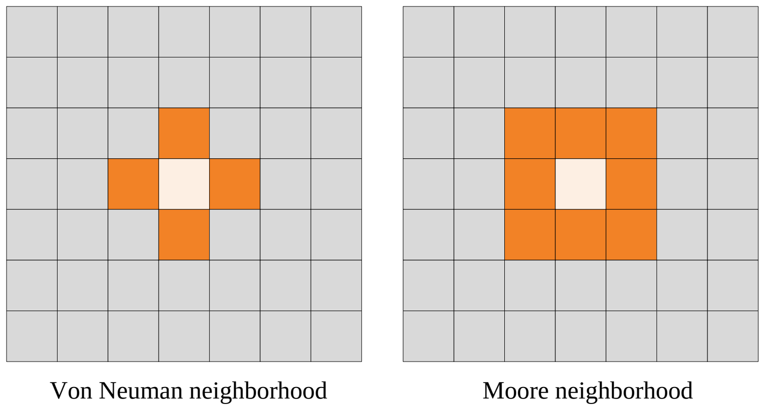

Figure II-12 Different cellular automata neighborhoods

II.6.2. Applications to MSRR

Cellular automata have lacked during a long time a real representation in hardware as pointed out by Murata [26]. Then, in 2001 CA were first employed in developing distributed reconfiguration controllers by Butler Z., Kotay K. and Rus D. [158, 159]. They use a cellular automata model to create "water-flow" like locomotion. They assume that the robot moves on the floor and there are no obstacles. A set of eight rules are presented in Figure II-13, these rules are used to move a robot (represented as a rectangular array of cells) eastward. A module uses only one rule in each direction and plans its own motion at the next moment according to the environmental information on the neighbors and rules. For example, if rule 3 (see Figure II-13) is applied, then the result is that the current cell moves one unit in the eastward direction. Figure II-14 shows the modules across an obstacle by using the rules in Figure II-13. During the process, modules always keep the connection whith each other, and no module is lost.

In 2003, Xu W. et al. [160] developed a set of rules for the class of planar lattice modules based on modules' local perception about their immediate neighbouring lattice cells.

In 2004, Butler Z. et al. [159] devised a set of transition rules for realizing water-flow motion by MoleCube, M-TRAN, and Crystal modules, in which a modular robot is considered as a particular type of Cellular Automata which runs local rules in each individual cell. Local rule sets are based only on the local configuration around a particular module, and consist of five and eight rules for water-flow in obstacle-free and obstacle-filled environments, respectively.

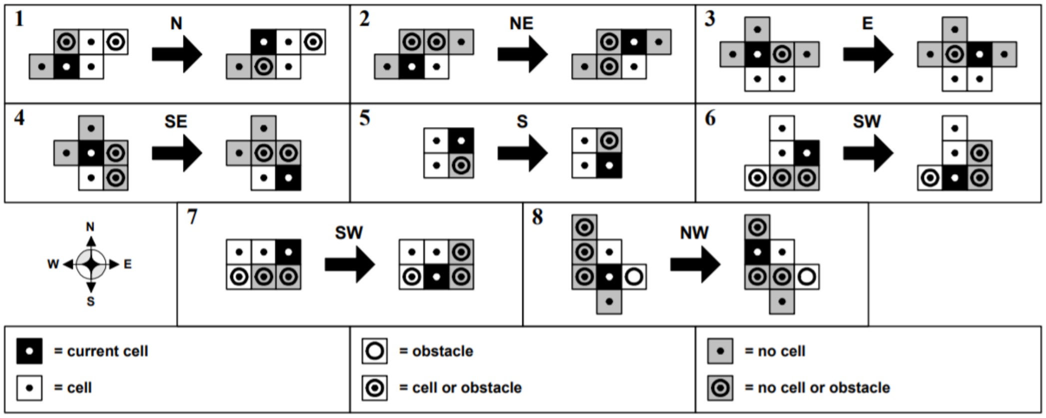

Figure II-13 Rules for eastward locomotion with obstacles

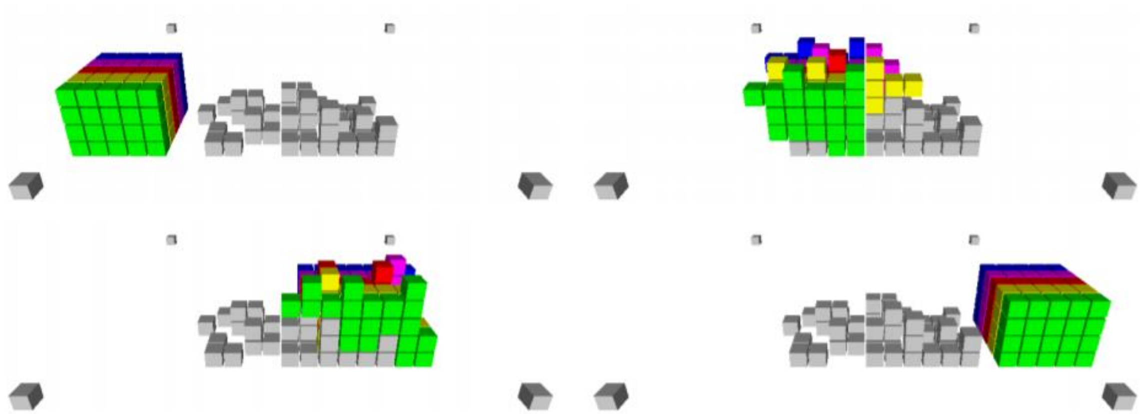

Figure II-14 Four snapshots of a simulation using the rule set in Figure II-13

In the same year, Kasper Stoy [161] proposed a seed-based self-assembly system in which gradients in the system were generated by seeds in order to produce growth in the system. Once gradient paths are generated, the automatically generated cellular automata (according to 3D CAD model description of the final configuration) are used to guide the growth process. Figure II-15 shows a Boing 747 is assembled from 9593 modules using Stoy's self-reconfiguration algorithms.

Figure II-15 Boing 747 in CAD (left); Boing 747 assembled from 9593 modules using seed-based self-reconfiguration algorithms (right)

In 2005, Wu Q. et al. [162] used CA for flow locomotion in the presence of obstacles by the M-Cubes lattice modules. In that work, the state of a cell is defined by the ID of modules located in front of its connectors and the next system state is computed by a transition rule generated by a two-layer artificial neural network with seven inputs (one for the cell state and six for states of neighboring cells) and one output (for the next state of the cell).

In 2012, Murata and Kurokawa [163] studied CA for generating the Flow operation based on an abstract model for a specific meta-module of M-TRAN called 'tile' model, in which a regular planar structure is considered as a plane filled with 2*2 tiles (cells). Their work considered these cells as objects of control (which are fixed in the environment) as opposed to conventional CA implementations that consider moving modules as control objects.

The above researches mainly focus on theory and lack practical application. The first step for applying the CA theory to MSRRs is to establish a MSRR that is suited to cellular automaton movement mechanism. For instance, for the block type ideal cellular automaton, the module of MSRR should have the connection ability between each other and can slide on their surfaces. Stoy and Kurokawa (see [164-166] for details) claimed that although several algorithms have been developed and validated based on their model, they have failed to be successfully deployed to the physical environment due to limitations in building reconfigurable robots that can satisfy necessary motion characteristics.

II.7. Conclusion

In this chapter, we have introduced modular robot systems along with their features, applications, and classification. In the physical composition aspect, actuation system and connection system are amongst the main parts of a modular robot. Three methods for miniaturization are detailed; these methods provide inspiration for the design of our MSRR. Contributions to the design of the distributed algorithms have been detailed. Cellular automata for controlling MSRRs have also been presented in this chapter. Although several algorithms have been developed and validated, people have generally failed to successfully deploy this algorithm to the physical environment due to limitations in manufacturing reconfigurable robots that can satisfy necessary motion characteristics.

References in Chapter II

[1] El Baz D., Boyer V., Bourgeois J., Dedu, E., and Boutoustous, K.. Distributed discrete state acquisition and concurrent pattern recognition in a MEMS-based smart surface[C]. Hardware and Software Implementation and Control of Distributed MEMS (DMEMS), 2010 First Workshop on. IEEE, 2010: 78-85.

[2] Delettre A, Laurent G J, Le Fort-Piat N. A new contactless conveyor system for handling clean and delicate products using induced air flows [C]. Intelligent Robots and Systems (IROS), 2010 IEEE/RSJ International Conference on. IEEE, 2010: 2351-2356.

[3] El Baz D., Boyer, V., Bourgeois, J., Dedu, E., and Boutoustous, K. Distributed part differentiation in a smart surface [J]. Mechatronics, 2012, 22(5) : 522-530.

[4] Boutoustous K., Laurent G. J., Dedu E., Matignon, L., Bourgeois, J., and Le Fort-Piat, N. Distributed control architecture for smart surfaces [C]. Intelligent Robots and Systems (IROS), 2010 IEEE/RSJ International Conference on. IEEE, 2010: 2018-2024.

[5] Piranda B., Laurent G. J., Bourgeois J., Clévy, C., Möbes, S., and Le Fort-Piat, N. A new concept of planar self-reconfigurable modular robot for conveying microparts [J]. Mechatronics, 2013, 23(7): 906-915.

[6] El Baz D, Piranda B, Bourgeois J. A distributed algorithm for a reconfigurable modular surface [C]. Parallel & Distributed Processing Symposium Workshops (IPDPSW), 2014 IEEE International. IEEE, 2014: 1591-1598.

[7] Laurent G. J., Delettre A., Zeggari R., Yahiaoui, R., Manceau, J. F., and Le Fort-Piat, N. Micropositioning and fast transport using a contactless micro-conveyor [J]. Micromachines, 2014, 5(1): 66-80.

[8] Murata S, Kurokawa H. Self-reconfigurable robots [J]. IEEE Robotics & Automation Magazine, 2007, 14(1): 71-78.

[9] Stoy K. Reconfigurable Robots [M]. KACPRZYK J, PEDRYCZ W. Springer Handbook of Computational Intelligence. Springer Berlin Heidelberg, 2015:1407-1421.

[10] Yim M, White P, Park M, et al. Modular self-reconfigurable robots [M]. Encyclopedia of complexity and systems science. Springer New York, 2009: 5618-5631.

[11] Fukuda T, Nakagawa S. Dynamically reconfigurable robotic system [C]. Robotics and Automation, 1988. Proceedings., 1988 IEEE International Conference on. IEEE, 1988: 1581-1586.

[12] Murata S, Kurokawa H, Yoshida E, et al. A 3-D self-reconfigurable structure [C]. Robotics and Automation, 1998. Proceedings. 1998 IEEE International Conference on. IEEE, 1998, 1: 432-439.

[13] Hossain S G M, Nelson C A, Dasgupta P. Hardware design and testing of modred: A modular self-reconfigurable robot system [M]. Advances in Reconfigurable Mechanisms and Robots I. Springer, London, 2012: 515-523.

[14] Gilpin K, Knaian A, Rus D. Robot pebbles: One centimeter modules for programmable matter through self-disassembly [C]. Robotics and Automation (ICRA), 2010 IEEE International Conference on. IEEE, 2010: 2485-2492.

[15] Miyashita S, Hadorn M, Hotz P E. Water floating self-assembling agents [C]. KES International Symposium on Agent and Multi-Agent Systems: Technologies and Applications. Springer, Berlin, Heidelberg, 2007: 665-674.

[16] Miyashita S, Lungarella M, Pfeifer R. Tribolon: Water-Based Self-Assembly Robots [J]. Artificial life models in hardware, 2009: 161-184.

[17] Ahmadzadeh H, Masehian E, Asadpour M. Modular robotic systems: characteristics and applications [J]. Journal of Intelligent & Robotic Systems, 2016, 81(3-4): 317-357.

[18] Kurokawa H, Tomita K, Yoshida E, et al. Motion simulation of a modular robotic system [C]. Industrial Electronics Society, 2000. IECON 2000. 26th Annual Conference of the IEEE. IEEE, 2000, 4: 2473-2478.

[19] Kirby B, Campbell J, Aksak B, et al. Catoms: Moving robots without moving parts [C]. Proceedings of the National Conference on Artificial Intelligence. Menlo Park, CA; Cambridge, MA; London; AAAI Press; MIT Press; 1999, 2005, 20(4): 1730.

[20] Bourgeois J, Piranda B, Naz A, et al. Programmable matter as a cyber-physical conjugation [C]. Systems, Man, and Cybernetics (SMC), 2016 IEEE International Conference on. IEEE, 2016: 002942-002947.

[21] http://www.keyirobot.com/home.html

[22] https://www.modrobotics.com/cubelets

[23] Schmitz D, Khosla P, Kanade T. The CMU reconfigurable modular manipulator system [J]. 1988.

[24] Fukuda T, Nakagawa S. Method of Autonomous Approach, Docking and Detaching Between Cells for Dynamically Recontigurable Robotic System CEBOT [J]. JSME international journal. Ser. 3, Vibration, control engineering, engineering for industry, 1990, 33(2): 263-268.

[25] Yim M. A reconfigurable modular robot with many modes of locomotion [C]. Proc. of the JSME Int. Conf. on Advanced Mechatronics. 1993: 283-288.

[26] Murata S, Kurokawa H, Kokaji S. Self-assembling machine [C]. Robotics and Automation, 1994. Proceedings., 1994 IEEE International Conference on. IEEE, 1994: 441-448.

[27] Chirikjian G S. Kinematics of a metamorphic robotic system [C]. Robotics and Automation, 1994. Proceedings., 1994 IEEE International Conference on. IEEE, 1994: 449-455.

[28] Hirose S, Shiratsu T, Fukushima F E. A proposal for cooperative robot" Gunryu" composed of autonomous segments [C]. Intelligent Robots and Systems' 94.'Advanced Robotic Systems and the Real World', IROS'94. Proceedings of the IEEE/RSJ/GI International Conference on. IEEE, 1994, 3: 1532-1538.

[29] Pamecha A, Chiang C J, Stein D, et al. Design and implementation of metamorphic robots [C]. Proceedings of the 1996 ASME Design Engineering Technical Conference and Computers in Engineering Conference. Irvine, California, USA: ASME, 1996, 10.

[30] Pamecha A, Ebert-Uphoff I, Chirikjian G S. Useful metrics for modular robot motion planning [J]. IEEE Transactions on Robotics and Automation, 1997, 13(4): 531-545.

[31] Hamlin G J, Sanderson A C. Tetrobot modular robotics: Prototype and experiments [C]. Intelligent Robots and Systems' 96, IROS 96, Proceedings of the 1996 IEEE/RSJ International Conference on. IEEE, 1996, 2: 390-395.

[32] Kurokawa H, Murata S, Yoshida E, et al. A 3-d self-reconfigurable structure and experiments [C]. Intelligent Robots and Systems, 1998. Proceedings., 1998 IEEE/RSJ International Conference on. IEEE, 1998, 2: 860-865.

[33] Kotay K, Rus D, Vona M, et al. The self-reconfiguring robotic molecule [C]. Robotics and Automation, 1998. Proceedings. 1998 IEEE International Conference on. IEEE, 1998, 1: 424-431.

[34] Hosokawa K, Fujii T, Kaetsu H, et al. Self-organizing collective robots with morphogenesis in a vertical plane [J]. JSME International Journal Series C Mechanical Systems, Machine Elements and Manufacturing, 1999, 42(1): 195-202.

[35] Endo G, Togawa K, Hirose S. Study on self-contained and terrain adaptive active cord mechanism [J]. Journal of the Robotics Society of Japan, 2000, 18(3): 419-425.

[36] Will P M, Castaño A, Shen W M. Robot modularity for self-reconfiguration [C]. Sensor Fusion and Decentralized Control in Robotic Systems II. International Society for Optics and Photonics, 1999, 3839: 236-246.

[37] Ünsal C, Kiliççöte H, Khosla P. I (CES)-cubes: a modular self-reconfigurable bipartite robotic system [J]. 1999.

[38] Tummala R L, Mukherjee R, Aslam D, et al. Reconfigurable adaptable micro-robot [C]. Systems, Man, and Cybernetics, 1999. IEEE SMC'99 Conference Proceedings. 1999 IEEE International Conference on. IEEE, 1999, 6: 687-691.

[39] Yoshida E, Kokaji S, Murata S, et al. Miniaturized self-reconfigurable system using shape memory alloy [C]. Intelligent Robots and Systems, 1999. IROS'99. Proceedings. 1999 IEEE/RSJ International Conference on. IEEE, 1999, 3: 1579-1585.

[40] Rus D, Vona M. A physical implementation of the self-reconfiguring crystalline robot [C]. Robotics and Automation, 2000. Proceedings. ICRA'00. IEEE International Conference on. IEEE, 2000, 2: 1726-1733.

[41] Yoshida E, Murata S, Kokaji S, et al. Micro self-reconfigurable robotic system using shape memory alloy [J]. Distributed autonomous robotic systems, 2000, 4: 145-154.

[42] Togawa K, Mori M, Hirose S. Study on three-dimensional active cord mechanism: development of ACM-R2 [C]. Intelligent Robots and Systems, 2000. (IROS 2000). Proceedings. 2000 IEEE/RSJ International Conference on. IEEE, 2000, 3: 2242-2247.

[43] Bojinov H, Casal A, Hogg T. Emergent structures in modular self-reconfigurable robots [C]. Robotics and Automation, 2000. Proceedings. ICRA'00. IEEE International Conference on. IEEE, 2000, 2: 1734-1741.

[44] Bojinov H, Casal A, Hogg T. Multiagent control of self-reconfigurable robots [C]. MultiAgent Systems, 2000. Proceedings. Fourth International Conference on. IEEE, 2000: 143-150.

[45] Yim M, Duff D G, Roufas K D. PolyBot: a modular reconfigurable robot [C]. Robotics and Automation, 2000. Proceedings. ICRA'00. IEEE International Conference on. IEEE, 2000, 1: 514-520.

[46] Mori M, Hirose S. Development of active cord mechanism ACM-R3 with agile 3D mobility [C]. Intelligent Robots and Systems, 2001. Proceedings. 2001 IEEE/RSJ International Conference on. IEEE, 2001, 3: 1552-1557.

[47] Yoshida E, Murata S, Kokaji S, et al. Get back in shape! [SMA self-reconfigurable microrobots] [J]. IEEE Robotics & Automation Magazine, 2002, 9(4) : 54-60.

[48] Yim M, Zhang Y, Roufas K, et al. Connecting and disconnecting for chain self-reconfiguration with PolyBot [J]. IEEE/ASME Transactions on mechatronics, 2002, 7(4): 442-451.

[49] Inou N, Kobayashi H, Koseki M. Development of pneumatic cellular robots forming a mechanical structure [C]. Control, Automation, Robotics and Vision, 2002. ICARCV 2002. 7th International Conference on. IEEE, 2002, 1: 63-68.

[50] Suh J W, Homans S B, Yim M. Telecubes: Mechanical design of a module for self-reconfigurable robotics [C]. Robotics and Automation, 2002. Proceedings. ICRA'02. IEEE International Conference on. IEEE, 2002, 4: 4095-4101.

[51] Brown H B, Weghe J M V, Bererton C A, et al. Millibot trains for enhanced mobility[J]. IEEE/ASME transactions on mechatronics, 2002, 7(4): 452-461.

[52] Kawakami A, Torii A, Motomura K, et al. SMC rover: planetary rover with transformable wheels [C]. SICE 2002. Proceedings of the 41st SICE Annual Conference. IEEE, 2002, 1: 157-162.

[53] Kurokawa H, Kamimura A, Yoshida E, et al. M-TRAN II: Metamorphosis from a four-legged walker to a caterpillar [C]. Intelligent Robots and Systems, 2003. (IROS 2003). Proceedings. 2003 IEEE/RSJ International Conference on. IEEE, 2003, 3: 2454-2459.

[54] Kamimura A, Kurokawa H, Yoshida E, et al. Distributed adaptive locomotion by a modular robotic system, M-TRAN II [C]. Intelligent Robots and Systems, 2004. (IROS 2004). Proceedings. 2004 IEEE/RSJ International Conference on. IEEE, 2004, 3: 2370-2377.

[55] Inou N, Minami K, Koseki M. Group Robots Forming a Mechanical Structure-Development of slide motion mechanism and estimation of energy consumption of the structural formation [C]. Computational Intelligence in Robotics and Automation, 2003. Proceedings. 2003 IEEE International Symposium on. IEEE, 2003, 2: 874-879.

[56] Tokashiki H, Amagai H, Endo S, et al. Development of a transformable mobile robot composed of homogeneous gear-type units [C]. Intelligent Robots and Systems, 2003. (IROS 2003). Proceedings. 2003 IEEE/RSJ International Conference on. IEEE, 2003, 2: 1602-1607.

[57] Mondada F, Pettinaro G C, Guignard A, et al. SWARM-BOT: A new distributed robotic concept [J]. Autonomous robots, 2004, 17(2-3): 193-221.

[58] Dorigo M. SWARM-BOT: An experiment in swarm robotics [C]. Swarm Intelligence Symposium, 2005. SIS 2005. Proceedings 2005 IEEE. IEEE, 2005: 192-200.

[59] Jorgensen M W, Ostergaard E H, Lund H H. Modular ATRON: Modules for a self-reconfigurable robot [C]. Intelligent Robots and Systems, 2004. (IROS 2004). Proceedings. 2004 IEEE/RSJ International Conference on. Ieee, 2004, 2: 2068-2073.

[60] Goldstein S C, Mowry T C. Claytronics: An instance of programmable matter [J]. 2004.

[61] Campbell J, Pillai P, Goldstein S C. The robot is the tether: active, adaptive power routing modular robots with unary inter-robot connectors [C]. Intelligent Robots and Systems, 2005. (IROS 2005). 2005 IEEE/RSJ International Conference on. IEEE, 2005: 4108-4115.

[62] Zhang L, Zhao J, Cai H G. A substructure based motion planning method for a modular self-reconfigurable robot [C]. Robot Motion and Control, 2004. RoMoCo'04. Proceedings of the Fourth International Workshop on. IEEE, 2004: 371-376.

[63] Bertolote T, Hentsch V. Design and prototyping of an underwater modular robot[J]. Unpublished Master Thesis, Laboratory of Intelligent Systems, EPFL, 2004.

[64] Griffith S T. Growing machines [D]. Massachusetts Institute of Technology, 2004.

[65] White P J, Kopanski K, Lipson H. Stochastic self-reconfigurable cellular robotics [C]. Robotics and Automation, 2004. Proceedings. ICRA'04. 2004 IEEE International Conference on. IEEE, 2004, 3: 2888-2893.

[66] Gonzalez-Gomez J, Aguayo E, Boemo E. Locomotion of a Modular Worm-like Robot using a FPGA-based embedded MicroBlaze Soft-processor [M]. Climbing and Walking Robots. Springer, Berlin, Heidelberg, 2005: 869-878.

[67] White P, Zykov V, Bongard J C, et al. Three Dimensional Stochastic Reconfiguration of Modular Robots [C]. Robotics: Science and Systems. 2005: 161-168.

[68] Østergaard E H, Christensen D J, Eggenberger P, et al. Hydra: From cellular biology to shape-changing artefacts [C]. International Conference on Artificial Neural Networks. Springer Berlin Heidelberg, 2005: 275-281.

[69] Zykov V, Mytilinaios E, Adams B, et al. Robotics: Self-reproducing machines [J]. Nature, 2005, 435(7039): 163-164.

[70] Brunete A, Hernando M, Gambao E. Modular multiconfigurable architecture for low diameter pipe inspection microrobots [C]. Robotics and Automation, 2005. ICRA 2005. Proceedings of the 2005 IEEE International Conference on. IEEE, 2005: 490-495.

[71] Bishop J, Burden S, Klavins E, et al. Programmable parts: A demonstration of the grammatical approach to self-

organization [C]. Intelligent Robots and Systems, 2005. (IROS 2005). 2005 IEEE/RSJ International Conference on. IEEE, 2005: 3684-3691.

[72] Salemi B, Moll M, Shen W M. SUPERBOT: A deployable, multi-functional, and modular self-reconfigurable robotic system [C]. Intelligent Robots and Systems, 2006 IEEE/RSJ International Conference on. IEEE, 2006: 3636-3641.

[73] Shen W M, Krivokon M, Chiu H, et al. Multimode locomotion via superbot robots [C]. Robotics and Automation, 2006. ICRA 2006. Proceedings 2006 IEEE International Conference on. IEEE, 2006: 2552-2557.

[74] Shimizu M, Ishiguro A, Kawakatsu T. A modular robot that exploits a spontaneous connectivity control mechanism [C]. Intelligent Robots and Systems, 2005. (IROS 2005). 2005 IEEE/RSJ International Conference on. IEEE, 2005: 1899-1904.

[75] Shimizu M, Mori T, Ishiguro A. A development of a modular robot that enables adaptive reconfiguration [C]. Intelligent Robots and Systems, 2006 IEEE/RSJ International Conference on. IEEE, 2006: 174-179.

[76] Terada Y, Murata S. Modular stucture assembly using blackboard path planning systems [C]. International Symposium on Automation and Robotics in Construction. 2006: 852-857.

[77] Stoy K. The deformatron robot: a biologically inspired homogeneous modular robot [C]. Robotics and Automation, 2006. ICRA 2006. Proceedings 2006 IEEE International Conference on. IEEE, 2006: 2527-2531.

[78] Donald B R, Levey C G, McGray C D, et al. An untethered, electrostatic, globally controllable MEMS micro-robot [J]. Journal of microelectromechanical systems, 2006, 15(1): 1-15.

[79] Ramchurn V, Richardson R C, Nutter P. ORTHO-BOT: a modular reconfigurable space robot concept [J]. Climbing and Walking Robots, 2006: 659-666.

[80] Moeckel R, Jaquier C, Drapel K, et al. Exploring adaptive locomotion with YaMoR, a novel autonomous modular robot with Bluetooth interface [J]. Industrial Robot: An International Journal, 2006, 33(4): 285-290.

[81] Liu J G, Wang Y C, Li B, et al. Center-configuration selection technique for the reconfigurable modular robot [J]. Science in China Series F: Information Sciences, 2007, 50(5): 697-710.

[82] Li B, Ma S, Liu J, et al. AMOEBA-I: a shape-shifting modular robot for urban search and rescue [J]. Advanced Robotics, 2009, 23(9): 1057-1083.

[83] Koseki M, Minami K, Inou N. Cellular robots forming a mechanical structure [M]. Distributed Autonomous Robotic Systems 6. Springer, Tokyo, 2007: 139-148.

[84] Yim M, Shirmohammadi B, Sastra J, et al. Towards robotic self-reassembly after explosion [C]. Intelligent Robots and Systems, 2007. IROS 2007. IEEE/RSJ International Conference on. IEEE, 2007: 2767-2772.

[85] Gilpin K, Kotay K, Rus D, et al. Miche: Modular shape formation by self-disassembly [J]. The International Journal of Robotics Research, 2008, 27(3-4): 345-372.

[86] Escalera J A, Ferre M, Aracil R, et al. ROBMAT: Teleoperation of a modular robot for collaborative manipulation [C]. International Conference on Knowledge-Based and Intelligent Information and Engineering Systems. Springer Berlin Heidelberg, 2007: 1204-1213.

[87] Yoon Y, Rus D. Shady3d: A robot that climbs 3d trusses [C]. Robotics and Automation, 2007 IEEE International Conference on. IEEE, 2007: 4071-4076.

[88] Carmichael B L, Gifford C M. Modeling and Simulation of the Seismic TETwalker Concept [J]. Center for Remote Sensing of Ice Sheets, University of Kansas, KS, Tech. Rep., CReSIS TR, 2007, 134.

[89] White P J, Yim M. Scalable modular self-reconfigurable robots using external actuation [C]. Intelligent Robots and Systems, 2007. IROS 2007. IEEE/RSJ International Conference on. IEEE, 2007: 2773-2778.

[90] Kurokawa H, Tomita K, Kamimura A, et al. Distributed self-reconfiguration of M-TRAN III modular robotic system [J]. The International Journal of Robotics Research, 2008, 27(3-4): 373-386.

[91] An B K. Em-cube: cube-shaped, self-reconfigurable robots sliding on structure surfaces [C]. Robotics and Automation, 2008. ICRA 2008. IEEE International Conference on. IEEE, 2008: 3149-3155.

[92] Li D, Fu H, Wang W. Ultrasonic based autonomous docking on plane for mobile robot [C]. Automation and Logistics, 2008. ICAL 2008. IEEE International Conference on. IEEE, 2008: 1396-1401.

[93] Zhang H, Gonzalez-Gomez J, Me Z, et al. Development of a low-cost flexible modular robot GZ-I [C]. Advanced Intelligent Mechatronics, 2008. AIM 2008. IEEE/ASME International Conference on. IEEE, 2008: 223-228.

[94] Yu C H, Haller K, Ingber D, et al. Morpho: A self-deformable modular robot inspired by cellular structure [C]. Intelligent Robots and Systems, 2008. IROS 2008. IEEE/RSJ International Conference on. IEEE, 2008: 3571-3578.

[95] Lyder A, Garcia R F M, Stoy K. Mechanical design of odin, an extendable heterogeneous deformable modular robot [C]. Intelligent Robots and Systems, 2008. IROS 2008. IEEE/RSJ International Conference on. Ieee, 2008: 883-888.

[96] Kernbach S, Meister E, Schlachter F, et al. Symbiotic robot organisms: REPLICATOR and SYMBRION projects [C]. Proceedings of the 8th workshop on performance metrics for intelligent systems. ACM, 2008: 62-69.

[97] Hjelle D, Lipson H. A robotically reconfigurable truss [C]. Reconfigurable Mechanisms and Robots, 2009. ReMAR 2009. ASME/IFToMM International Conference on. IEEE, 2009: 73-78.

[98] Mampel J, Gerlach K, Schilling C, et al. A modular robot climbing on pipe-like structures [C]. Autonomous Robots and Agents, 2009. ICARA 2009. 4th International Conference on. IEEE, 2009: 87-91.

[99] Sproewitz A, Billard A, Dillenbourg P, et al. Roombots-mechanical design of self-reconfiguring modular robots for adaptive furniture [C]. Robotics and Automation, 2009. ICRA'09. IEEE International Conference on. IEEE, 2009: 4259-4264.

[100] Galloway K C, Jois R, Yim M. Factory floor: A robotically reconfigurable construction platform [C]. Robotics and Automation (ICRA), 2010 IEEE International Conference on. IEEE, 2010: 2467-2472.

[101] Wang W, Yu W, Zhang H. JL-2: A mobile multi-robot system with docking and manipulating capabilities [J]. International Journal of Advanced Robotic Systems, 2010, 7(1): 9.

[102] Ryland G G, Cheng H H. Design of iMobot, an intelligent reconfigurable mobile robot with novel locomotion [C]. Robotics and Automation (ICRA), 2010 IEEE International Conference on. IEEE, 2010: 60-65.

[103] Belisle R, Yu C, Nagpal R. Mechanical design and locomotion of modular-expanding robots [J]. Proceedings of the IEEE, 2010: 17-23.

[104] Rasakatla S, Krishna K M, Indurkhya B. Mod-Leg a modular legged robotic system [C]. ACM SIGGRAPH 2010 Posters. ACM, 2010: 12.

[105] Merali R, Long D. Actuated responsive truss [J]. Modular Robots: The State of the Art, 2010, 36.

[106] Wei H, Chen Y, Tan J, et al. Sambot: A self-assembly modular robot system [J]. IEEE/ASME Transactions on Mechatronics, 2011, 16(4): 745-757.

[107] Tolley M T, Lipson H. Fluidic manipulation for scalable stochastic 3d assembly of modular robots [C]. Robotics and

Automation (ICRA), 2010 IEEE International Conference on. IEEE, 2010: 2473-2478.

[108] Neubert J, Cantwell A P, Constantin S, et al. A robotic module for stochastic fluidic assembly of 3D self-reconfiguring structures [C]. Robotics and Automation (ICRA), 2010 IEEE International Conference on. IEEE, 2010: 2479-2484.

[109] Kutzer M D M, Moses M S, Brown C Y, et al. Design of a new independently-mobile reconfigurable modular robot [C]. Robotics and Automation (ICRA), 2010 IEEE International Conference on. IEEE, 2010: 2758-2764.

[110] Lyder A, Garcia R F M, Stoy K. Genderless connection mechanism for modular robots introducing torque transmission between modules [C]. Proceedings of the ICRA Workshop on Modular Robots, State of the Art. 2010: 77-81.

[111] Zhao J, Cui X, Zhu Y, et al. A new self-reconfigurable modular robotic system UBot: Multi-mode locomotion and self-reconfiguration [C]. Robotics and Automation (ICRA), 2011 IEEE International Conference on. IEEE, 2011: 1020-1025.

[112] Garcia R F M, Hiller J D, Stoy K, et al. A vacuum-based bonding mechanism for modular robotics [J]. IEEE Transactions on Robotics, 2011, 27(5): 876-890.

[113] Delrobaei M, McIsaac K A. Design and steering control of a center-articulated mobile robot module [J]. Journal of Robotics, 2011, 2011.

[114] Kirby B T, Ashley-Rollman M, Goldstein S C. Blinky blocks: A physical ensemble programming platform [C]. CHI'11 Extended Abstracts on Human Factors in Computing Systems. ACM, 2011: 1111-1116.

[115] Yoneda K, Suzuki I, Yamamoto M, et al. Acquisition of adaptive behavior for virtual modular robot using evolutionary computation [C]. European Conference on Artificial Life. Springer, Berlin, Heidelberg, 2009: 181-188.

[116] Meng Y, Zhang Y, Sampath A, et al. Cross-ball: a new morphogenetic self-reconfigurable modular robot [C]. Robotics and Automation (ICRA), 2011 IEEE International Conference on. IEEE, 2011: 267-272.

[117] Faiña A, Orjales F, Bellas F, et al. First steps towards a heterogeneous modular robotic architecture for intelligent industrial operation [C]. Workshop Reconfigurable Modular Robotics: Challenges of Mechatronic and Bio-Chemo-Hybrid Systems, IROS. 2011: 6.

[118] Zhu Y, Wang X, Cui X, et al. Research on Locomotive Evolution Based on Worm-Shaped Configuration of Self-reconfigurable Robot HitMSR II [J]. Electrical Power Systems and Computers, 2011: 245-252.

[119] Wu Q, Luo Y, Chi X, et al. Motion error analysis of modular self-reconfigurable robot M-Cubes based screw theory [C]. Electronic and Mechanical Engineering and Information Technology (EMEIT), 2011 International Conference on. IEEE, 2011, 2: 859-866.

[120] Guan E, Fu Z, Yan W, et al. Self-reconfiguration path planning design for M-lattice robot based on genetic algorithm [J]. Intelligent Robotics and Applications, 2011: 505-514.

[121] Sadjadi H, Mohareri O, Al-Jarrah M A, et al. Design and implementation of HexBot: A modular self-reconfigurable robotic system [J]. Journal of the Franklin Institute, 2012, 349(7): 2281-2293.

[122] Baca J, Ferre M, Aracil R. A heterogeneous modular robotic design for fast response to a diversity of tasks [J]. Robotics and Autonomous Systems, 2012, 60(4): 522-531.

[123] Hong W, Wang S, Shui D. Reconfigurable robot system based on electromagnetic design [C]. Fluid Power and Mechatronics (FPM), 2011 International Conference on. IEEE, 2011: 570-575.

[124] Wolfe K C, Moses M S, Kutzer M D M, et al. M 3 Express: A low-cost independently-mobile reconfigurable modular robot [C]. Robotics and Automation (ICRA), 2012 IEEE International Conference on. IEEE, 2012: 2704-2710.

[125] Moubarak P, Ben-Tzvi P. Modular and reconfigurable mobile robotics [J]. Robotics and autonomous systems, 2012, 60(12): 1648-1663.

[126] Davey J, Kwok N, Yim M. Emulating self-reconfigurable robots-design of the SMORES system [C]. Intelligent Robots and Systems (IROS), 2012 IEEE/RSJ International Conference on. IEEE, 2012: 4464-4469.

[127] Qiao G, Song G, Zhang J, et al. Design of transmote: a modular self-reconfigurable robot with versatile transformation capabilities [C]. Robotics and Biomimetics (ROBIO), 2012 IEEE International Conference on. IEEE, 2012: 1331-1336.

[128] Romanishin J W, Gilpin K, Rus D. M-blocks: Momentum-driven, magnetic modular robots [C]. Intelligent Robots and Systems (IROS), 2013 IEEE/RSJ International Conference on. IEEE, 2013: 4288-4295.

[129] Wu C, Wang X, Zhuang G, et al. Motion of an underwater self-reconfigurable robot with tree-like configurations [J]. Journal of Shanghai Jiaotong University (Science), 2013, 18(5): 598-605.

[130] Pacheco M, Moghadam M, Magnússon A, et al. Fable: Design of a modular robotic playware platform [C]. Robotics and Automation (ICRA), 2013 IEEE International Conference on. IEEE, 2013: 544-550.

[131] Salem B. PetRo: development of a modular pet robot [C]. Robot and Human Interactive Communication, 2014 RO-MAN: The 23rd IEEE International Symposium on. IEEE, 2014: 483-488.

[132] Neubert J, Rost A, Lipson H. Self-soldering connectors for modular robots [J]. IEEE Transactions on Robotics, 2014, 30(6): 1344-1357.

[133] Romanishin J W, Gilpin K, Claici S, et al. 3D M-Blocks: Self-reconfiguring robots capable of locomotion via pivoting in three dimensions [C]. Robotics and Automation (ICRA), 2015 IEEE International Conference on. IEEE, 2015: 1925-1932.

[134] Zhang Y, Song G, Liu S, et al. A modular self-reconfigurable robot with enhanced locomotion performances: design, modeling, simulations, and experiments [J]. Journal of Intelligent & Robotic Systems, 2016, 81(3-4): 377-393.

[135] Parrott C, Dodd T J, Gross R. HyMod: A 3-DOF Hybrid Mobile and Self-Reconfigurable Modular Robot and its Extensions [C]. Distributed Autonomous Robotic Systems, The 13th International Symposium. Springer, 2016.

[136] Doyle M J, Xu X, Gu Y, et al. Modular Hydraulic Propulsion: A robot that moves by routing fluid through itself [C]. Robotics and Automation (ICRA), 2016 IEEE International Conference on. IEEE, 2016: 5189-5196.

[137] Zhao L, Wang H, Lin T, et al. Conceptual Design and Kinematic Analysis of the Diamobot: A Homogeneous Modular Robot [M]. Advances in Reconfigurable Mechanisms and Robots II. Springer, Cham, 2016: 693-703.

[138] Li Y, Zhu S, Wang Z, et al. The Kinematics Analysis of a Novel Self-Reconfigurable Modular Robot Based on Screw Theory [J]. DEStech Transactions on Engineering and Technology Research, 2016 (mime).

[139] Guimarães P P S, Nunes M M, Galembeck T F, et al. A Bio-inspired Apodal and Modular Robot [C]. Robotics Symposium and IV Brazilian Robotics Symposium (LARS/SBR), 2016 XIII Latin American. IEEE, 2016: 61-66.

[140] Moreno R, Liu C, Faina A, et al. The EMeRGE modular robot, an open platform for quick testing of evolved robot morphologies [C]. Proceedings of the Genetic and Evolutionary Computation Conference Companion. ACM, 2017: 71-72.

[141] Reddy C H S S, Patlolla S, Agrawal A, et al. HexaMob—A Hybrid Modular Robotic Design for Implementing Biomimetic Structures [J]. Robotics, 2017, 6(4): 27.

[142] Gilpin K, Rus D. Modular robot systems [J]. IEEE robotics & automation magazine, 2010, 17(3): 38-55.

[143] Terada Y, Murata S. Automatic Assembly System for Large Modular Structure [J]. Journal of the Robotics Society of

Japan, 2005, 23(5): 612-618.

[144] Støy K. Controlling self-reconfiguration using cellular automata and gradients [C]. Proceedings of the 8th international conference on intelligent autonomous systems (IAS-8). 2004: 693-702.

[145] Schultz U P. Distributed control diffusion: Towards a flexible programming paradigm for modular robots [C]. Proceedings of the 1st international conference on Robot communication and coordination. IEEE Press, 2007: 15.

[146] Shen W M, Salemi B, Will P. Hormone-inspired adaptive communication and distributed control for CONRO self-reconfigurable robots [J]. IEEE transactions on Robotics and Automation, 2002, 18(5): 700-712.

[147] Miao Y, Yan G, Lin Z. A distributed reconfiguration strategy for target enveloping with hexagonal metamorphic modules [C]. Robotics and Automation (ICRA), 2011 IEEE International Conference on. IEEE, 2011: 4804-4809.

[148] Mabed H, Bourgeois J. Towards programmable material: Flexible distributed algorithm for modular robots shape-shifting [C]. Advanced Intelligent Mechatronics (AIM), 2014 IEEE/ASME International Conference on. IEEE, 2014: 408-414.

[149] Naz A, Piranda B, Bourgeois J, et al. A distributed self-reconfiguration algorithm for cylindrical lattice-based modular robots [C]. Network Computing and Applications (NCA), 2016 IEEE 15th International Symposium on. IEEE, 2016: 254-263.

[150] Fitch R, Butler Z, Rus D. Reconfiguration planning among obstacles for heterogeneous self-reconfiguring robots [C]. Robotics and Automation, 2005. ICRA 2005. Proceedings of the 2005 IEEE International Conference on. IEEE, 2005: 117-124.

[151] Marbach D, Ijspeert A J. Co-evolution of configuration and control for homogenous modular robots [C]. Proceedings of the eighth conference on intelligent autonomous systems (IAS8). IOS Press, 2004 (BIOROB-CONF-2004-004): 712-719.

[152] Michel O. Cyberbotics Ltd. Webots™ : professional mobile robot simulation [J]. International Journal of Advanced Robotic Systems, 2004, 1(1): 5.

[153] Gonzalez-Gomez J, Gonzalez-Quijano J, Zhang H, et al. Toward the sense of touch in snake modular robots for search and rescue operations [C]. Proc. ICRA 2010 Workshop “Modular Robots: State of the Art. 2010: 63-68.

[154] Miyashita S, Hadorn M, Hotz P E. Water floating self-assembling agents [C]. KES International Symposium on Agent and Multi-Agent Systems: Technologies and Applications. Springer, Berlin, Heidelberg, 2007: 665-674.

[155] Mintchev S, Stefanini C, Girin A, et al. An underwater reconfigurable robot with bioinspired electric sense [C]. Robotics and Automation (ICRA), 2012 IEEE International Conference on. IEEE, 2012: 1149-1154.

[156] Bishop J, Burden S, Klavins E, et al. Programmable parts: A demonstration of the grammatical approach to self-organization [C]. Intelligent Robots and Systems, 2005. (IROS 2005). 2005 IEEE/RSJ International Conference on. IEEE, 2005: 3684-3691.

[157] https://en.wikipedia.org/wiki/Cellular_automaton

[158] Butler Z, Kotay K, Rus D, et al. Cellular automata for decentralized control of self-reconfigurable robots [C]. Proc. of the ICRA 2001 workshop on modular robots. 2001: 21-26.

[159] Butler Z, Kotay K, Rus D, et al. Generic decentralized control for lattice-based self-reconfigurable robots [J]. The International Journal of Robotics Research, 2004, 23(9): 919-937.

[160] Xu W, Wang S G, Wang A L, et al. Towards an efficient self-organizing reconfiguration method for self-reconfigurable

robots [J]. Journal of Intelligent & Robotic Systems, 2003, 37(4): 415-425.

[161] Støy K. Emergent control of self-reconfigurable robots [J]. The Maersk Mc-Kinney Moller Institute for Production Technology, University of Southern Denmark, 2003: 114-124.

[162] Wu Q, Wang Y, Cao G, et al. Locomotion control of distributed self-reconfigurable robot based on cellular automata [J]. Advances in Intelligent Computing, 2005: 179-188.

[163] Murata S, Kurokawa H. Robotic metamorphosis [J]. Self-Organizing Robots, 2012: 131-171.

[164] Stoy K, Kurokawa H. Current topics in classic self-reconfigurable robot research [C]. Proceedings of the IROS Workshop on Reconfigurable Modular Robotics: Challenges of Mechatronic and Bio-Chemo-Hybrid Systems. 2011.

[165] Butler Z, Rizzi A. Distributed and cellular robots [M]. Springer Handbook of Robotics. Springer Berlin Heidelberg, 2008: 911-920.

[166] Fitch R, Butler Z, Rus D. Reconfiguration planning for heterogeneous self-reconfiguring robots [C]. Intelligent Robots and Systems, 2003. (IROS 2003). Proceedings. 2003 IEEE/RSJ International Conference on. IEEE, 2003, 3: 2460-2467.

Chapter III. New Concept of Linear Motor

III.1. Introduction

As we have said in Chapter II, most actuators only have one function for connecting or moving; this chapter explores a new kind of fastenable linear motor for the smart distributed robot system. The organization of this chapter is as follows: Section III.2 introduces the Electro-permanent (EP) magnet and gives a brief introduction of magnetic materials. The mathematical calculation of the magnetic field of the solenoid will be given in section III.3. Section III.4 mainly talks about the new kind of linear motor which is based on a simplified electro-permanent magnet. Some experiments are discussed in section III.5. The conclusion is drawn in section III.6.

III.2. Electro-Permanent (EP) magnet

III.2.1. Magnetic Materials

There are two categories of ferromagnetic materials: hard and soft magnetic materials. A material in a magnetic sense is termed soft if the magnetization process is nearly reversible and hard if there is considerable hysteresis in the magnetization process. Soft magnetic materials are easily magnetized and demagnetized. They have the following characteristics: high *magnetic saturation* (saturation is the state reached when an increase in applied external magnetic field H cannot increase the magnetization of the material further) [1]; low *coercivity* (also called the coercive force. For ferromagnetic material, the coercivity is the intensity of the applied magnetic field required to reduce the magnetization of that material to zero after the magnetization of the sample has been driven to saturation) [2]; high *permeability* (the degree of magnetization of a material in response to a magnetic field) [3]; low *magnetocrystalline anisotropy* (a ferromagnetic material is said to have magnetocrystalline anisotropy if it takes more energy to magnetize it in certain directions than in others) [4]; low *core loss* (in Alternating Current (AC) devices the magnetic core cause energy losses due to hysteresis and eddy currents (Foucault currents), this energy losses called core loss) [5] and high *resistivity* (resistivity is a fundamental property that quantifies how strongly a given material opposes the flow of electric current) [6]. Hard magnetic materials are difficult to magnetize and demagnetize. Compare with soft magnetic;

they have high saturation magnetization, coercivity, magnetocrystalline anisotropy and maximum energy product.

Now we concentrate on the Alnico5 [7] magnet and the NdFeB [8] magnet; their characteristics are the foundation of our work.

Alnico5

The primary composition of Alnico5 magnet is Aluminum (Al), Nickel (Ni) and Cobalt (Co), hence the name. Although it has a high remanent induction, it has relatively low magnetic values because of its easy of demagnetization. However, it is resistant to heat and has good mechanical features.

NdFeB

Known as the third generation of rare earth magnets, Neodymium (NdFeB) magnets are the most powerful and advanced commercialized permanent magnet today. Since they are made from Neodymium, one of the most plentiful rare earth elements and inexpensive iron, NdFeB magnets offer the best value in cost and performance. Comparing with other magnets, NdFeB magnets have higher remanence, higher coercivity, and lower Tc (Curie temperature, the temperature at which the material loses its magnetism) than others.

NdFeB magnet has a very high coercivity, the Alnico5 magnet has a relatively lower coercivity (see Table III-1). However, both of them have about the same residual magnetism (see Table III-1, the residual magnetism is the magnetization left behind in a ferromagnetic material after an external magnetic field is removed, measured in Gauss or Tesla).

Table III-1 Residual magnetism and coercivity of NdFeB and Alnico5

Material	Residual magnetism	Coercivity
NdFeB	1.28 T	1120 kA/m
Alnico5	1.26 T	48 kA/m

III.2.2. Electro-Permanent (EP) Magnet

Electro-permanent (EP) magnet [9] is a solid-state device which allows an external magnetic field to be modulated by an electrical pulse. No electrical power is required to maintain the field. EP magnet contains two magnetic materials, one magnetically hard and one semi-hard, capped at both ends with a magnetically soft material (e.g. Iron) and wrapped with a coil. Because of the characteristic of coercivity and residual induction, NdFeB (hard) and Alnico5 (semi-hard) are the two most common materials used to make the EP magnet. The coil can wrap the NdFeB magnet and Alnico5 magnet together or only wrap the Alnico5 magnet.

Figure III-1 details the principle of EP magnet. When current passes through the coil, the direction of the axial magnetic field of Alnico5 magnet changes with the direction of the current. When the magnetization direction of Alnico5 magnet is the same as NdFeB magnet, the external of magnetic flux reaches the maximum value. This correspondent to the ON configuration. When the magnetization direction of Alnico5 is opposite to that of NdFeB magnet, some or all the flux circulates inside the device; the external magnetic flux reaches the minimum value. This correspondent to the OFF configuration.

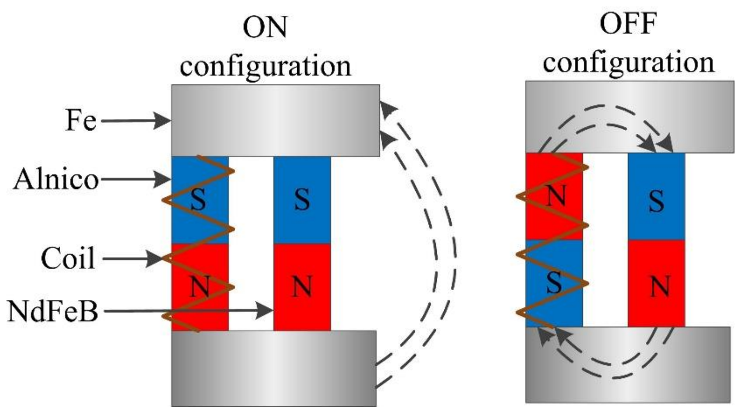

Figure III-1 Principle of Electro-permanent (EP) magnet

It is obvious that the EP magnet consumes power only when it changes the status to ON or OFF, otherwise, it does not need a power supply. Due to the energy saving characteristics, EP magnet can be used in some small-scale projects, such as Ara (Google module phone) [10] and Pebbles robot system (modular self-reconfiguring robotic system from MIT) [11]. Figure III-2 shows a module of Ara; the module can be locked and unlocked from the phone, each module fastens tight to the motherboard via EP magnet actuator. When users want to change a module, such as a camera module or a battery module, the circuit generates some pulses to release these modules. The EP magnet is shown in the red circle in Figure III-2.

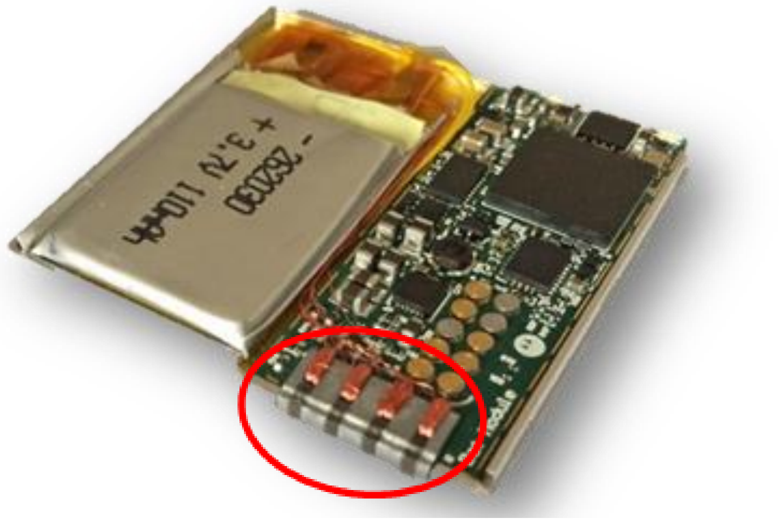

Figure III-2 EP magnets in a Ara (Google modular phone) module

Figure III-3 presents the EP magnet which is used in Pebbles; it can hold up a 250g test mass. The magnetic rods are Grade N40SH NdFeB, and Cast Alnico5, both of them are 1.587mm in diameter and 3.175mm in length, and magnetized through their length. The pole pieces are Grade ASTM-A848 soft magnetic iron. An 80-turns coil is wrapped around the magnetic rods, the material of the coil is #40 AWG magnet wire with 390˚C solder-strippable insulation [9].

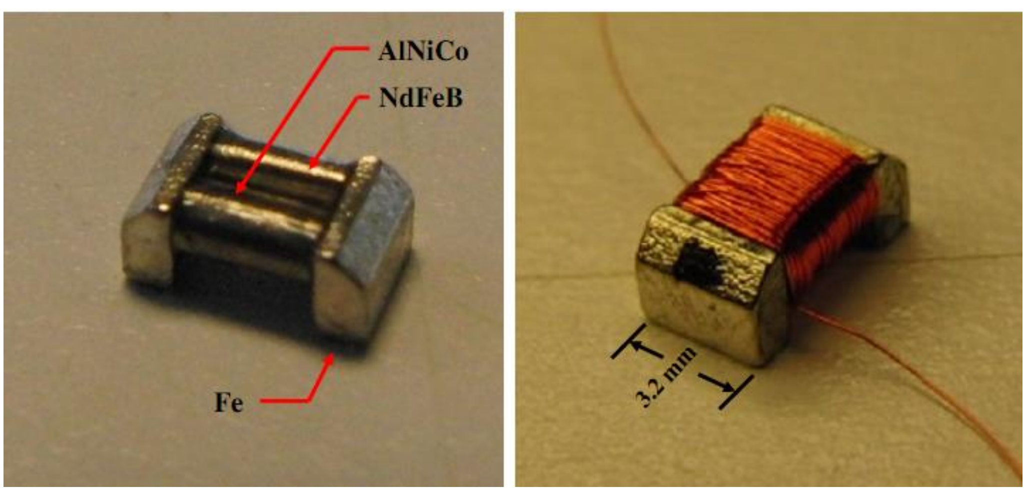

Figure III-3 EP magnets on Robot Pebbles (MIT)

III.3. Analysis of Magnetic Field in the Solenoid

Section 2 has introduced the basic principle and structure of EP magnet. The most important part that we can learn is to change the direction of the magnetic field of Alnico5 with a solenoid. The magnetic field in the solenoid needs to be large enough, and greater than the coercivity of Alnico5. This section mainly analyzes the magnetic field within the solenoid [12, 13].

For tightly (without interval) wound infinite solenoid, the internal magnetic field is simple, it is a uniform magnetic field, and its direction is along the solenoid axis. It can be simply represented by the following formula:

$$B_{in} = \mu_0 nI \ , \qquad (3.1)$$

where μ_0 is the vacuum permeability ($\mu_0 = 4\pi\times10^{-7}$ H/m, μ_0 is an ideal, (baseline) physical constant, which is the value of magnetic permeability in a classical vacuum), n is the number of turns along the axial in unit length, I is the current intensity in the solenoid in Ampere.

But in reality, there is no such a kind of infinite solenoid. So, we need to analyze the magnetic field of the non-tight-wound solenoid.

Figure III-4 presents a part of the solenoid. Assuming that the current is I, the number of turns of the solenoid is N, the radius is R, the pitch is, and the number of turns along the axial in unit length is $n=\frac{1}{d}$ (regardless of the diameter). Define the right-hand coordinate system as shown in Figure III-4, the origin (point O) of the coordinate is the point to be measured; the center axis of the solenoid is the x-axis; assume that a plane passes through the origin, perpendicular to the central axis, and intersects the solenoid at point Q; y-axis passes through point O and Q; the position of the z-axis can be obtained by the right-hand rule.

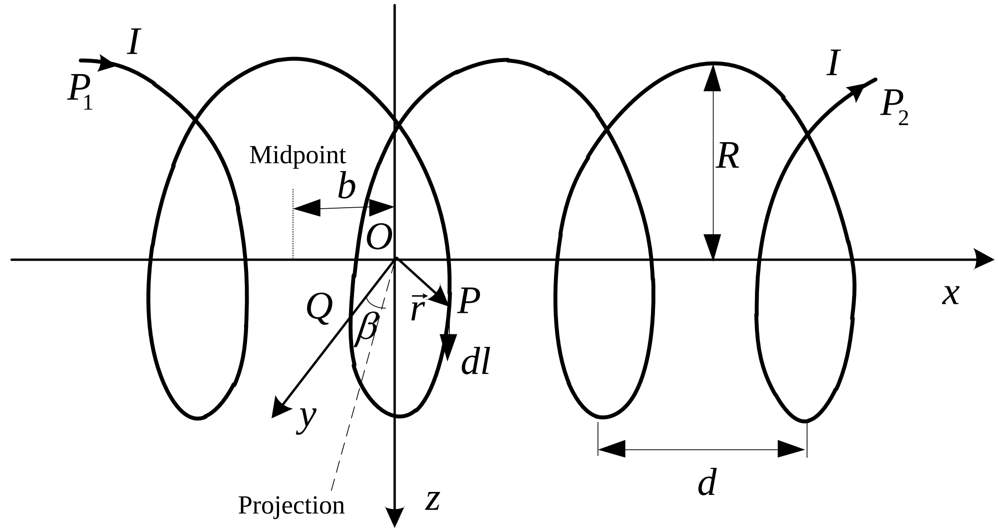

Figure III-4 Structure of solenoid

We take a line element $d\vec{l}$ at point P on the solenoid. The displacement vector from point O to point P is $\vec{r}$; the projection of the $\vec{r}$ in the yz plane is shown by the dotted line in Figure III-4. The angle between the projection and the y-axis is β . Thus, the coordinates of point P are:

$$\begin{cases} x = \dfrac{\beta}{2\pi} d = \dfrac{\beta}{2\pi n} \\ y = R\cos\beta \\ z = R\sin\beta \end{cases} \tag{3.2}$$

The individual components of $d\vec{l}$ are:

$$\begin{cases} dl_x = dx = \dfrac{d\beta}{2\pi n} \\ dl_y = dy = -R\sin\beta \cdot d\beta \\ dl_z = dz = R\cos\beta \cdot d\beta \end{cases} \tag{3.3}$$

From Biot-Savart Law, the magnetic induction intensity at the point O is:

$$\vec{B}=\frac{\mu_o I}{4\pi}=\int_{P_1}^{P_2}\frac{d\vec{l}\times\vec{r}'}{r^3} \tag{3.4}$$

where $\vec{r}'$ is the displacement vector from point P to point O, $\vec{r}'=-\vec{r}$, P_1 and P_2 are the left and right endpoints of the solenoid, respectively. In order to get the components of the magnetic induction intensity at the point O. We firstly calculate:

$$\begin{cases}\left(d\vec{l}\times\vec{r}'\right)_x = r_z' dl_y - r_y' dl_z = R^2\cdot d\beta \\ \left(d\vec{l}\times\vec{r}'\right)_y = r_x' dl_z - r_z' dl_x = \dfrac{R}{2\pi n}\left(\sin\beta-\beta\cos\beta\right)\cdot d\beta \\ \left(d\vec{l}\times\vec{r}'\right)_z = r_y' dl_x - r_x' dl_y = -\dfrac{R}{2\pi n}\left(\cos\beta+\beta\sin\beta\right)\cdot d\beta \end{cases} \tag{3.5}$$

$$r=\sqrt{x^2+y^2+z^2}=\frac{1}{2\pi n}\sqrt{\left(2\pi nR\right)^2+\beta^2} \tag{3.6}$$

Then, combining (3.4), (3.5), and (3.6), we can get:

$$\begin{cases}B_x=\dfrac{\mu_0 I}{4\pi}\left(2\pi n\right)^3 R^2\displaystyle\int_{\beta_1}^{\beta_2}\frac{d\beta}{\left[\left(2\pi nR\right)^2+\beta^2\right]^{\frac{3}{2}}} \\ B_y=\mu_0 I\pi n^2 R\displaystyle\int_{\beta_1}^{\beta_2}\frac{\sin\beta-\beta\cos\beta}{\left[\left(2\pi nR\right)^2+\beta^2\right]^{\frac{3}{2}}}d\beta \\ B_z=-\mu_0 I\pi n^2 R\displaystyle\int_{\beta_1}^{\beta_2}\frac{\cos\beta+\beta\sin\beta}{\left[\left(2\pi nR\right)^2+\beta^2\right]^{\frac{3}{2}}}d\beta \end{cases} \tag{3.7}$$

Assume distance between the midpoint of one circle of the solenoid and point O is b. The azimuth angles of point P_1 and P_2 are:

$$\begin{cases}\beta_1=-\dfrac{N}{2}2\pi-\dfrac{b}{d}2\pi=-N\pi-2\pi bn \\ \beta_2=\dfrac{N}{2}2\pi-\dfrac{b}{d}2\pi=N\pi-2\pi bn\end{cases} \tag{3.8}$$

Put formula (3.8) into formula (3.7); we can get the distribution of magnetic field in the solenoid:

$$\begin{cases} B_x = \frac{1}{2}\mu_0 nI\left(\frac{\frac{N}{2n}-b}{\sqrt{R^2+\left(\frac{N}{2n}-b\right)^2}}+\frac{\frac{N}{2n}+b}{\sqrt{R^2+\left(\frac{N}{2n}+b\right)^2}}\right) \\ B_y = \mu_0 I\pi n^2 R\int_{\beta_1}^{\beta_2}\frac{\sin\beta-\beta\cos\beta}{\left[(2\pi nR)^2+\beta^2\right]^{\frac{3}{2}}}d\beta \\ B_z = -\mu_0 I\pi n^2 R\int_{\beta_1}^{\beta_2}\frac{\cos\beta+\beta\sin\beta}{\left[(2\pi nR)^2+\beta^2\right]^{\frac{3}{2}}}d\beta \end{cases} \quad (3.9)$$

When the solenoid is infinite, that is $N \to \infty$, the magnetic field in the infinite solenoid is:

$$\begin{cases} \beta_x = \mu_0 nI \\ \beta_y = 0 \\ \beta_z = -\mu_0 nI\left[2\pi nRk_0(2\pi nR)+k_1(2\pi nR)\right] \end{cases} \quad (3.10)$$

where $k_0(t)$ and $k_1(t)$ are the zero derivative and the first derivative of the second kind of deformed Bessel function.

When the solenoid is tightly wound, that is $n \to \infty$, due to $K_0(2\pi nR) \to 0$ and $K_1(2\pi nR) \to 0$, we can get the magnetic field as follows:

$$\begin{cases} B_x = \mu_0 nI \\ B_y = 0 \\ B_z = 0 \end{cases} \quad (3.11)$$

The above calculation only considers a solenoid with limited length. In fact, the Alnico5 inside the solenoid also has an effect on the magnetic field. Moreover, the applied current will be a non-linear pulse current, which will also make the calculation process more complex. Therefore, this calculation is only for reference; Chapter IV will detail numerical simulations via software like COMSOL

Multiphysics.

III.4. Linear Motor Based on Simplified Electro-Permanent (SEP) Magnets

For EP magnets, due to their small power consumption, they are primarily used to provide a force to fasten objects. This section will introduce a new concept of the linear motor (actuator) that contains both motion and connection functions. The linear motor is composed of simplified electro-permanent (SEP) magnets.

III.4.1. Principle of Simplified Electro-Permanent (SEP) magnet

The main principle of SEP magnet is shown in Figure III-5. The Alnico5 is wrapped by the copper coil; its magnetic field direction can be changed when a positive pulse or a negative pulse passes the coil. Note that magnetic field also changes with polarity, for a facility of the presentation we emphasize on polarity change. It is not difficult to see that this principle is similar to the EP magnet, the difference is that the Alnico5 magnet is not placed in parallel with NdFeB magnet, and there is no soft magnet part. Since the structure of this new type actuator is only a part of the EP magnet, thus, we call it SEP magnet, where S means simplified.

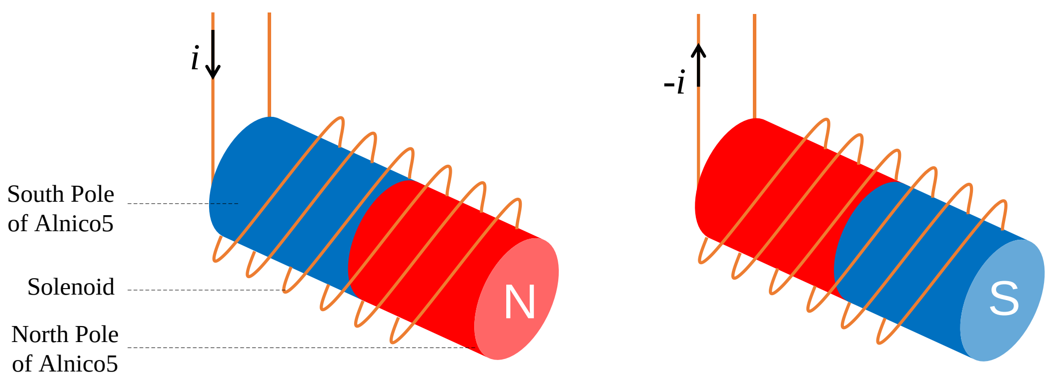

Figure III-5 The principle of SEP

III.4.2. Motion and connection mechanisms

Figure III-6 displays an example of motion mechanism of SEP magnets. According to the basic principle of the magnets, the same polarities repel themselves, and different polarities attract themselves. As shown in this figure, there are two SEP magnets; one produces repulsive force, another one produces attractive force at the same time; thus, the permanent magnet NdFeB can be moved by the magnetic field. Figure III-6 is just a schematic diagram, in a real situation (see chapter V), the two kinds of magnets are embedded in a cube. Thus, the permanent magnet will not roll. Since SEP magnets are controllable, the direction of movement is also controllable. In fact, the two SEP magnets and the permanent magnet combine into a new concept of the linear motor. In this linear motor, the SEP magnets are the stator; the NdFeB magnet is the rotor. We note that the NdFeB magnet also can be the stator; in that case, the SEP magnet becomes the rotor relatively.

Besides motion, there is a fastening force when Alnico5 magnet and NdFeB magnet have different polarities. Thus, this linear motor naturally contains a function of connection.

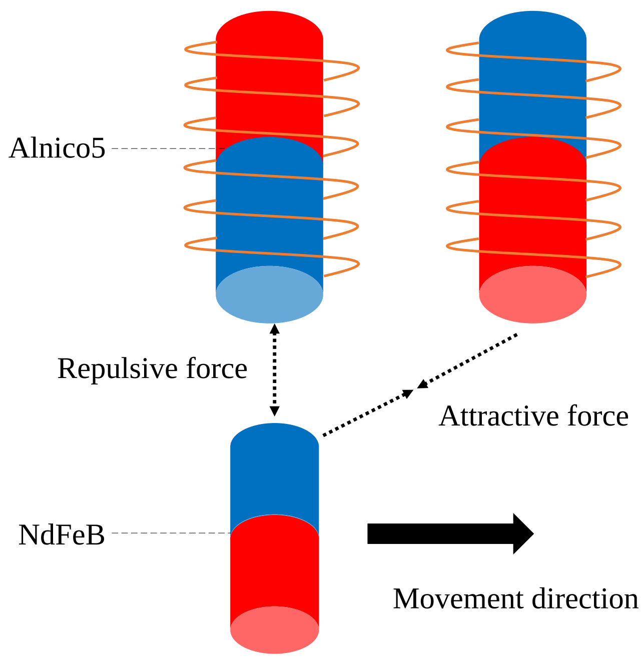

Figure III-6 Motion mechanism of new linear motor

Figure III-7 displays a series of motion and the status of magnetic field of SEP magnets. The NdFeB (rotor) moves from right to the left. The initial polarity of NdFeB and SEP magnets are the same. At each step, only one SEP magnet need to change its polarity. There is only one permanent magnet in Figure III-7, but the rotor can be composed of a plurality of permanent magnets.

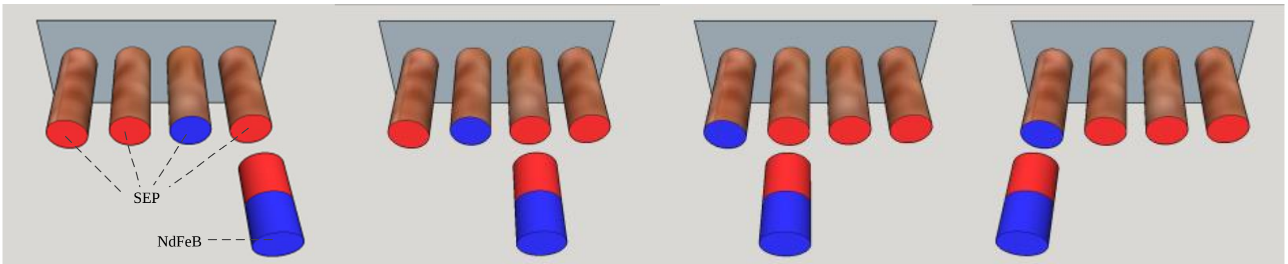

Figure III-7 Status of magnetic filed of SEP magnets in motion

Except for providing both driving force and fastening force, the new linear motor can move in any direction, with the proper arrangement of permanent magnets or SEP magnets in the plane. Figure III-8 and Figure III-9 give two examples of using this actuator to achieve circular motion. As shown in Figure III-8, we assume that the initial magnetic field directions of NdFeB magnet, No. 0 SEP magnet and No. 7 SEP magnet are the same. The NdFeB magnet can have circular motion when changing the direction of the magnetic field of SEP from No.1 to No.7 in turn. The NdFeB magnet can also have circular motion in the opposite direction by changing the direction of the magnetic field of SEP magnet from No.7 to No.1 in turn.

As mentioned before, both SEP magnet and NdFeB magnet can be the stator and the rotor. This provides a great convenience when designing the structure of the robot. If we need to simplify the motion structure and do not even contain any circuit, we can set the NdFeB magnet as a rotor, just as shown in Figure III-8. But if we want to save costs and reduce the difficulty of the control system, we can design the structure as shown in Figure III-9. In this example, we only need to control two SEP magnets rather than eight. Since we need to control the movement direction, we need at least two SEP magnets to be the rotor. The possibilities of motion are shown in Figure III-10. As can be seen, the more intensive SEP magnets are arranged, the more possibilities of the movement direction.

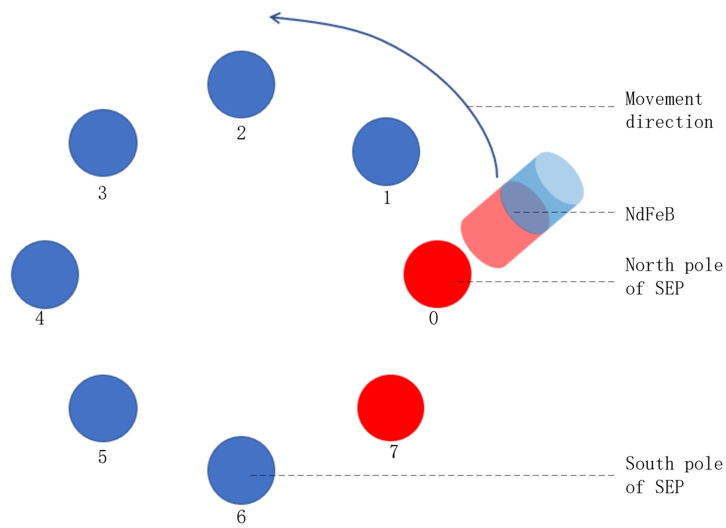

Figure III-8 Circular motion, NdFeB is the rotor

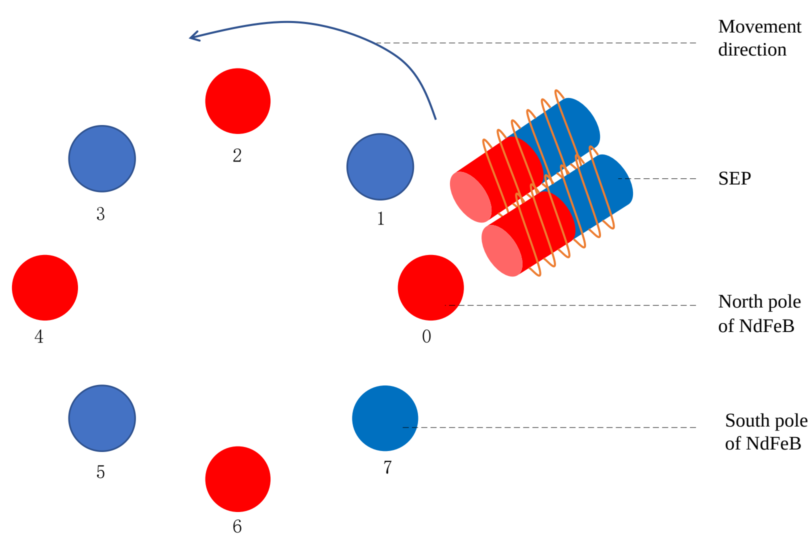

Figure III-9 Circular motion, SEP is the rotor

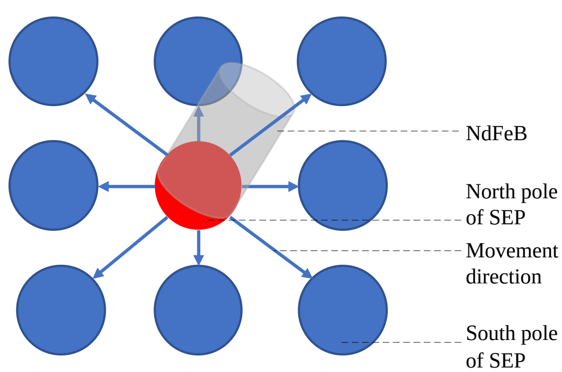

Figure III-10 Possibilities of motion

III.4.3. Enhanced magnetic field

Compared with the normal electromagnet and EP magnet, the advantages of SEP magnets are obvious: SEP magnets can achieve both motion and connection functions. Besides them, another advantage of SEP magnets is the possibility to have another mode that is the enhanced magnetic field. As shown in Figure III-11, when small electric current passes through the coil of the SEP magnet, the coil becomes an electromagnet. When the direction of the magnetic field of the electromagnet coincides with the direction of the magnetic field of Alnico5 magnet, the magnetic field shown by the entire SEP magnet will be enhanced as shown in this figure. Thus, the motion speed and the connection force between the two kinds of magnets are enhanced. But this function also consumes more power, generates heat and reduces the life of the system, so this function is only recommended when large adsorption forces (such as vertical motion and carrying objects) or when quick movements are needed.

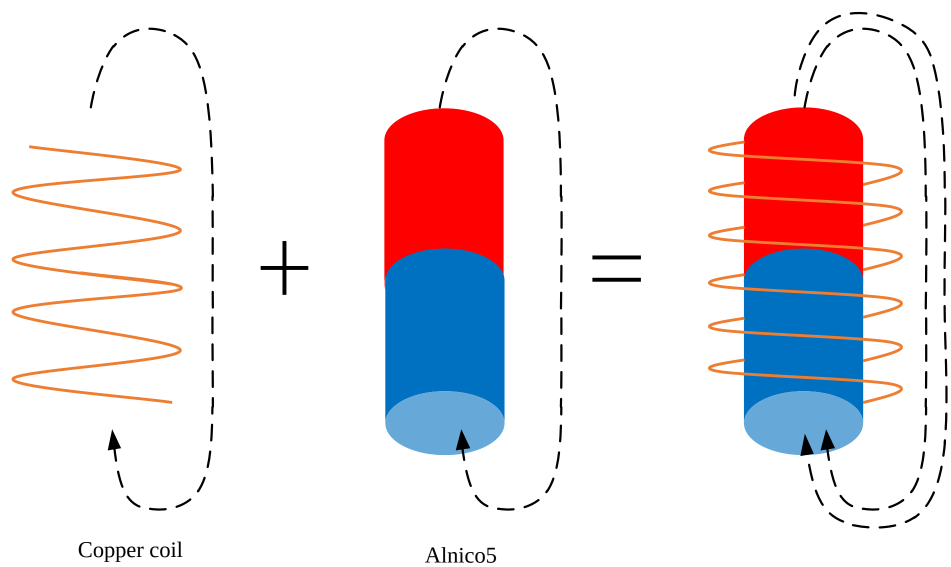

Figure III-11 Principle of enhanced magnetic field

III.5. Fabrication of a SEP Magnet and Tests

We make a simple SEP magnet to test its characteristics. The Alnico5 magnet is 8mm in length, 3 mm in diameter, and wound around by a 360-turn coil. We use the pulse generator to produce rectangular pulses, the amplitude of each pulse is 9.2 volt, and the width is 400 microseconds. Figure III-12 presents the result of the test. In the beginning, no pulse passes through the SEP magnet, and then we separate the two magnets. After passing 10 pulses through the SEP magnet, the polarity of Alnico5 is changed. Then we change the direction of NdFeB magnet (which can be seen via the white mark on NdFeB magnet) and put it close to SEP magnet. The SEP magnet and NdFeB magnet attract each other, which means the SEP magnet is reversely magnetized by pulses. Otherwise, the NdFeB magnet will be excluded away. This test validates our design of SEP magnet. In theory, SEP magnet can be made as tiny as possible.

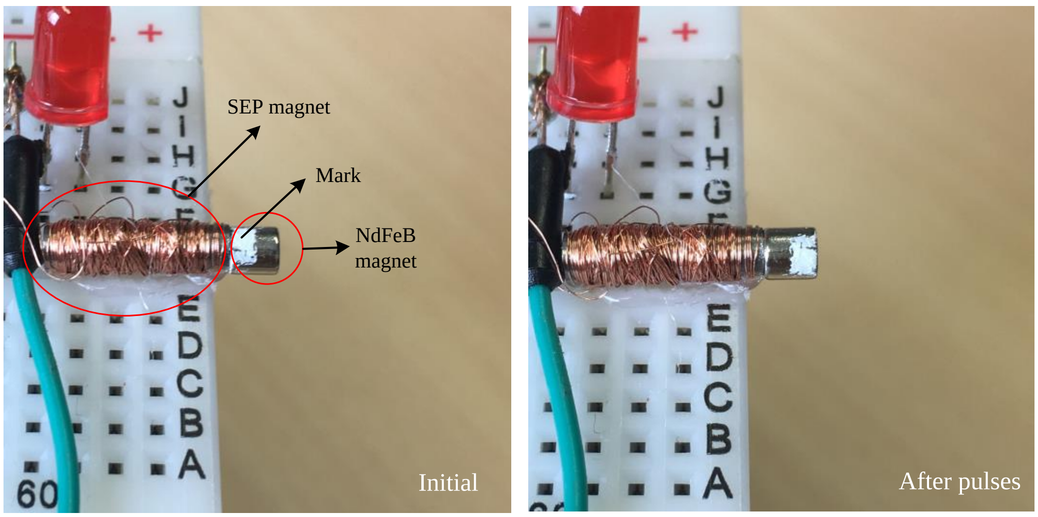

Figure III-12 Alnico5 magnet reversely magnetized

III.6. Conclusion

This chapter is mainly a presentation of the concept of SEP magnet. SEP magnet is a simplified EP magnet; its principle can be described by analyzing the magnetic field in a solenoid. SEP magnet can be used in a linear motor, which can achieve both moving and connection with only one system and does not require energy consumption while connected. By using this concept, the complexity of the structure of modular robot systems can be greatly reduced; the size of the robot modules can also be greatly reduced; moreover, this motor can save energy, which is very important especially for robots at a small scale.

References in Chapter III

[1] Bakshi, V.U., U.A.Bakshi. Basic Electrical Engineering [M]. Technical Publications. 2009: pp. 3–31.

[2] Tumanski, S. Handbook of magnetic measurements [M]. Boca Raton, FL: CRC Press. 2011

[3] Jackson, John David. Classical Electrodynamics (2nd ed.) [M]. New York: Wiley. 1975.

[4] Chikazumi, Sōshin. Physics of Ferromagnetism [M]. Clarendon Press.1997.

[5] Kazimierczuk, Marian K. High-frequency magnetic components (Second ed.) [M]. Chichester: Wiley. 2014

[6] Lowrie. Fundamentals of Geophysics [M]. Cambridge University Press. 2007

[7] Brady, George Stuart; Clauser, Henry R.; Vaccari, John A. Materials Handbook: An Encyclopedia for Managers. McGraw-Hill Professional. 2002: p. 577.

[8] Campbell, Peter. Permanent magnet materials and their application [M]. Cambridge University Press, 1996.

[9] Knaian A N. Electropermanent magnetic connectors and actuators: devices and their application in programmable matter [D]. Massachusetts Institute of Technology, 2010.

[10] http://www.projectara.com

[11] Gilpin K, Knaian A, Rus D. Robot pebbles: One centimeter modules for programmable matter through self-disassembly [C]. Robotics and Automation (ICRA), 2010 IEEE International Conference on. IEEE, 2010: 2485-2492.

[12] D. Howard Dellinger; L. E. Whittmore, R. S. Ould. Radio Instruments and Measurements [M]. NBS Circular. National Bureau of Standards.1924

[13] https://en.wikipedia.org/wiki/Solenoid

Chapter IV. Design and Numerical Simulation of Simplified Electro-Permanent Magnet

IV.1. Introduction

In Chapter III we have introduced the principles of SEP magnet, but we did not give details on the value of the different parameters in order to build a SEP magnet with low power consumption, small size, strong connecting force and strong driving force. This chapter aims at validating our design and finding the most reasonable parameters of the SEP magnet such as the number of coil turns, coil coverage area, copper wire diameter, current size and so on.

Section IV.2 presents the hysteresis loop and the whole process of the polarization change in the SEP magnet. Section IV.3 details the Jiles-Atherton model, which is used in the numerical simulation model. The design of the model and numerical simulation via COMSOL Multiphysics are presented in section IV.4. Section IV.5 discusses the effect of some important parameters like the number of coil turns and coverage area of the coil in the model. The conclusion of this chapter is given in section IV.6.

IV.2. Hysteresis Loop

Magnetic hysteresis is an inherent characteristic of some materials; it occurs when an external magnetic field is applied to a ferromagnet (such as the iron), and the atomic dipoles align themselves with it. Even when the field is removed, part of the alignment will remain, which means the material has become magnetized. Once magnetized, the magnet will stay magnetized indefinitely. It requires heat or a magnetic field in the opposite direction in order to demagnetize the magnet [1].

The relationship between field strength H and magnetization M is not linear in these materials. If a magnet is demagnetized (H=M=0), the relationship between H and M is plotted for increasing levels of field strength, M follows the initial magnetization curve. This curve increases rapidly at first and then approaches an asymptote called magnetic saturation. If the magnetic field is now reduced monotonically, M follows a different curve. When the strength becomes zero, the magnetization is offset from the origin by an amount called the remanence. If the H-M relationship is plotted for all values of the magnetic field, the result is a hysteresis loop called the main loop. The width of the middle section along the H axis is twice the coercivity of the material [2].

Figure IV-1 describes the limit hysteresis loop, that is, the largest one of all hysteresis loops. In the beginning, at point o, the ferromagnetic material is in the magnetic neutral state ($H=B=M=0$). When the material is placed in the external magnetic field H, the material begins to magnetize; the curve travels along ***o-b***. When reaching the saturation state (point ***a***), the magnetization intensity M is at the saturation value M_s and no longer increases with the increase of the magnetic field strength H; the curve starts parallel to the H axis and extends to point b, and the curve ***o-a-b*** is the starting magnetization curve. When the magnetic field strength H starts to reduce, since the change of magnetization intensity M is lag the change of magnetic field strength H, the magnetization intensity curve returns not in accordance with the original path but along the curve ***a-c-d-e***. When the magnetic field strength H is reduced to zero, the intersection of the curve and the M axis is the residual magnetization intensity, M_r. By adding an opposite magnetic field H_c, the magnetization M could be reduced to zero, H_c is a coercive force.

When the reverse magnetic field strength reaches Hs, the material will reach the saturation state (point d) in the opposite magnetize direction. In this case, the corresponding magnetization M is $-M_s$. If H is increased at this time, the curve will reach the positive saturation state according to the *path* ***d-f-g-a***. The curve ***a-c-d-f-g-a*** constitutes a closed hysteresis loop, this hysteresis loop is an irreversible magnetization process, and one H value corresponds to two M values. Curve ***a-b*** and ***e-d*** are reversible magnetization processes.

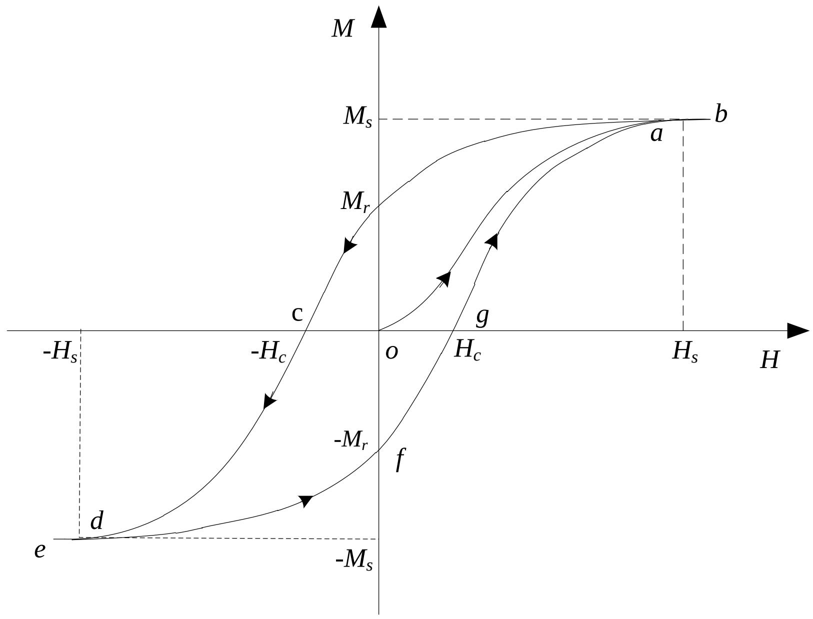

Figure IV-1 Hysteresis loop

IV.3. Jiles-Atherton Model

In order to accurately express the magnetization properties of ferromagnetic materials, it is necessary to handle their various magnetization curves and hysteresis loops correctly. Nowadays, the study of the hysteresis loop theory and its model building method is described in the literature. The Jiles-Atherton (J-A) [3-5], Preisach [6] and Stoner-Wohlfarth (S-W) [7] are three classical models in magnetization modelling. The advantages and disadvantages of the above four models in the simulation of ferromagnetic materials are described systematically by [8]. Jiles-Atherton (J-A) model was introduced by D.C. Jiles and D.L. Atherton in 1983. This model passed through the experimental verification, and has been widely used for practical applications. Based on the Weiss ferromagnetism theory [9], it requires a wide magnetic field for a ferromagnetic material to reach saturation magnetization from the initial state. In this magnetic field, there is a strong interaction between the atomic moments of the ferromagnetic material, which tends to rotate to be parallel to each other. The role of the external magnetic field is only to change the magnetic direction of the formation of spontaneous magnetization. Weiss names this strong internal range as ferromagnet to be magnetized from the initial magnetization to saturation magnetization. In a magnetic field as a molecular field H_m, and assume that the expression is $H_m = aM$, where a is the molecular field parameter, M is the magnetization intensity. If the direction of the external magnetic field is parallel to the direction of the magnetization, then the effective magnetic field inside the ferromagnetic is:

$$H_e = H + H_m = H + aM \tag{4.1}$$

Then according to the paramagnetic magnetization theory and the definition of Langevin function $L(z)$, we can get:

$$M(z) = M_s L(z) = M_s \coth(z - \frac{1}{z}) \tag{4.2}$$

where M_s is the saturation magnetic polarization intensity, which is often provided by the manufacturer, $M_s = Nm$ and N is the number of molecules per unit volume; m is the modulus of the atomic magnetic moment; $z = He/a$, $\alpha = kT/m$, where k is the Boltzmann constant, T is the temperature of the material (in unit Kelvin).

We replace M in the formula (4.2) by M_{an}; then the equation can represent the relationship between the magnetization and the external magnetic field strength during the ideal magnetization of the ferromagnet. M_{an} is called the non-hysteresis magnetization. According to formula (4.2), if the value of external magnetic field strength is given, M_{an} can be uniquely determined.

Jiles-Atherton hysteresis model is based on the above Weiss molecular field theory. The hysteresis of ferromagnetic materials is described by a set of differential equations which can be expressed as a full differential magnetic susceptibility:

$$\frac{\mathrm{d}M}{dH} = \frac{(1-c)dM_{irr}/dH_e + cdM_{an}/dH_e}{1-\alpha cdM_{an}/dH_e - \alpha(1-c)dM_{irr}/dH_e} \tag{4.3}$$

where H is the magnetic field strength, M_{an} is the modified Langevin function:

$$M_{an}(H) = M_s\left[\coth\left(\frac{H_e}{a}\right) - \frac{a}{H_e}\right] \tag{4.4}$$

Formula (4.3) can be used to describe the non-hysteresis magnetization; M_s is the saturation magnetization; M_{irr} is the irreversible magnetization; M_{rev} is the reversible magnetization; the total magnetization M equals to the sum of M_{irr} and M_{rev}; c is related to the ratio M_{rev}/M; H_e is the effective field strength of the material,

$$H_e = H + \alpha M \tag{4.5}$$

where α is the material-related parameter; the total magnetization M, the relationship between M_{irr} and H_e is as follows:

$$\frac{\mathrm{d}M_{irr}}{dH_e} = \frac{M_{an} - M_{irr}}{k\delta} \tag{4.6}$$

$$M = M_{irr} + c\left(M_{an} - M_{irr}\right) \tag{4.7}$$

where k quantifies average energy required to break pinning site in the magnetic material, δ depends on the direction of changes of magnetizing field H with $\delta = 1$ for increasing field, $\delta = -1$ for decreasing field.

When the magnetization is known, the corresponding magnetization value can be known by calculating the formula (4.3). In the formula (4.3) - (4.7), there are five parameters: a, α, M_s, k, and c. The characteristics of the magnetic material are uniquely determined by a set of five parameters.

These parameters have different effects on the shape and size of the hysteresis loop [3]:

• M_s only affects the highest point of hysteresis loop, with the increase of M_s, the highest point of hysteresis loop is also increasing;

• α affects the inclination of knee part (***c-d*** in Figure V-1) of hysteresis loop, the greater the value, the steeper the knee;

• a affects the inclination of hysteresis loop, including the knee part, the greater the value, the gentler the hysteresis loop;

• k affects the coercive force, the larger the value, the wider the hysteresis loop;

• c affects the slope but does not affect the knee part, the greater the value, the gentler the hysteresis loop.

In the simulation process, we have adjusted the above five parameters in order to calibrate the hysteresis loop of Alnico5. This will be shown in the sequel of this chapter.

IV.4. Numerical Simulation with COMSOL Multiphysics

COMSOL Multiphysics is a numerical simulation software for engineering. It originated in the Toolbox of Matlab, originally named Toolbox 1.0. Then it was renamed as Femlab 1.0 (FEM for the finite element, LAB is taken from the Matlab), the name has been used to Femlab3.1. Since version 3.2, COMSOL Multiphysics become its official name [10].

COMSOL Multiphysics can achieve direct coupling of multi-physics fields. Due to its superior multi-field direct coupling capability and efficient analytical and computational power, it has been universally accepted and widely used in the domain of numerical simulation. COMSOL Multiphysics offers a variety of modules for different areas, including AC/DC, microelectromechanical systems, RF, acoustics, chemical engineering, geoscience, structural mechanics, and so on. We mainly use the AC/DC module in our work.

IV.4.1. Model

In the sequel, we present simulation results of SEP magnet with COMSOL 5.2 [11]. Since the structure of the SEP magnet is axisymmetric, we only need to establish a two-dimensional symmetric model, which is shown in Figure IV-2. The model consists of three parts, the first part is Alnico5 (see Figure IV-3 (a)), it has a size of 1.5mm * 8mm; the second part is a copper coil, with an initial size of 0.7 * 10mm (see Figure IV-3 (b)), its size is changeable; the third part is air (see Figure IV-3 (c)).

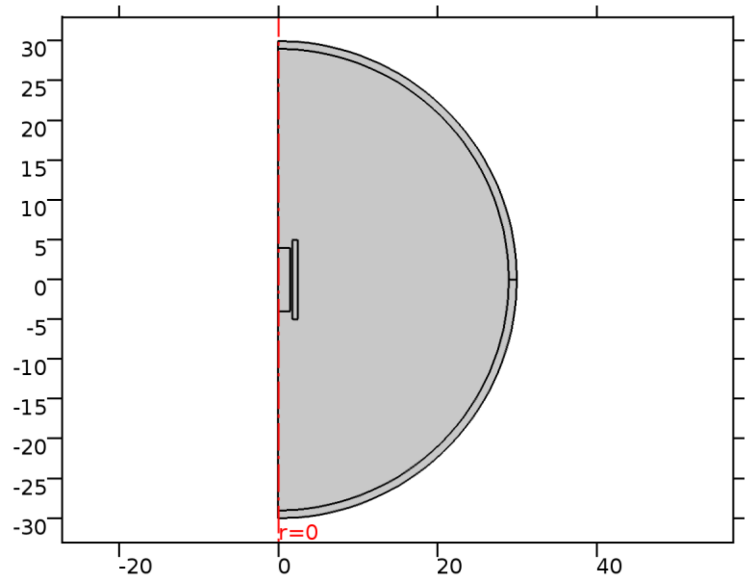

Figure IV-2 2D domain of the numerical simulation including Alnico5, coil and surrounding air

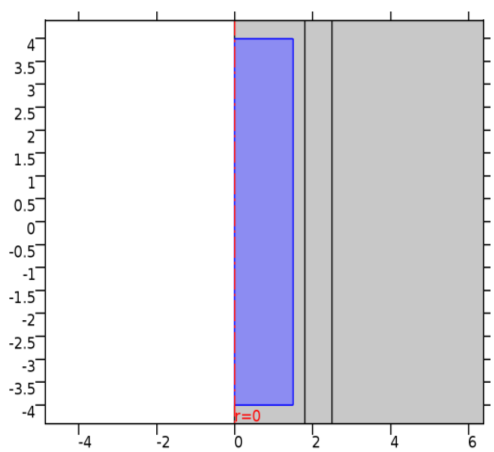

(a)

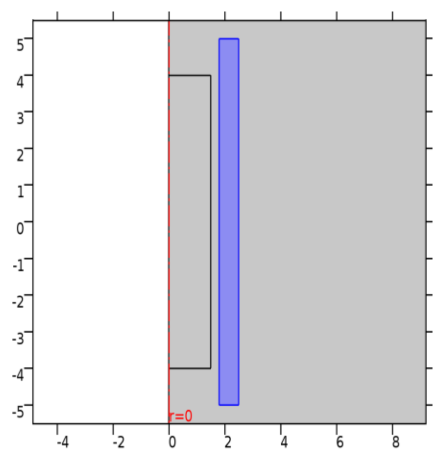

(b)

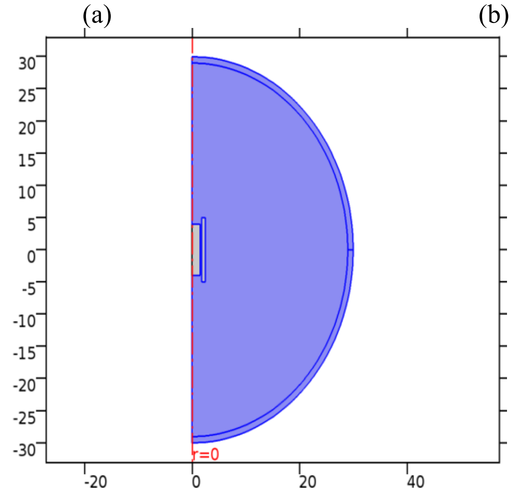

(c)

Figure IV-3 Three views at SEP magnet model: (a) Alnico5, (b) Copper, (c) Air

IV.4.2. Physical parameters

The definition of physical parameters includes the definition of material properties and the setting of boundary conditions and initial values. When the model contains multiple subdomains, and their physical parameters are not the same, we also need to define the physical parameters for each subdomain. In order to simplify the simulation experiment, we use parametric modelling, that is, the whole simulation can be controlled by some global parameters, these parameters include geometric parameters, operating parameters, coil parameters, condition parameters, solver parameters, material parameters. Table IV-1 shows the parameters of the entire simulation model in COMSOL.

Table IV-1 Global parameters for simulation with COMSOL

Name	Expression	Initial Value	Description
Radius	1.5[mm]	0.0015 m	Geometric parameters: the radius of Alnico5
Length	8[mm]	0.008 m	Geometric parameters: the length of Alnico5
R_coil_in	1.8[mm]	0.0018 m	Geometric parameters: the inside diameter of coil
R_coil_out	2.5[mm]	0.0025 m	Geometric parameters: the outside diameter of coil
I_current_Amp	20[A]	20 A	Operating parameters: coil current
N_coil	100	100	Coil parameters: coil turns
d_wire_coil	0.2[mm]	2E−4 m	Coil parameters: the diameter of the copper wire
L_coil	10[mm]	0.01 m	Geometric parameters: the length of coil
Pulse_Period_p	0.4[ms]	4E−4 s	Condition parameters: positive magnetization pulse period
P_rise	0.01[ms]	1E−5 s	Condition parameters: magnetization pulse rise / fall edge width
solver_step	P_rise*0.05	5E−7 s	Solver parameters: time of step
Pulse_Period_n	0.4[ms]	4E−4 s	Condition parameters: negative magnetization pulse time
Pulse_hold	0.4[ms]	4E−4 s	Condition parameters: positive and negative pulse hold time
F_sin	2[Hz]	2 Hz	Condition parameters: sinusoidal demagnetization period
Br	0.3[T]	0.3 T	Material parameters: initial residual magnetic flux density
Mr_z	Br/mu0_const	2.3873E5 A/m	Material parameters: initial residual magnetization
Bs	2[T]	2 T	Material parameters: saturated magnetic flux density
Ms_z	Bs/mu0_const	1.5915E6 A/m	Material parameters: saturation magnetization

IV.4.3. Mesh

The accuracy of the calculation and the speed of the computation are directly related to the discrete model / mesh (finite element representation). The more detailed the representation, the more accurate the calculation, but also the greater the computing time. Therefore, it is important to combine the different factors and rationally carry out finite element meshing.

COMSOL Multiphysics provides two ways for meshing: Free meshing and Mapped meshing. The Free meshing uses tetrahedron, quadrilateral or triangles to mesh, and changes the mesh quality by side length curvature and grid number. It is usually used for spatial free surface and complex entities meshing. The Mapped meshing uses the parameters such as the number of grids and the length of the cells to strictly control the mesh quality.

In our model, the Alnico5 and copper coil are meshed by Mapped (see Figure IV-4), and the remaining air is made with Free triangular. The specific element size parameters are shown table IV-2. The global meshed model is shown in Figure IV-5.

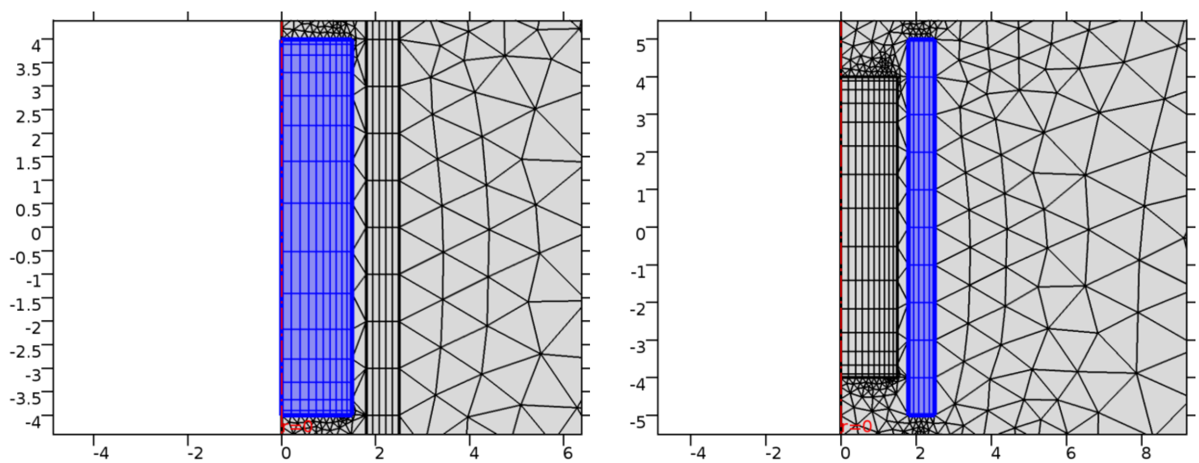

Figure IV-4 Mapped mesh of Alnico5 and copper coil

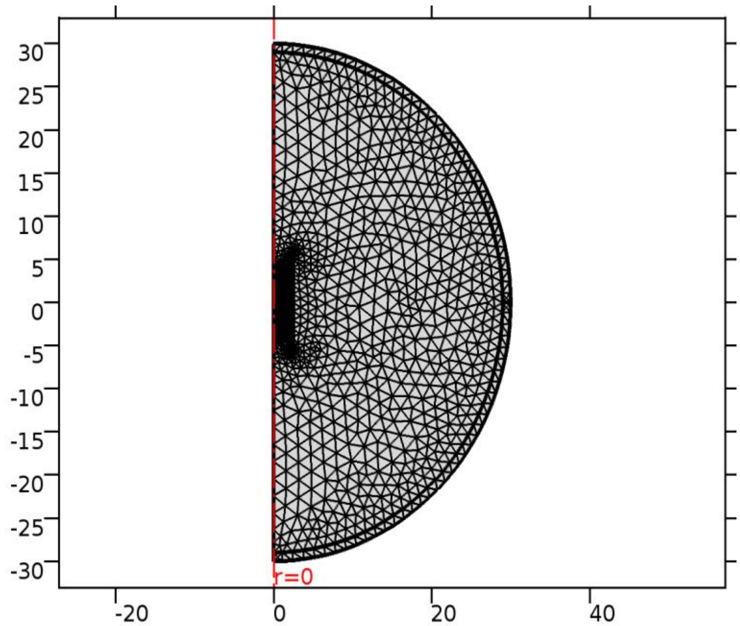

Figure IV-5 Meshed model

Table IV-2 Mesh data

Description	Value
Minimum element quality	0.1359
Average element quality	0.8917
Triangular elements	1864
Quadrilateral elements	200
Edge elements	260
Vertex elements	14

IV.4.4. Study and model calibration

To simulate the process of Alnico5 magnetization and reverse magnetization, we have to adjust the five parameters of Jiles-Atherton theory in the formula (4.3) - (4.7) so that the hysteresis loop is similar to the real one tested in [12]. So, parameter calibration is the first step. In the real tests of the hysteresis loop, the excitation is a sinusoidal function. Thus, we use the same type of signal for model calibration.

Figure IV-6 shows the hysteresis loop resulting from the COMSOL simulation. Figure IV-7 displays the internal average magnetic field B_z (unit is Tesla, in the z-direction) and the coil current intensity I (unit is 10 Amperes) in function of the time given in seconds. It is obvious that there is a phase lag between current and B_z, this is the magnetic hysteresis. If we take a look at the two figures, then it can be observed that at $t = 0$ s the Alnico5 material begins to be magnetized and reaches the maximum near 0.1 s; then magnetization begins to decrease, and reverses near 0.28 s; near 0.36 s, it reaches the maximum in the reverse direction; when $t = 0.52$ s, it becomes zero again. This is the first hysteresis phase, and the process repeats again. It should be noted that from then on, the Alnico5 is no longer without magnetization. Thus, the hysteresis loop cannot coincide with the first period. In the hysteresis loop, when H increases from zero to its maximum value and then decreases to zero, some residual magnetism remains (see point a), at this point the value of the magnetic flux density is also known as the remanent flux density.

The Hysteresis loops in Figure IV-6 do not coincide, which is because we use the Jiles-Atherton theory. In this theory, each step of the magnetization process is related to the previous step, and numerical simulation results depends on magnetization history. When the period is long enough, it will eventually stabilize.

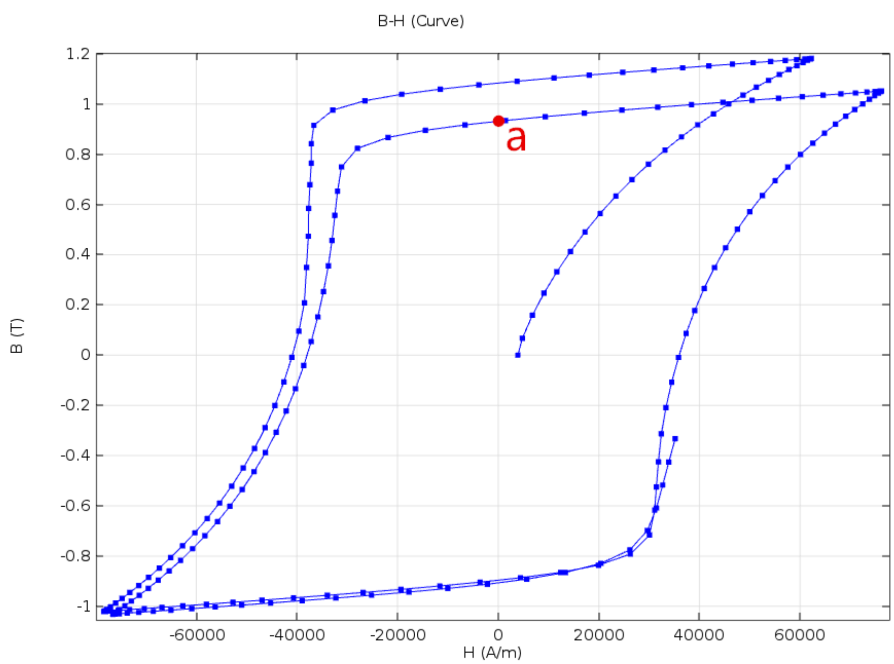

Figure IV-6 Calibrated hysteresis loop by COMSOL

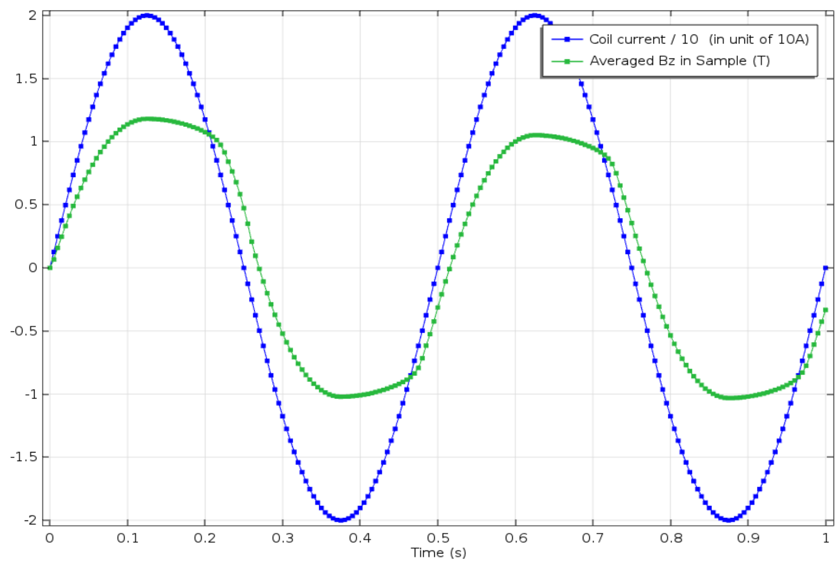

Figure IV-7 Relationship of the coil current intensity I (unit is 10 *A*) and internal average magnetic field B_z in function of the time (*s*).

Figure IV-8 shows the 3D magnetic flux density view. Figure IV-9 displays four important phases of the magnetization process. Figure IV-9 (a) shows the magnetic flux density when it reaches the maximum value. Figure IV-9 (b) shows the directions of the magnetic field when it starts to reverse. At this moment, it is obvious that the directions of the magnetic field in Alnico5 and outside are opposite. The interaction of the magnetic fields of the Alnico5 and the coil also causes the nearby magnetic field to become disordered. In Figure IV-9 (c), the Alnico5 is demagnetized. In Figure IV-9 (d), the magnetic flux density reaches the maximum value in the opposite direction.

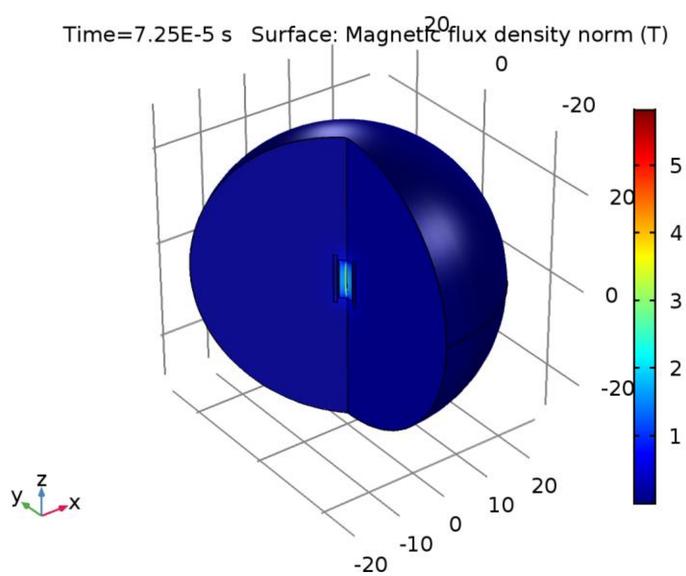

Figure IV-8 3D magnetic flux density view

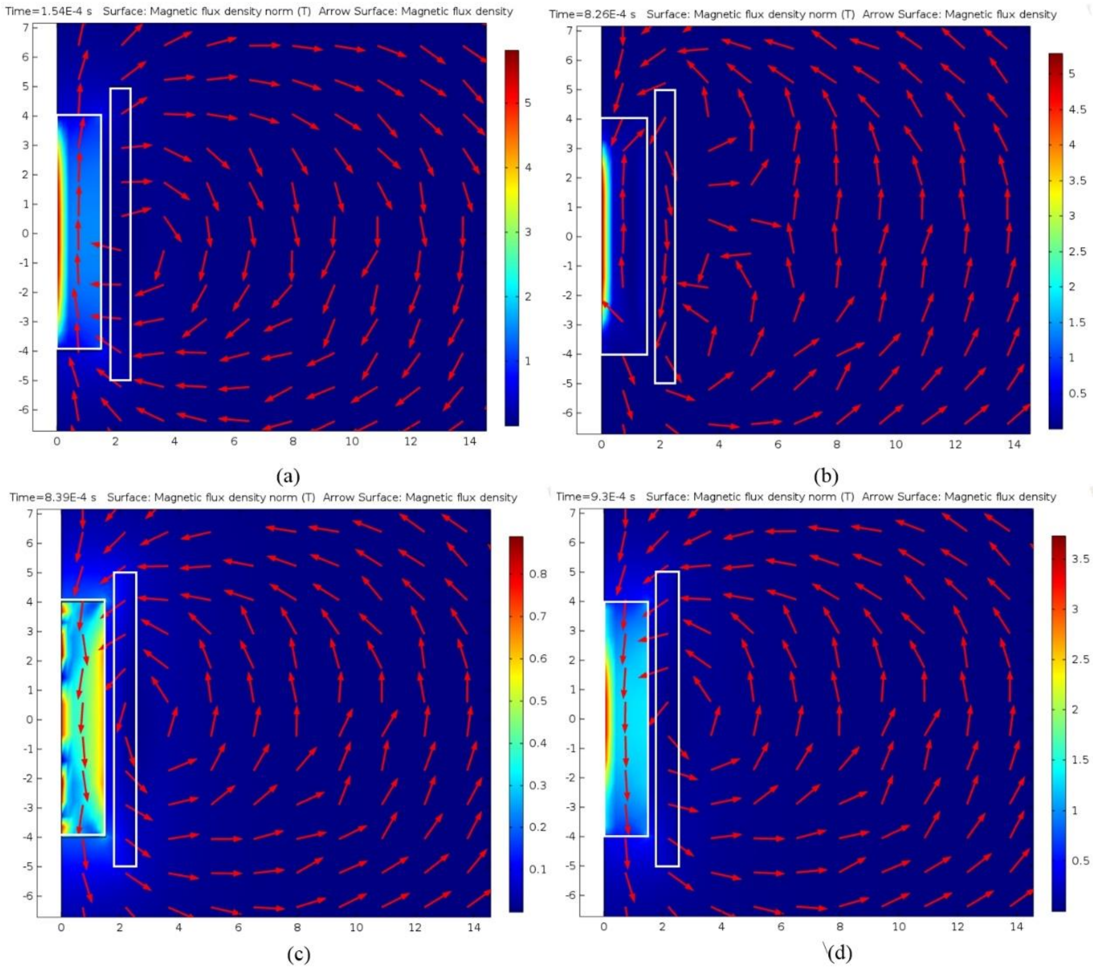

Figure IV-9 Magnetic flux density (in Tesla) at four representative times for sinusoidal excitation. (a) Maximum value of the flux density. (b) The flux density begins to change the direction. (c) Alnico 5 is demagnetized. (d) Maximum value of flux density in opposite direction

We use a pulse signal to change the magnetic field of SEP magnet. The pulse signal consists of a positive pulse followed by a negative pulse. To the best of our knowledge, COMSOL Multiphysics does not provide such a signal. Referring to Table IV-1, we first define two positive pulse signals *rect1* (see Table IV-3 and Figure IV-10) and *rect2* (see Table IV-4 and Figure IV-11).

Table IV-3 Definition of positive pulse signal: *rect1*

Description	**Value**
Lower limit	P_rise
Upper limit	Pulse_Period_p + P_rise*2

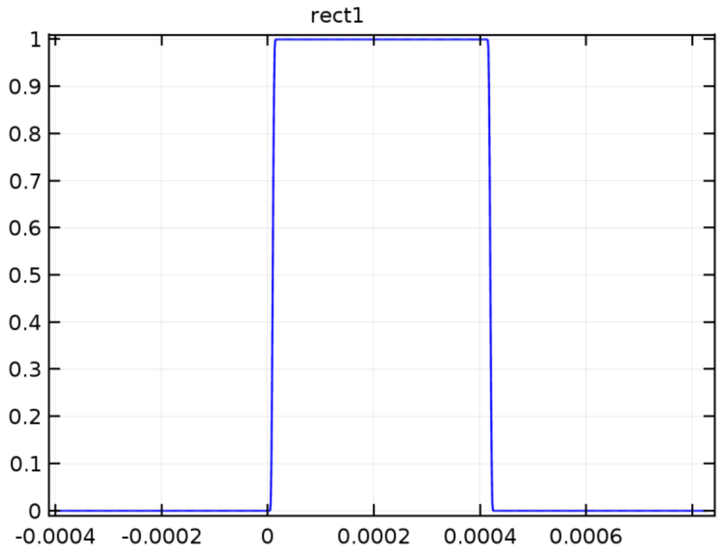

Figure IV-10 Positive pulse signal: *rect1*

Table IV-4 Definition of positive pulse signal: *rect2*

Description	Value
Lower limit	Pulse_Period_p + Pulse_hold + P_rise*4
Upper limit	Pulse_Period_p + Pulse_hold + P_rise*4 + Pulse_Period_n + P_rise*2

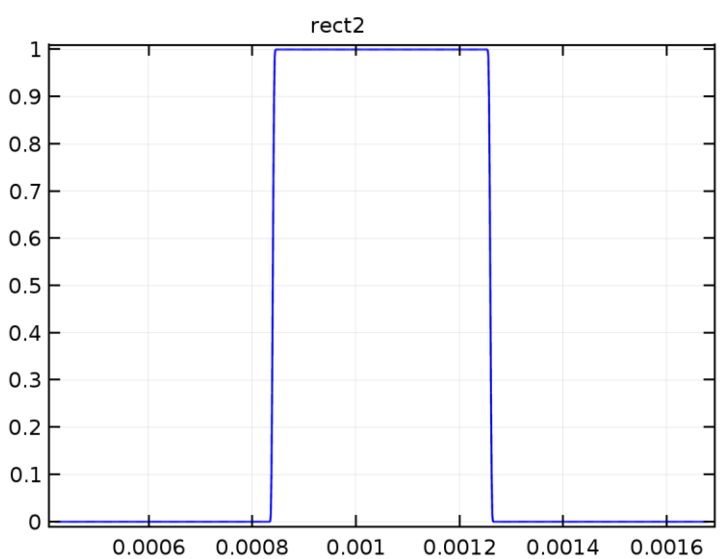

Figure IV-11 Positive pulse signal: *rect2*

Finally, we combine the two signals to obtain the complete pulse signal pw1 (see Table IV-5 and Figure IV-12).

Table IV-5 Definition of the complete pulse signal: pw1

Start	End	Function
0	Pulse_Period_p+Pulse_hold+P_rise*4	rect1(t)
Pulse_Period_p+Pluse_hold+P_rise*4	Pulse_Period_p+Pulse_hold+P_rise*4+Pulse_Period_n+Pulse_hold+2*P_rise	-rect2(t)

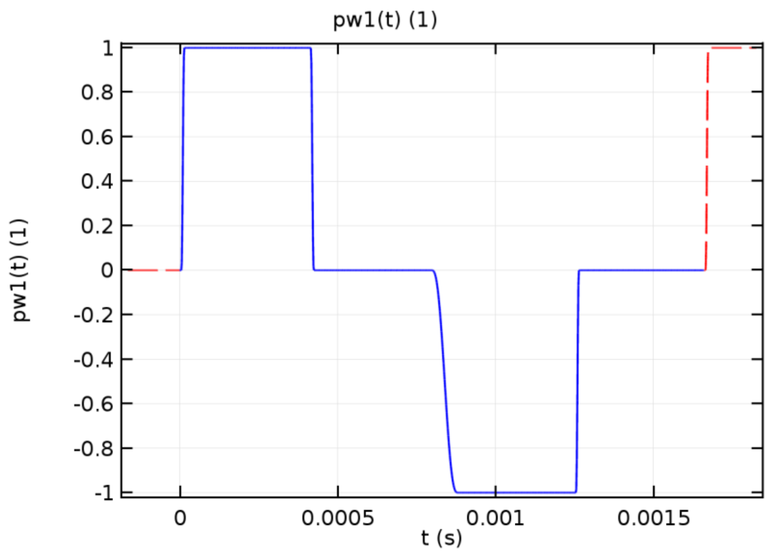

Figure IV-12 The complete pulse signal: pw1

We consider now the case where the excitation signal is a pulse. Pulse peak is 20 *A*. We get the new B-H curve, which is shown in Figure IV-13; where the internal average magnetic field B_z is in Tesla. The coil current intensity *I* (unit is 10 Amperes) is shown in Figure IV-14. Compare the point **a** in Figure IV-13 and Figure IV-6, the value in Figure IV-13 (0.8 T) is less than the one in Figure IV-6 (0.9 T); this is due to the non-linearity of the pulse signal, and the effect of non-linear inductance elements. When generating a magnetic field, eddy currents (Foucault currents) are also generated in Alnico5. These eddy currents, in turn, generates the anti-magnetic field, which will hinder the magnetization process, and prevents the Alnico5 from being completely saturated. This anti-magnetic field is enhancing radially from outside to the inside of Alnico5. Non-uniform magnetization often occurs when magnetizing the permanent magnet with a large cross-section, since the magnet surface is in the saturation state, but the middle portion is not. Figure IV-15 details the anti-magnetic fields in Alnico5 with COMSOL. The magnetizing current pulse width is short; pulse rise time is much shorter. When the pulse current increases, the anti-magnetic field becomes more apparent. Therefore, when designing SEP magnet, the diameter of Alnico5 cannot be too big.

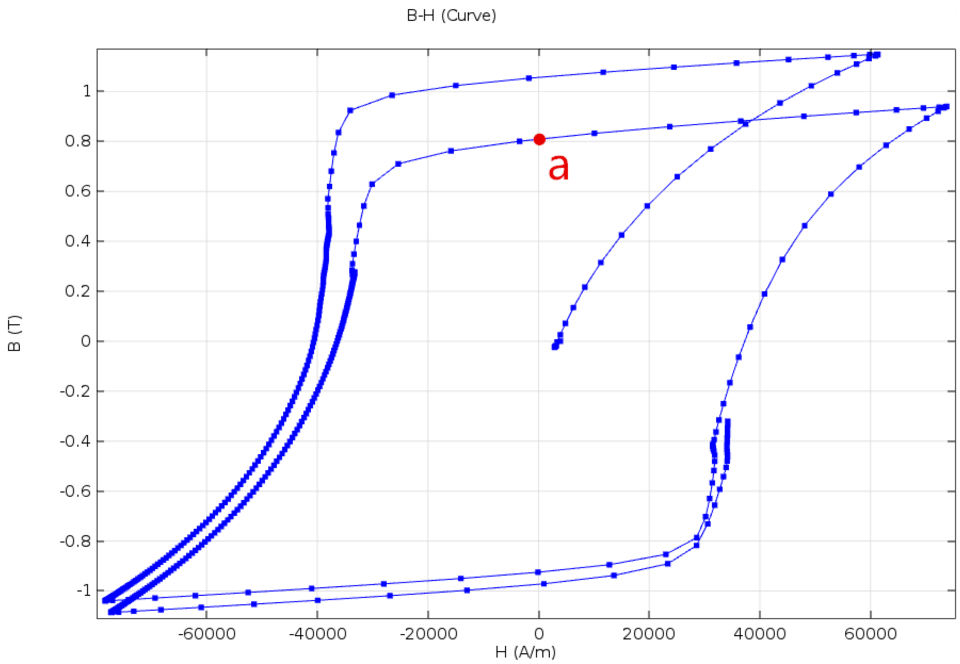

Figure IV-13 B-H curve of the pulse signal

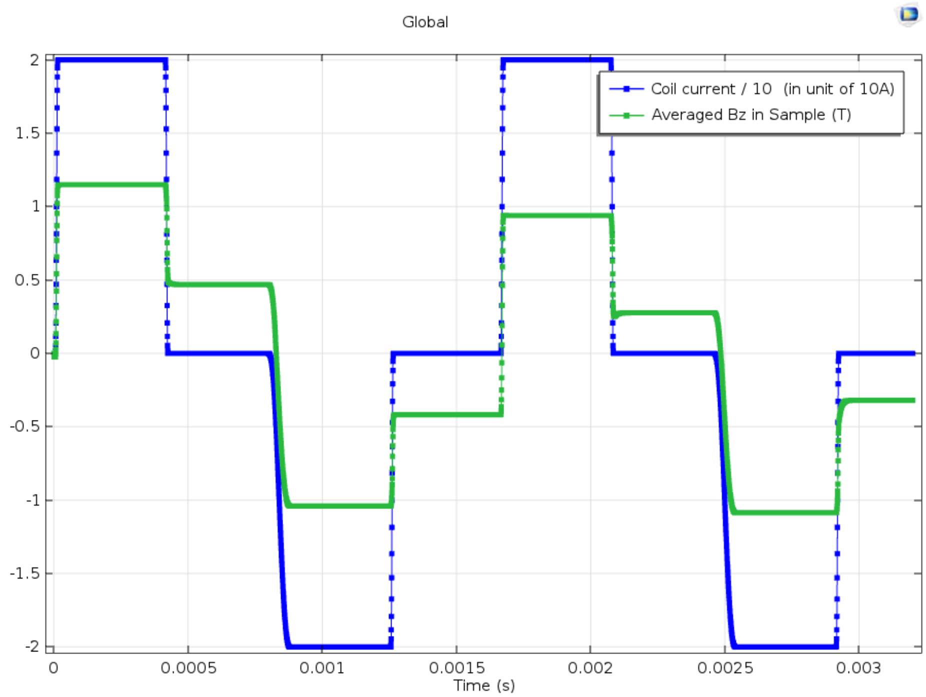

Figure IV-14 Relationship between internal average magnetic field B_z and the coil current intensity I (pulse case, unit is 10A)

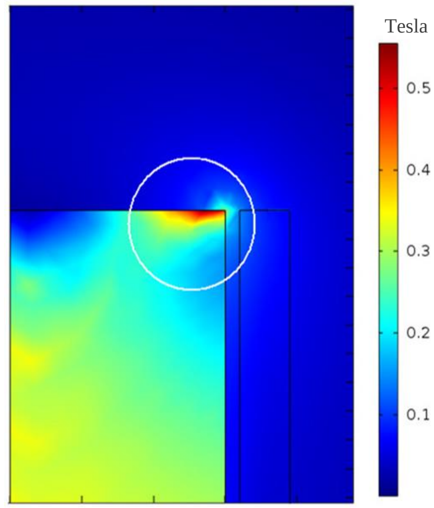

Figure IV-15 Anti-magnetic field in Alnico5

By comparing Figure IV-6 and Figure IV-13, we can see that the sinusoidal signal is more favourable to achieve greater magnetic flux density than the pulse signal. Nevertheless, its frequency is too low for practical use in a modular robot where modules have to move rapidly. Thus, when a module needs to move quickly, we use pulses; and when it reaches a specified position, we use a sinusoidal signal in order to make the connection between the modules more efficient. This conclusion is very important, and we provide the sequel guidance for programming and control strategies.

IV.5. Simulation Results

We concentrate now on several points in relationship with the design of the SEP magnet. In the sequel, we detail the effect of coil turns, pulse intensity, the coverage area of the coil on the global behaviour of the SEP magnet.

IV.5.1. Effect of the number of coil turns

To analyze the effect of the number of coil turns, we make tests with up to 500 coil turns and measure the magnetic flux density. Figure IV-16 shows the trends of the magnetic flux density of Alnico5 center, B_{center}. In the beginning, B_{center} increases with the number of coil turns. The growth rate is significantly reduced at 200 turns; B_{center} reaches a maximum value at 300 turns, and does not increase anymore. As a conclusion, it is better to choose the number of coil turns between 200 to 300.

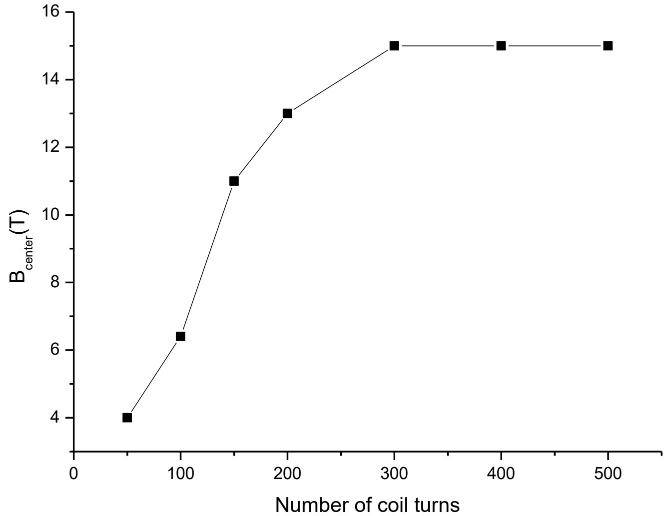

Figure IV-16 Effect of number of coil turns

IV.5.2. Effect of the pulse intensity

We analyze now the effect of the intensity of the pulse, and consider peaks from 1 A to 30 A. Figure IV-17 shows the trends of the magnetic flux density B_{center} of Alnico5 center, and the average magnetic flux density $B_{average}$. We observe that the greater the intensity of the pulse, the greater the magnetic flux density. We note that when the intensity is below 5 A, the hysteresis curve is distorted. At 20 - 30 A, although the pulse peak is large a few energy is required since the pulse is very short, and it will not cause damage to the circuit. Thus, it is better to choose a current intensity that is sufficiently large but that avoids the destruction of the circuits and equipment.

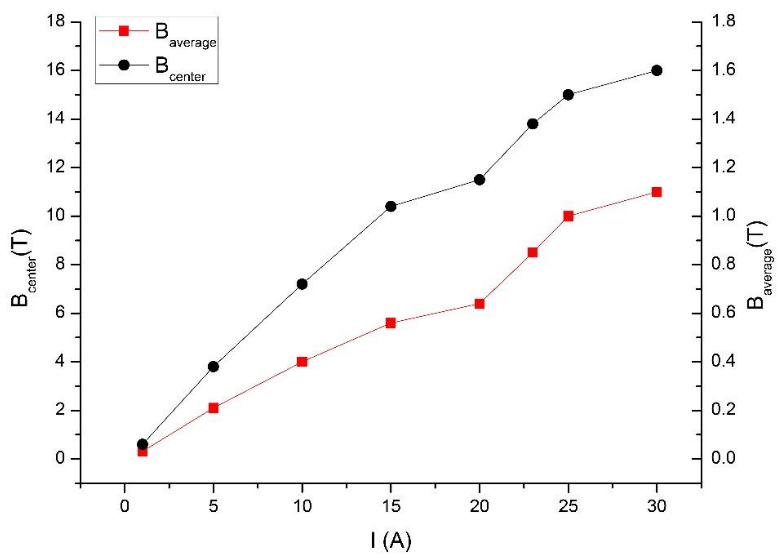

Figure IV-17 Effect of pulse peak

IV.5.3. Effect of the coverage area of coil

For a fixed number of coil turns and fixed current intensity, we consider now three configurations in the simulation:

a) Alnico 5 is half wrapped (see Figure 18 (a));

b) Alnico 5 is exactly wrapped (see Figure 18 (b));

c) Alnico 5 is extra wrapped (see Figure 18 (c)).

These three configurations correspond to tight, loose and very loose wrapping, respectively. Figure IV-20 displays the distribution of the magnetic flux density according to the coverage area. In Figure IV-18 (a), it can be seen that, if the Alnico5 is not fully covered, then the two ends (in the circle) cannot be magnetized. In Figure IV-18 (b) and Figure IV-18 (c), we observe that the Alnico5 can be totally magnetized, there are no significant differences, but the larger the coverage area, the smaller the magnetic flux density of Alnico5 center. This is because, when the coverage area increases, the magnetic flux density which is distributed to Alnico5 center becomes smaller. Thus, when manufacturing SEP magnet, it is better to exactly wrap Alnico5 with copper coil.

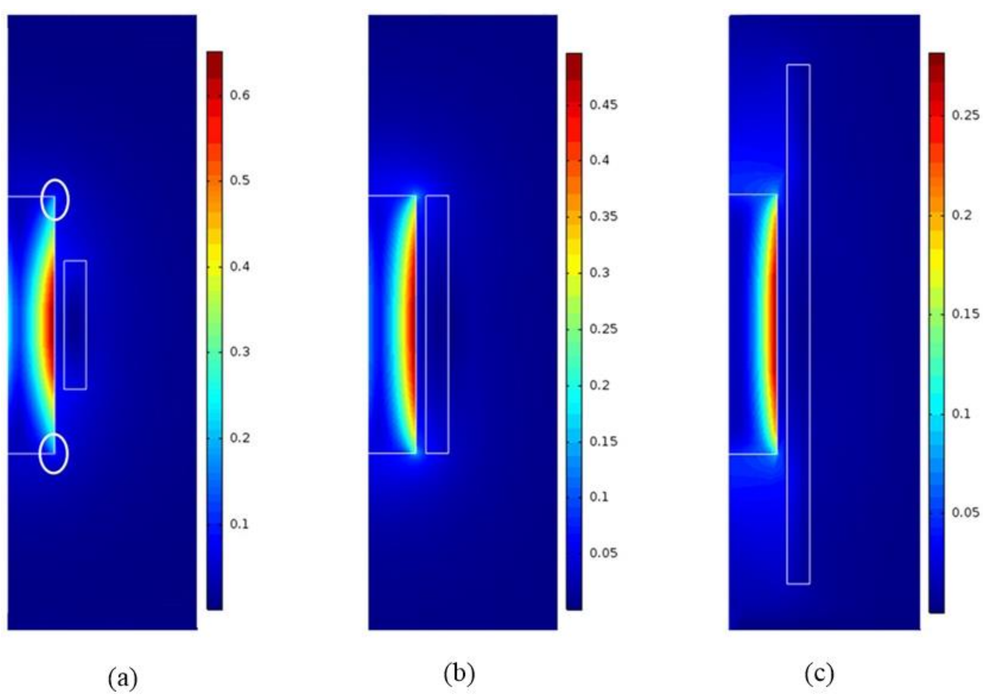

Figure IV-18 Effect of the coverage area of coil. (a) half wrapped. (b) exactly wrapped. (c) extra wrapped.

IV.5.4. Effect of the diameter of copper wire

We analyze now the effect of the diameter of copper wire which is used for making the coil. Figure IV-19 shows the trends of the magnetic flux density B_{center} of Alnico5 center. We can notice that there is no significant difference when changing the diameter of copper wire between 0.01 mm and 0.2 mm. So, when choosing the copper wire, we only need to consider the maximum current it can withstand according to the American Wire Gauge (AWG), which is also known as the Brown & Sharpe wire gauge. AWG is a standardized wire gauge system used since 1857 predominantly in North America for the diameters of round, solid, nonferrous, electrically conducting wire.

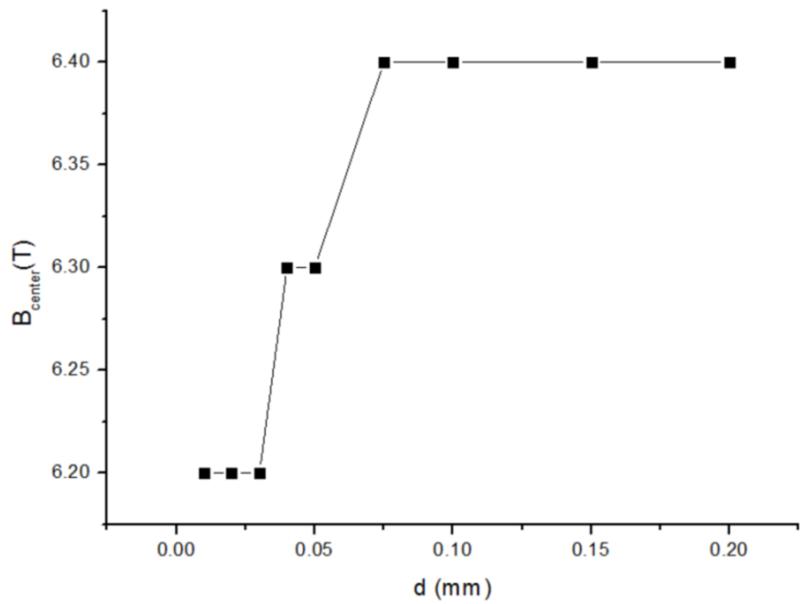

Figure IV-19 Effect of the diameter of copper wire

Table IV-6 shows some standard wires in AWG. We take a close look at the fusing current; it is easy to see that the wire can withstand bigger current when the time is shorter. In our case, the pulse period is much shorter than 32 ms. Besides, in order to reduce the size of the SEP magnet, the smaller the diameter of the copper wire, the better. So, we choose the wire with the diameter between 0.127mm and 0.202mm.

Table IV-6 AWG wire sizes

AWG	Diameter	Turns of wire, without insulation	Area	Resistance/length	Fusing current	
	（mm）	（per cm）	(mm^2)	($m\Omega/m$)	1s (A)	32ms (A)
26	0.405	24.7	0.129	133.9	39	218
27	0.361	27.7	0.102	168.9	31	174
28	0.321	31.1	0.081	212.9	24	137
29	0.286	35.0	0.0642	268.5	20	110
30	0.255	39.3	0.0509	338.6	15	86
31	0.227	44.1	0.0404	426.9	12	69
32	0.202	49.5	0.0320	538.3	10	54
33	0.180	55.6	0.0254	678.8	7.7	43
34	0.160	62.4	0.0201	856.0	6.1	34
35	0.143	70.1	0.0160	1079	4.8	27
36	0.127	78.7	0.0127	1361	3.9	22
37	0.113	88.4	0.01	1716	3.1	17
38	0.101	99.3	0.00797	2164	2.4	14

IV.6. Conclusion

This chapter first introduces the Magnetic hysteresis and the Jiles-Atherton model. Then based on the former theories we build a model in COMSOL Multiphysics. Finally, we have performed a series of numerical simulations to study the effect of different parameters like the number of coil turns or wrapping area. The simulation results play a guidance role in validating the design of SEP magnet. Some important conclusions can be given:

1) It is better to choose the number of coil turns between 200 and 300.

2) The greater the intensity of the pulse, the greater the magnetic flux density. It is better to choose an intensity that is big enough but also avoids the destruction of the circuits and equipment.

3) When manufacturing SEP magnet, it is better to wrap Alnico5 with copper coil exactly.

4) There is no significant difference when changing the diameter of copper wire between 0.01 mm and 0.2 mm. Considering the voltage and current, it is better to choose the wire with the diameter between 0.127mm and 0.202mm.

We also need to note that, the numbers of the coil turns, the diameter of the copper wire, the thickness of coil and the coverage area of the coil are interrelated, and their relationship can be calculated.

References in Chapter IV

[1] Chikazumi, Sōshin. Physics of ferromagnetism (2nd ed.) [M]. Oxford: Oxford University Press.1997.

[2] Chikazumi S., Graham C. D. Physics of Ferromagnetism 2e [M]. Oxford University Press on Demand, 2009.

[3] Jiles D. C.，Atherton D. L．Theory of ferromagnetic hysteresis [J]. Journal of Magnetism and Magnetic Materials，2001,61(1-2):48-60．

[4] Jiles D. C．Numerical determination of hysteresis parameters for the modelling of magnetic properties using the theory of ferromagnetic hysteresis [J]．IEEE Transactions on Magnetics，1992, 28(1): 35-37．

[5] Annakkage U. D., McLaren P. G., Dirks E., et al. A current transformer model based on the Jiles-Atherton theory of ferromagnetic hysteresis [J]. IEEE transactions on power delivery, 2000, 15(1): 57-61.

[6] Preisach F. Über die magnetische Nachwirkung [J]. Zeitschrift für Physik A Hadrons and Nuclei, 1935, 94(5): 277-302.

[7] Stoner E. C., Wohlfarth E. P. A mechanism of magnetic hysteresis in heterogeneous alloys [J]. Philosophical Transactions of the Royal Society of London A: Mathematical, Physical and Engineering Sciences, 1948, 240(826): 599-642.

[8] Hiders J, Bergqvist. A Simple Vector Generalization of the Jiles-Atherton Model of Hysteresis [J]. IEEE Transactions on Magnetics，1996,32(5):4213-4215.

[9] Dupré L, Melkebeek J. Electromagnetic hysteresis modelling: from material science to finite element analysis of devices [J]. International Compumag Society Newsletter, 2003, 10(3): 4-15.

[10] https://www.comsol.com/release-history

[11] Multiphysics C. 5.2, 2015 [J]. COMSOL Multiphysics: a finite element analysis, solver and simulation software for various physics and engineering application, especially coupled phenomena, or multiphysics. URL http://www. comsol. com.

[12] Campbell P., Al-Murshid S. A model of anisotropic alnico magnets for field computation [J]. IEEE Transactions on Magnetics, 1982, 18(3): 898-904.

Chapter V. Hardware Design: Circuit and Structure

V.1. Introduction

The design of SEP magnet and the linear motor made of SEP magnets build the foundation of our distributed modular robot system. This Chapter is mainly a presentation of the design and hardware of our distributed modular robot system, whose name is DILI.

The DILI modular robot was designed after the Smart Block project as seen in the previous chapters. In this chapter, we present our contributions regarding, in particular, the design of an electronic circuit which allows us to achieve fast and smooth module motion. We also detail the design of the DILI module. As already mentioned in Chapter III, SEP magnets move thanks to current pulses. Each DILI module will contain several linear motors. We recall that each linear motor needs at least two SEP magnets. As a consequence, the control system and control strategy are complex. In Section V.2, we consider the design of the electronic circuit dedicated to pulse generation (our goal is to obtain a simple and small system, with high execution speed). Section V.3 introduces the microcontroller and circuit board.

The structure of the modular robot is very important, as described in Chapter II. There is a variety of modular robot structures. The structure directly determines the motion possibilities. At the same time, a reasonable structure can also ensure energy savings during the process of moving. We also note that, in the case of 2D motion, the robotic module needs to have the function of connection and motion. In Section V.4, we concentrate on the physical implementation of the DILI robot.

Section V.5 presents the motion and connection principle or DILI robot. In Section V.6, we test the performance of the DILI robot via a series of experiments, such as the speed on different surfaces, holding force. We test its vertical force, which also laid the foundation for DILI to achieve 3D movement in the future. The conclusion of this chapter is given in section V.7.

V.2. Pulse Signal Generation Circuit

As mentioned in chapter III, pulse signals are used to change the direction of magnetic field of SEP magnets. Coercive force (intrinsic) is the property of the material that decides what magnetic field strength is needed for magnetization. Axial and diametrical magnetization can be made in standard inductors, i.e. solenoids. However, radial, multiple poles, or any other complex kind of magnetization must be obtained thanks to a special magnetization device.

When the pulse signal passes through the solenoid, it generates a pulse magnetic field in its interior. In general, when the peak value of the pulse magnetic field reaches 3-5 times the material coercivity, the material can be fully magnetized [1].

V.2.1. Capacitance pulse discharge

There are two main methods for generating large pulse current, using a strong pulse power or using a capacitor [2]. Since distributed robot systems generally require a smaller volume, we choose the latter one. Capacitance pulse discharge also has the advantage of a simple structure; it requires low power and is easy to control. Figure V-1 displays a schematic diagram of it.

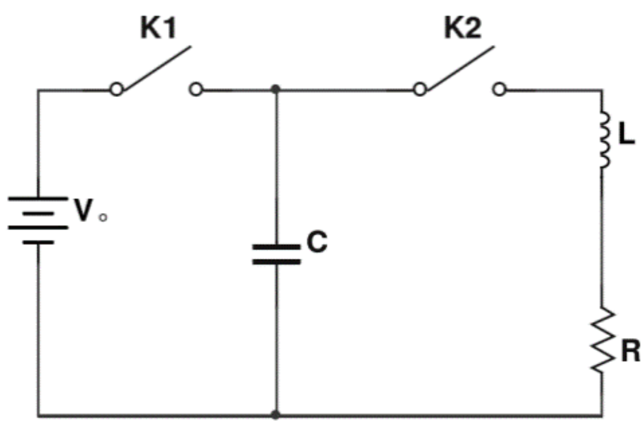

Figure V-1 Schematic diagram of capacitance pulse discharge

As shown in Figure V-1, when the switch *K1* is closed, capacitor *C* will be charged by the power source. Then disconnect *K1*, close *K2*; the circuit forms a typical RLC oscillator circuit. In this case, a constant coefficient second order linear homogeneous differential equation can be formed; *u* is as an unknown quantity. That is given as follows,

$$LC\frac{d^2u_c}{dt^2}+RC\frac{d\ u_c}{dt}+u_c=0\,, \tag{5.1}$$

Let β be the damping coefficient, $\beta=\frac{R}{2}\sqrt{\frac{L}{C}}$, and ω to be the angular frequency $\omega=\sqrt{\frac{1}{LC}}$, $i=-C\frac{du_c}{dt}$.

The initial conditions are when $t = 0^+$, $u_c = U_0$, $i = 0$. Depending on different circuit parameters, the following three conditions are calculated:

1) When $\beta = 1,\ R=2\sqrt{\frac{L}{C}}$, the circuit is in critically damped state,

$$LC\frac{d^2u_c}{dt^2}+RC\frac{d\ u_c}{dt}+u_c=0\,, \tag{5.2}$$

2) When $\beta > 1, R>2\sqrt{\frac{L}{C}}$, the circuit is in over-damped state,

$$\mathrm{i}(t)=\frac{CU_0\omega}{\sqrt{\beta^2-1}}e^{-\beta\omega t}sh\left(w\sqrt{\beta^2-1t}\right), \tag{5.3}$$

3) When $0<\beta < 1, R<2\sqrt{\frac{L}{C}}$, the circuit is in under-damped ringing state,

$$\mathrm{i}(t)=\frac{CU_0\omega}{\sqrt{1-\beta^2}}e^{-\beta\omega t}\sin\left(w\sqrt{1-\beta^2 t}\right) \tag{5.4}$$

Waveforms of the signal associated with three different states are shown in Figure V-2. Intuitive looking, the current peak in the case of the second state is too low. In the third case we have a high-current peak, but the presence of a negative pulse will play the role of degaussing. So, the case of first state is suitable for magnetization.

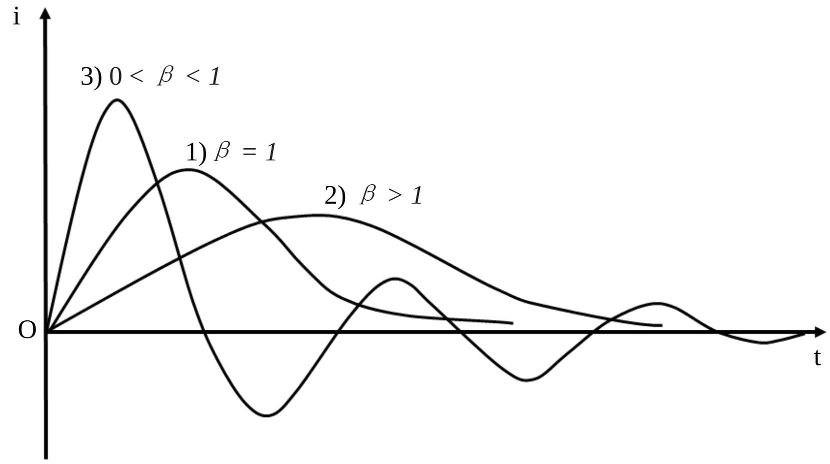

Figure V-2 Waveforms of the three states of the capacitance pulse discharge

V.2.2. H-bridges for controlling the magnetization direction

In Figure V-1, we can observe that the width of the pulse is determined by the time to turn-on and turn-off the switch K2. Since we want to control the SEP magnet to achieve both positive and negative direction of the magnetization, we must use a special switch to obtain two-way current control; this special switch is H-bridge. H bridge is an electronic circuit that enables a voltage to be applied across a load in either direction. This circuit is often used in robotics and other applications to allow DC motors to run forward or backward [3].

An H bridge is built with four switches (electronical or mechanical). By controlling the four switches, we can control the load to move forward, move backward and stop. Figure V-3 shows its topology, and its working principle, the load is a motor. When the switches S 1, S 4 are closed, and S 2, S 3 are opened, a voltage is applied across the motor from left to right. When the switches S 1, S 4 are opened, and S 2, S 3 switches are closed, the voltage is applied across the motor from right to left. Table V-1 details the status of switches in H-bridge and its result. If only one switch is closed, H-bridge cannot work. Thus, these states are not included in the table.

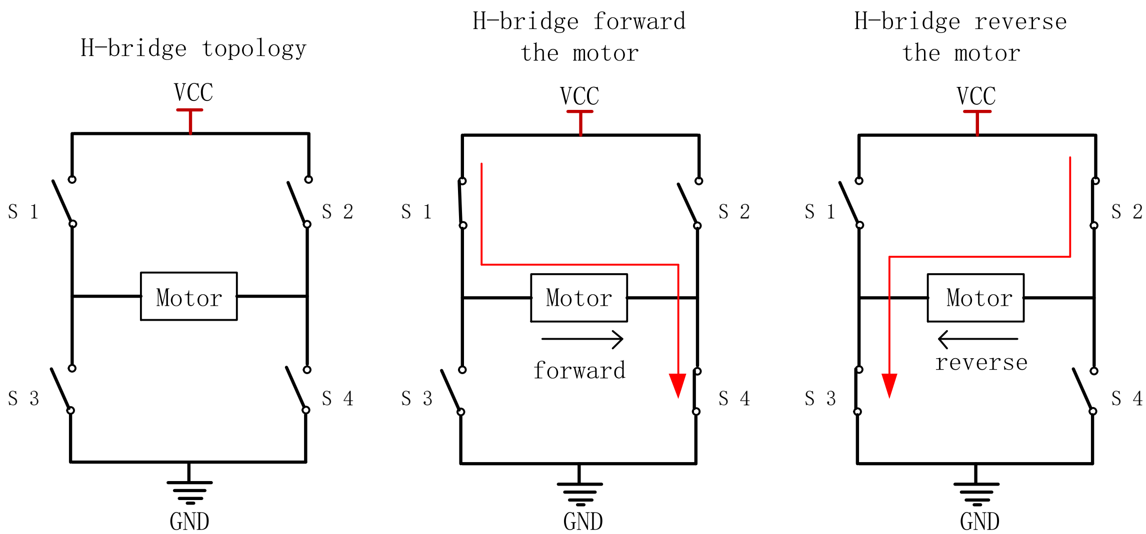

Figure V-3 Principle of H-bridge

Table V-1 Status of switches of H-bridge

Motor status	**Switch status (1 for close, 0 for open)**			
	S1	**S2**	**S3**	**S4**
Motor moves right	1	0	0	1
Motor moves left	0	1	1	0
Motor brakes	0	1	0	1
	1	0	1	0
Short circuit	1	1	0	0
	0	0	1	1
	0	1	1	1
	1	0	1	1
	1	1	0	1
	1	1	1	0
	1	1	1	1

V.2.3. Dead-time in H-bridges

MOSFET [3] technology responds quickly and can pass high current; it is used as a switch of H-bridge for robots. Figure V-4 is a typical scheme of H-bridge made from MOSFET. In a practical case, we found that such a circuit has a dead-time phenomenon. Dead-time is also called as shoot-through protection or no-overlap PWM (Pulse Width Modulation). Generally speaking, its presence is a good thing in most instances.

When turning one MOSFET off, while turning the other MOSFET on, for a short while both the low and high-side MOSFETs are potentially conducting to a certain degree, creating a relatively low resistance path from the supply to the ground. This can result in a current spike which is quite problematic. The dead-time permits one to avoid this problem.

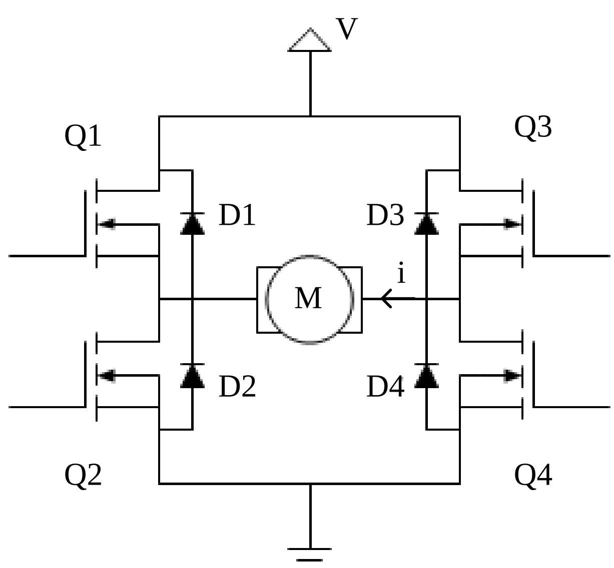

Figure V-4 Scheme of H-bridge circuit

Dead-time is an inherent characteristic of MOSFET. It is mainly due to a small amount capacitance in MOSFET. This capacitance information is usually found in the MOSFET data sheet. Table V-2 displays the capacitance parameters of two common transistors.

Table V-2 Capacitance parameters of two MOSFET

Items	**MOSFET**	
	Irf8736pbf	**Irf9310pbf**
Input Capacitance	2315 pF	5250 pF
Output Capacitance	449 pF	1300 pF
Reverse Transfer Capacitance	219 pF	880 pF

V.2.4. Drawbacks of dead-time

The presence of dead-time can be a drawback of SEP magnet. A MOSFET is limited in its speed to switch on and off by the amount of time that it takes to charge and discharge the small amount capacitance in its structure. The most direct consequence of dead-time is to cause a delay. Theoretically, the dead-time can be calculated. The most important parameters are turn-on and turn-off times.

In addition to the delay, there are other effects of dead-time. In Figure V-4, we suppose that in the beginning, during the dead-time, Q1 is open, Q2, Q3, and Q4 are off. Since the current flows in different directions, the power unit output level will be different. As shown in Figure V-5, when the current flowing through the power unit is greater than 0, that is $i > 0$, the power unit output voltage is U_{dc}, conversely when $i < 0$, the output level is 0. Therefore, during the dead-time, since the current flows to a different direction, the actual output voltage of the power unit is as shown in Figure V-5 (e) and (f). Obviously, when $i > 0$, the actual output voltage will increase by amount that corresponds to $U_{\mathrm{d}}T_d/T_s$, when i < 0, the actual output voltage will decrease by amount that corresponds to $U_{\mathrm{d}}T_d/T_s$. This will cause the distortion of the output waveform; generate new harmonic components; reduce the effect of active filtering.

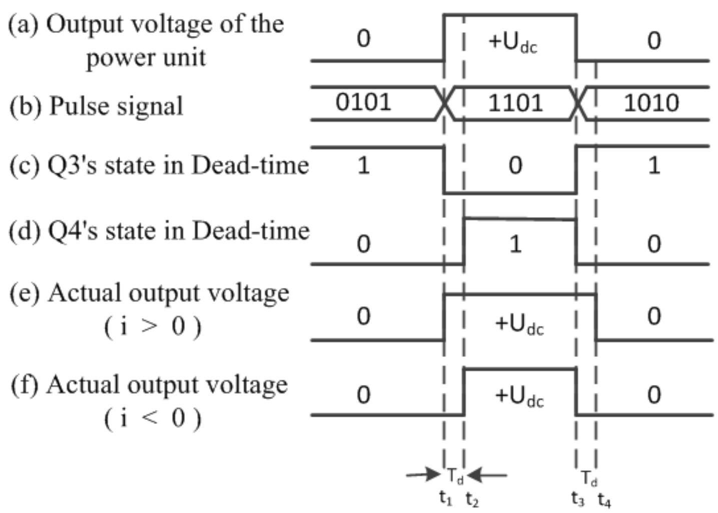

Figure V-5 Timing diagram showing the effect of dead-time

V.2.5. Dead-time controllable H-bridge

We measured the dead-time with an oscilloscope. It is equal to 130ms. This is longer than charging time of the capacitor (100ms). So, we improved the H-bridge whose dead-time is controllable; the improved circuit is presented in Figure V-6. In this new circuit, each MOSFET can be controlled independently by one Input / Output (I/O) of micro-controller, instead of one I/O to control a half-bridge like in [4]. The advantage is that the ON and OFF time of each MOSFET can be precisely calculated and can be directly controlled by the microcontroller. Meanwhile, the dead-time can be controlled according to the expected speed of modules.

In addition to re-improving the H-bridge, we also used a half-bridge multiplex design. With this design, the complexity of the circuit can be reduced. Thereby, the size and weight of actuator can also be reduced. This is necessary for micro-robots. The specific structure is as shown in Figure V-7, the switches S 1 and S 2 form a common semi-H-bridge, like switches S 3 and S 4 or S 5 and S 6 or S 7 and S 8, respectively. Thus, the common semi-H-bridge and the other three semi-H-bridges form a total of two pairs of H-bridges, with a total of four semi-H-bridges instead of six. For example, when the magnetization direction of SEP 2 need to be controlled in positive, we only need to close switch S 1 and switch S 6, the other remains open. We note that this design cannot simultaneously magnetize two SEP magnets since we could obtain incomplete magnetization.

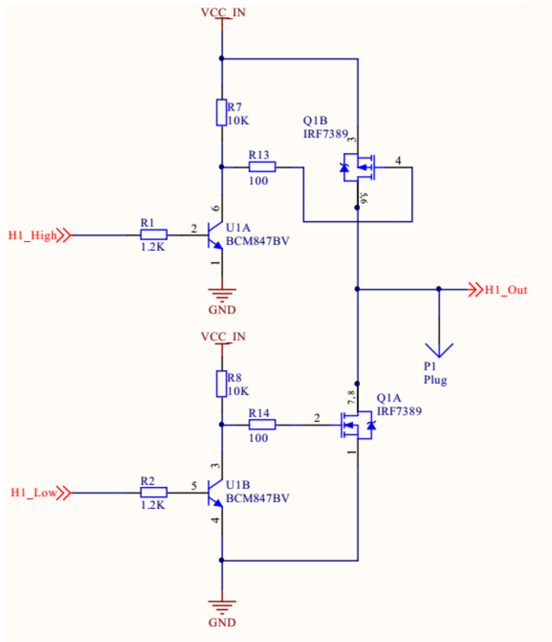

Figure V-6 Dead-time controllable semi-H-bridge

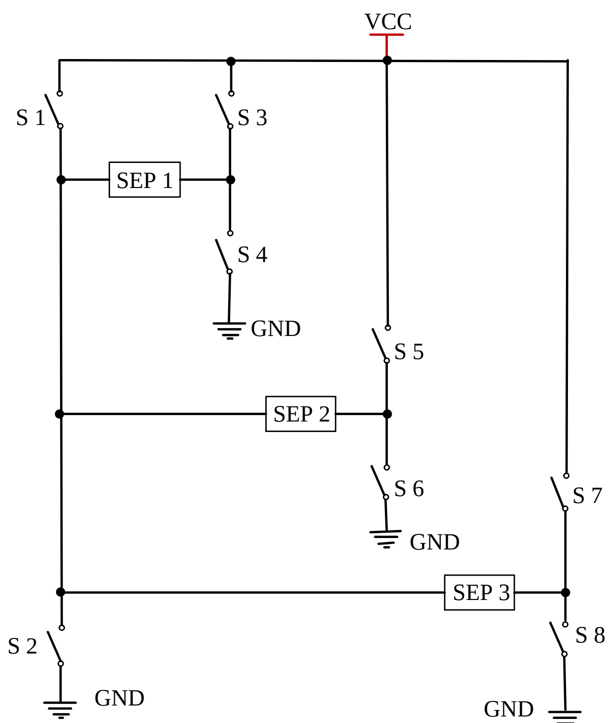

Figure V-7 Half-bridge multiplex design

V.3. Microcontroller and Circuit

DILI robot system uses the STM32F103, a 32-bit enhanced flash memory microcontroller as the core. STM32F103ZE is based on Cortex-M 3, which is specifically designed to meet the requirements of embedded systems that must meet high performance, low power, and real-time applications. The maximum operating frequency of this core is up to 72 MHz. Its rich interface resources greatly simplify the system hardware, while greatly reducing system power consumption. This also lays the foundation for the future functional upgrading of the system. Table V-3 presents the key features of STM32F103. The circuit that we designed is shown in Figure V-8, it is a 35mm*35mm board. The PCB (Printed Circuit Board) and real circuit board are shown in Figure V-9. In order to facilitate the scalability of this system, we designed another board which contains only 8 semi-H-bridges, it has the same size as the main circuit and can connect to the main board. Figure V-10 shows the detail of the bridge circuit board.

Table V-3 Key features of STM32F103 microcontroller

Key features	Description
Low power consumption	Three low power modes: Hatch, Stop and Standby.
Debug mode	Support for serial debug (SWD) and JTAG interface download.
Memory	With built-in high-speed memory (512K Flash and 64K SRAM), it does not need to use a special external Flash or ROM.
I/O port	26/36/51/80 compatible 5V multi-function bi-directional I/O port, all I/O port can be mapped to the external 16 interrupts.
Timer	It has up to 11 timers: four 16-bit timers, two 16-bit 6-channel advanced control timers, two watchdog timers (an independent watchdog and window watchdog), Systick timer and two 16-bit basic timers for driving the DAC.
communication interfaces	It also has up to 13 communication interfaces: two IIC interface (SMBus/PMBus), five USART interface, three SPI interfaces (18Mbit/s), one CAN interface (2.0B), one USB2. 0 full-speed interface and one SDIO interface.
Two 12-bit AD/C converters	16 input channels, conversion time, is 1 microsecond (measuring range 0-3.6V), with dual sampling, hold function.

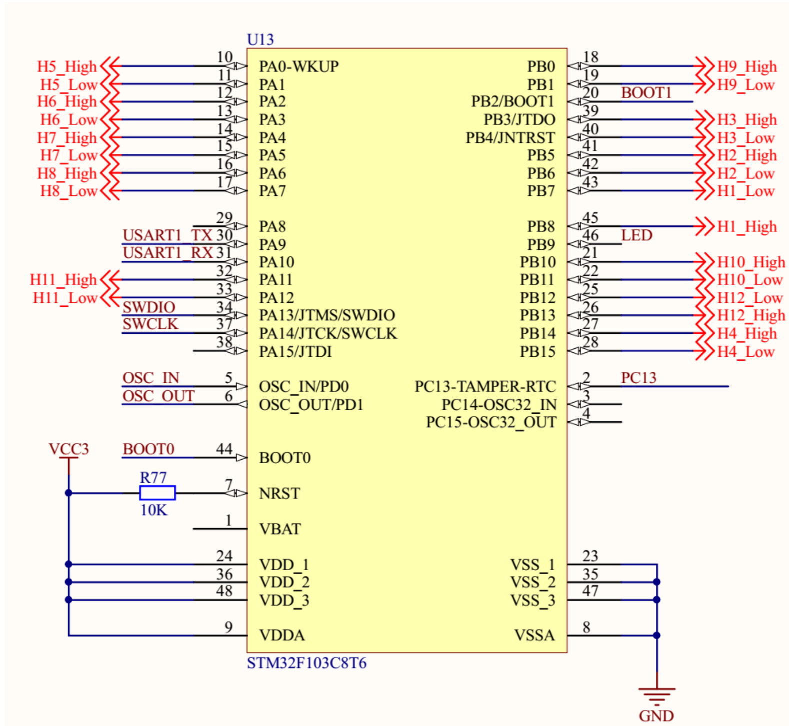

Figure V-8 Circuit of the main board

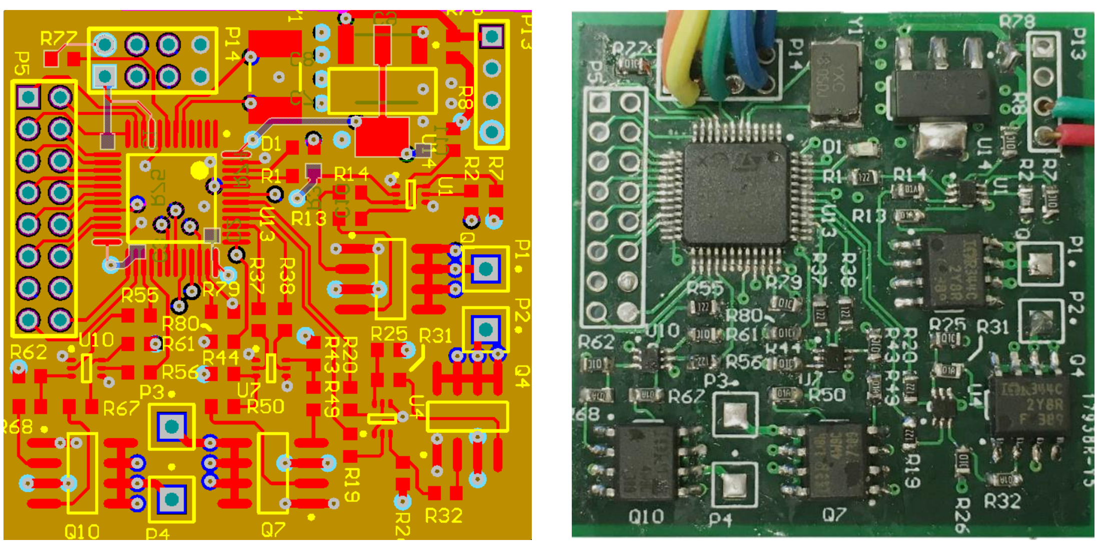

Figure V-9 PCB and the real main board for controlling our robot

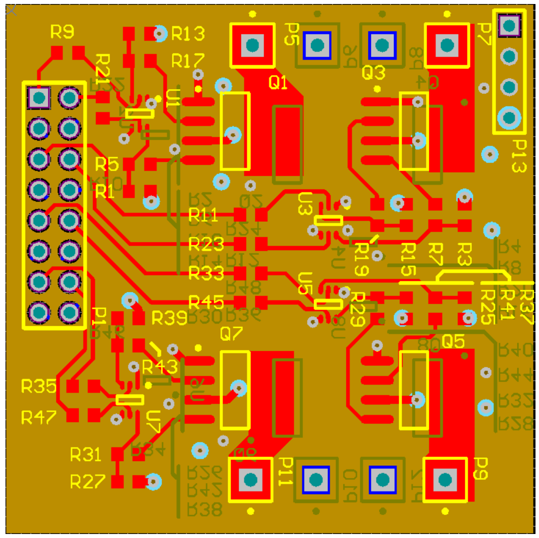

Figure V-10 Bridge circuit board

For controlling propose, we connect a Bluetooth module to the main board the serial port. Thus, we can send information to the main board by smartphone or PC.

V.4. Structure of DILI Robot

This subsection is devoted to the presentation of the DILI module. As shown in Figure V-11, we design DILI according to a cubic shape with sides 1.5 cm. The basic structure is built in one part via 3D print technology with the material of PLA (Poly Lactic Acid). In addition to the top and bottom, each module has four work surfaces devoted to both motion and connection. The bottom is smooth and used for sliding. Each module has six large holes for SEP magnets and four small holes for NdFeB magnets; they are placed in two layers. The only strict limit of the distance between the NdFeB magnets is half bigger than the distance between the EP magnets so that cubes can move in the desired direction. The Alnico5 magnet in SEP magnet has a size of 1.5 mm in diameter and 8 mm in length and wrapped with 250 turns of 0.15 mm enamel copper wire.

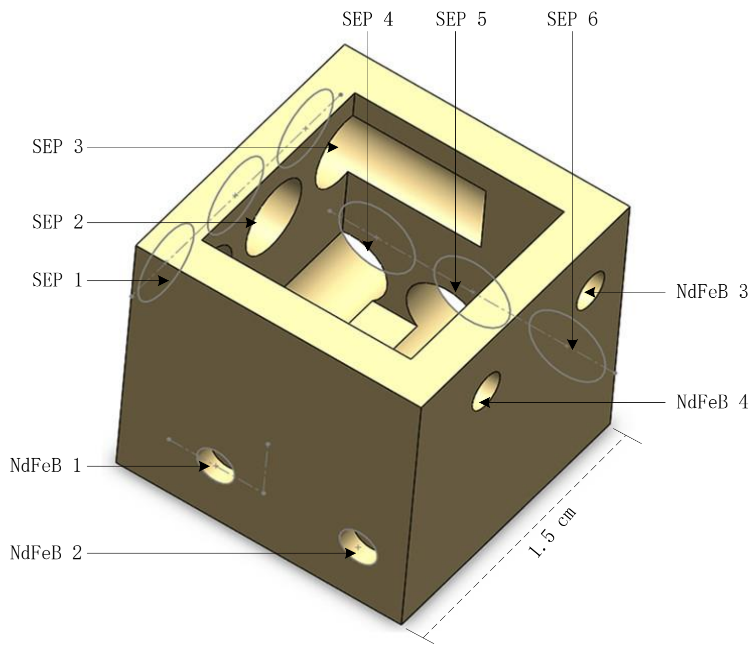

Figure V-11 Structure of DILI robot

Figure V-12 and Figure V-13 are section views of large holes and small holes on DILI module. The diameter of the large holes are 4 mm, they penetrate from the outer wall to the inner; the four holes that are close to the wall are embedded inside the wall. This kind of design can not only save space but also can reduce the weight. We expect also this design to improve the stability of the module and lead to smooth motion. The diameter of the holes are 2 mm, in order to install NdFeB magnets precisely and keep them parallel to the outer wall, the small holes are not situated in the wall. Figure V-14 shows the 4 working surfaces (a), 6 SEP magnets (b) and 4 NdFeB magnets (c) with real DILI module. We place the small holes and big holes sufficiently apart so that the magnetic field generated by SEP magnet does not affect the NdFeB magnets which could have an impact on the motion of modules and the strength of connections between modules.

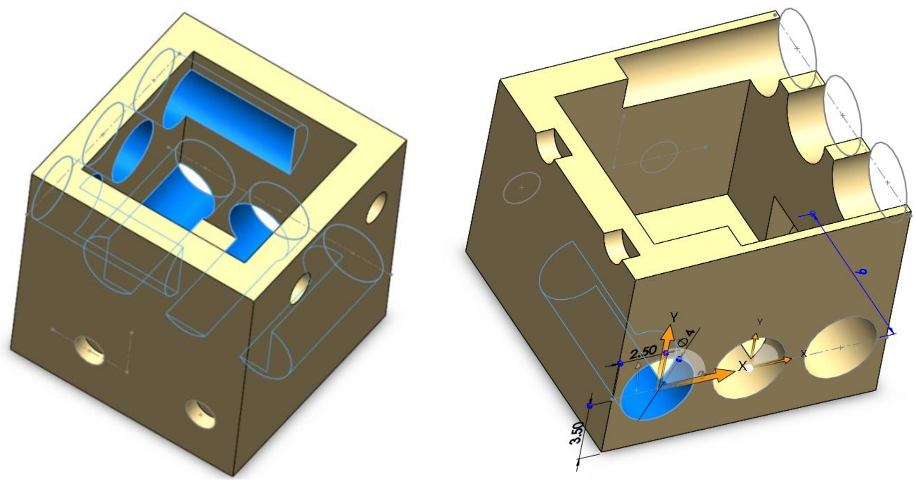

Figure V-12 Details of big holes on DILI for SEP magnets, right part corresponds to a cut of DILI module

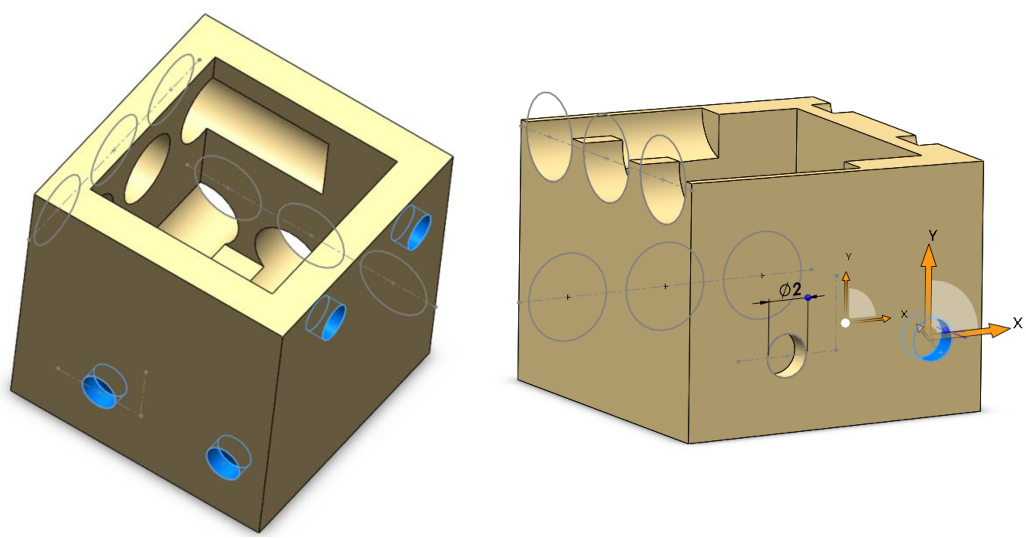

Figure V-13 Details of small holes on DILI for NdFeB magnets, right part corresponds to a cut of DILI module

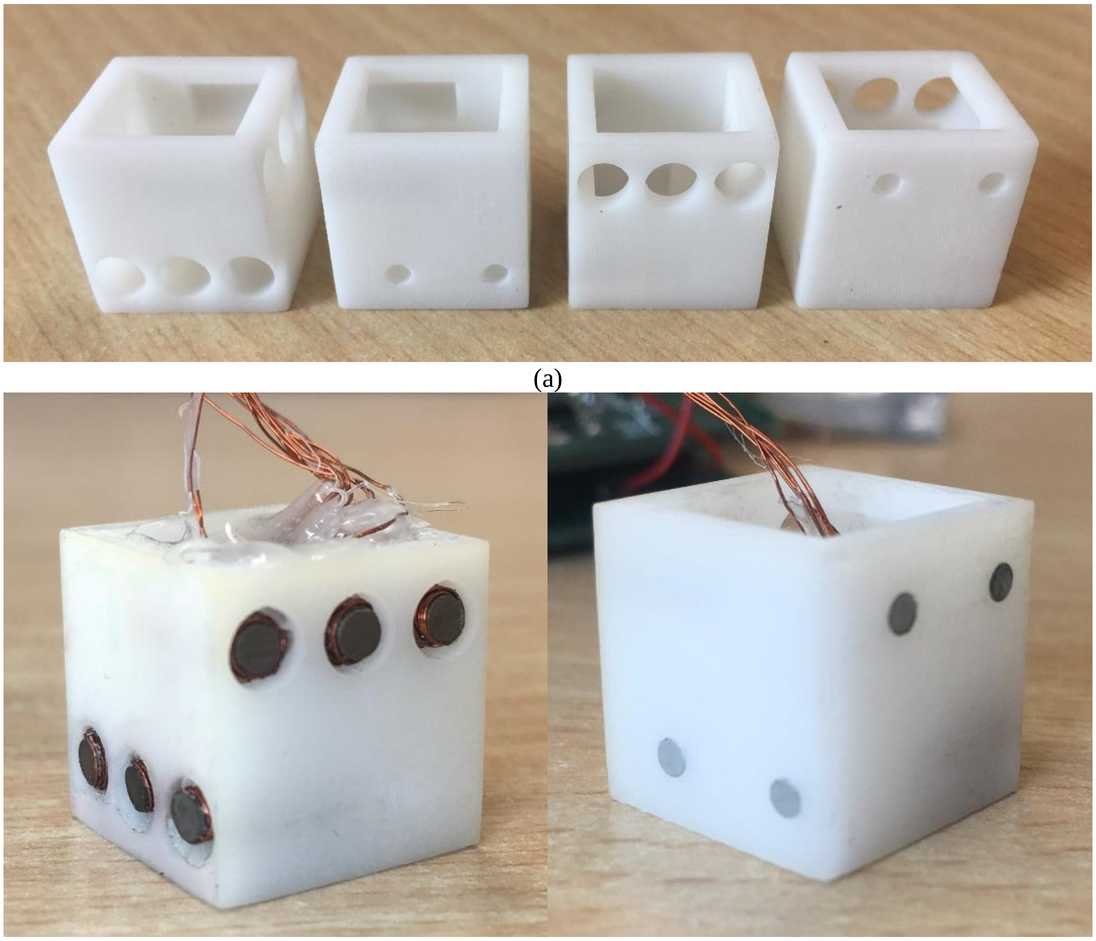

(a)

(b) (c)

Figure V-14 Real DILI module: (a) working surfaces of DILI module; (b) two sides with SEP magnets; (c) two sides with NdFeB magnets

In DILI, the working surfaces between modules are divided into two layers according to the height. The surface with NdFeB magnets faces the surface with SEP magnets in the same height, as shown in Figure V-15. The three SEP magnets and two NdFeB magnets form a linear motor. Thus, each module can move by itself or can be driven by other modules. Placing the SEP magnets and NdFeB magnets in two layers can not only guarantee every side has the ability of motion, but also makes full use of the space and reduces the volume.

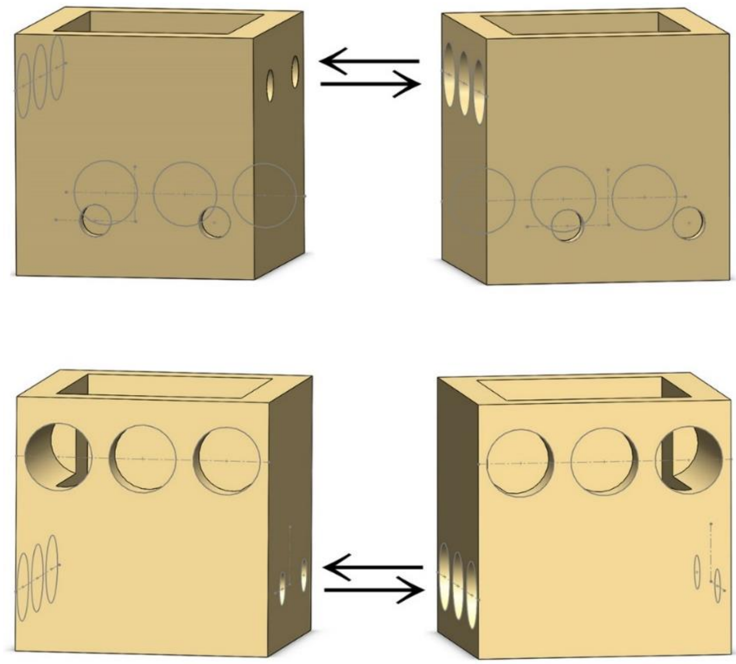

Figure V-15 Relative positions of two DILI modules for working purpose

V.5. Motion and Connection Principle of DILI Robot

Figure V-16 shows the status of SEP magnets in a complete movement process along a distance of one module (from left to right). Six steps are needed to achieve the whole motion. At each step, only one SEP magnet changes its status and the system only needs energy at that time. The order of the SEP magnets which change the status is **3-1-2-3-1-2**. When the movement ends, modules do not need the energy to fasten to each other, since modules can fasten each other by the permanent magnetic field generated by Alnico5 magnets and NdFeB magnets. The new linear motor can be made as tiny as possible; the limitation is the size of Alnico5 magnet and coil. The new linear motor is easy to build and can provide both driving force and fastening force. Another advantage of the linear motor is that it can move in any direction, due to the controllability of the polarity of Alnico5 magnet. For example, if we want to return the module to the original location, we only need to change the status of SEP magnets in order **1-3-2-1-3-2.**

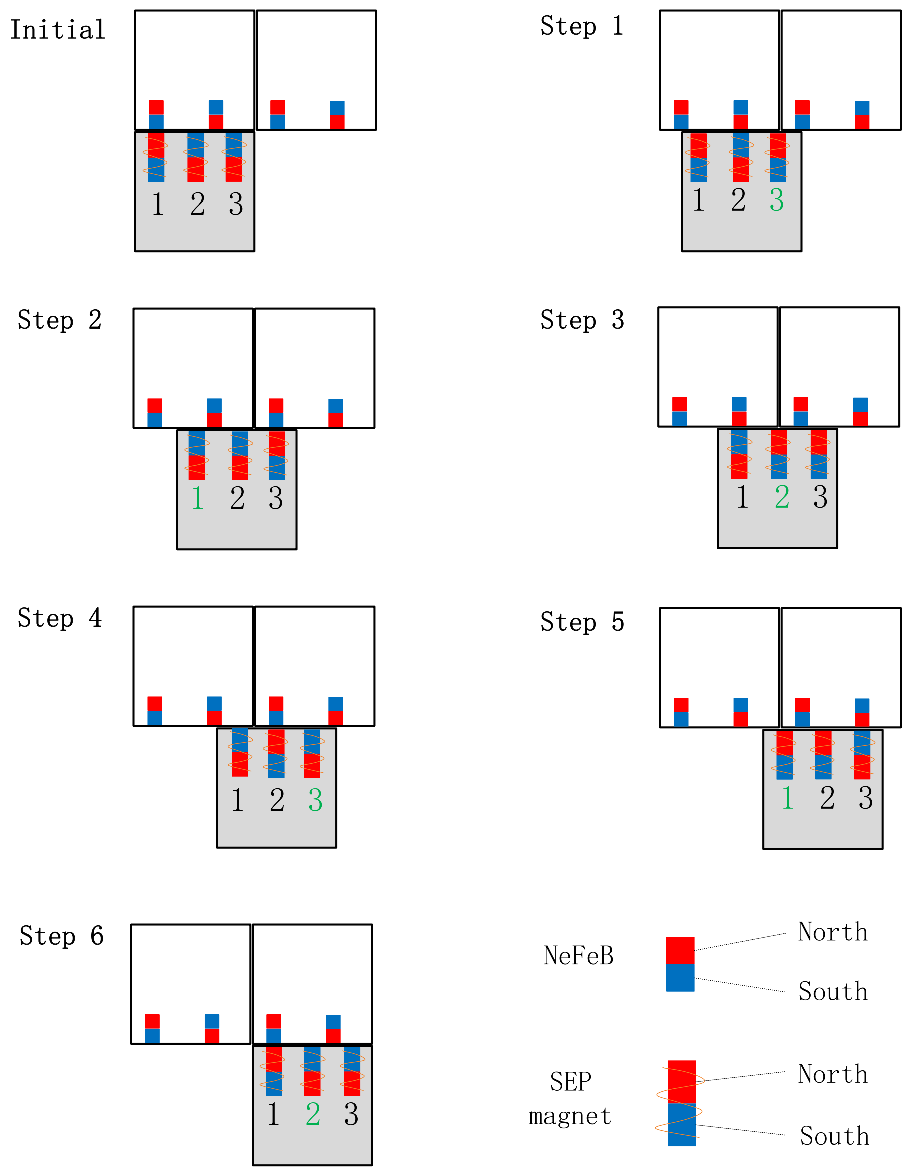

Figure V-16 Status of SEP magnets in one complete movement process

V.6. Experiments

We concentrate on the motion and connection functions. We have built a platform to test the two functions. For the speed, we have designed an ultrasonic velocity tester, by detecting the send and return signal to determine the speed of modules. We use a miniature tensile force measure instrument to measure the holding force.

V.6.1. Speed test

Table V-4 shows the speed of DILI on different surfaces for three operating modes. These three modes are:

- the stable mode;
- the enhanced mode;
- the fastest mode.

In the stable mode, the DILI module can move without error. The parameters of stable mode are chosen after many experiments; this mode can not only guarantee fast motion but also ensures the stability of the system.

The enhanced mode is relatively similar to the stable mode; the difference is that a 0.8 A continuous current is applied to the coil (for more details we refer to subsection 2.3).

The fastest mode is achieved by reducing the dead-time to few microseconds. We also reduce the time between two consecutive pulses as much as possible. It should be noted that, in the fastest mode, the motion may present some error, like an incomplete motion. The reason is that the Alnico5 magnet is not fully magnetized in the fastest mode.

Table V-4 Speed test on different surfaces

Materials / Mode	Glass	Paper	Wood	Cement
Fastest mode	20mm/s	20mm/s	18mm/s	18mm/s
Stable mode	13mm/s	13mm/s	12mm/s	12mm/s
Enhanced mode	9mm/s	9mm/s	9mm/s	9mm/s

We sort the friction between the surfaces and the DILI from small to large: $V_{glass} < V_{paper} < V_{wood} < V_{cement}$. For each mode, we note that the speed is almost indistinguishable on the different surfaces.

The reason that the surface has slight effects on the speed is that the movement of DILI is controlled by pulses. The movement is stepping forward rather than linear. When the block moves from one position to the next position, the initial speed is zero; the final speed is also zero, there is no speed accumulation. So, the previous move did not affect the next move. Figure V-17 is the screenshot of the test. A video of our test is presented in [5]. On the video, we observe a particularly smooth motion of the module; experiments were carried out on a wood surface with the Stable mode in Table1.

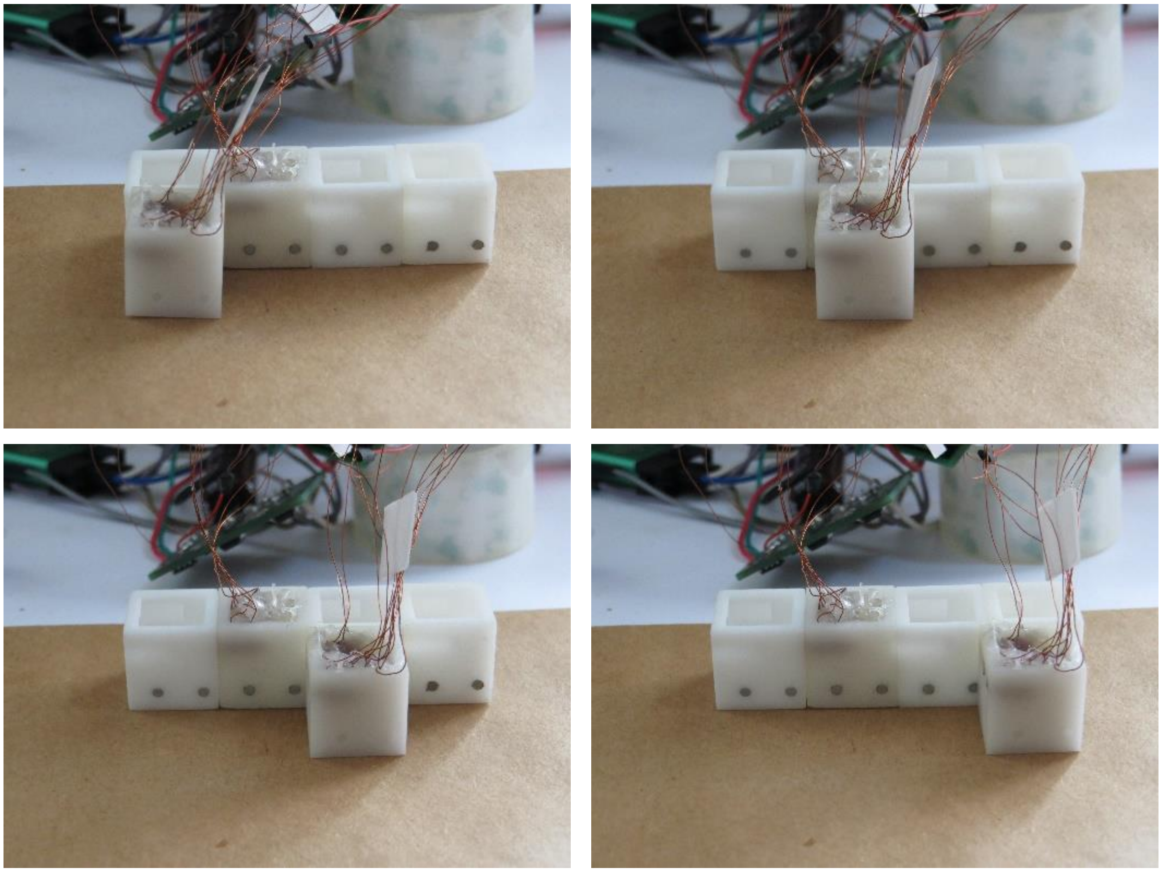

Figure V-17 Speed test

V.6.2. Holding force test

The holding force that we tested is the positive tension between two blocks. The holding force is related to the magnetic field of Alnico5 magnet in SEP magnet, holding force reaches the maximum when Alnico5 magnet reaches saturation. The intensity of the magnetic field of Alnico5 magnet is related to the number of pulses and the applied voltage. Figure V-18 shows the results of holding force test in millinewton at different voltage values and a different number of pulses. We can summarize the following results:

a) If the voltage is less than 4 V, the circuit cannot produce a holding force.

b) Holding force increases as the voltage rises.

c) Generally, the higher the number of pulses, the greater the holding force. But there is a saturation value, when the saturation value is reached, if the voltage does not change, then the holding force does not increase as the number of pulses increases.

d) The greater the voltage, the less the number of pulses required to reach a saturated holding force. For example, when the voltage is 16 V, only one pulse is needed to reach the saturated holding force.

We also note that the sinusoidal signal is more favourable than a pulse for the magnetization of the magnet to achieve greater magnetic flux density. So, we changed the pulse to sinusoidal signal and measured the holding force again. The result is displayed in Figure V-19. Obviously, with a sinusoidal signal, the holding force can be greatly increased. In some case, with the same voltage (i.e. 16 V), the holding force generated by the sinusoidal signal (140 mN) is nearly twice as much as the holding force generated by pulse signal (75 mN).

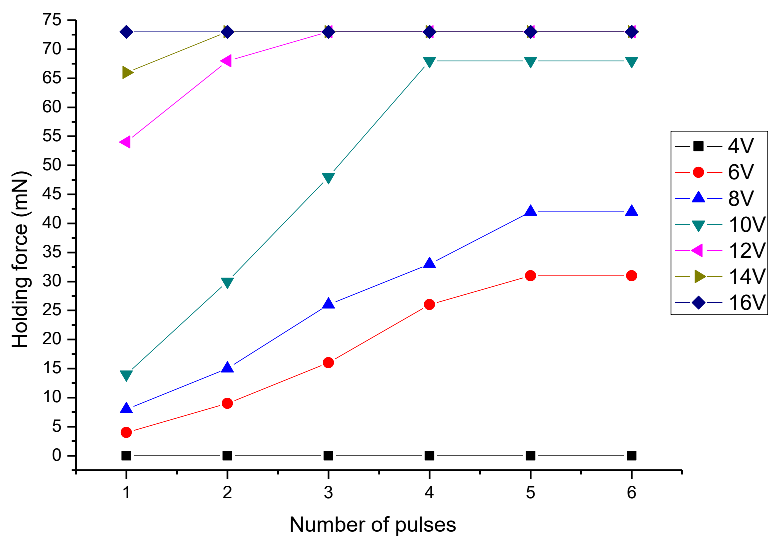

Figure V-18 Holding force test with pulse signal

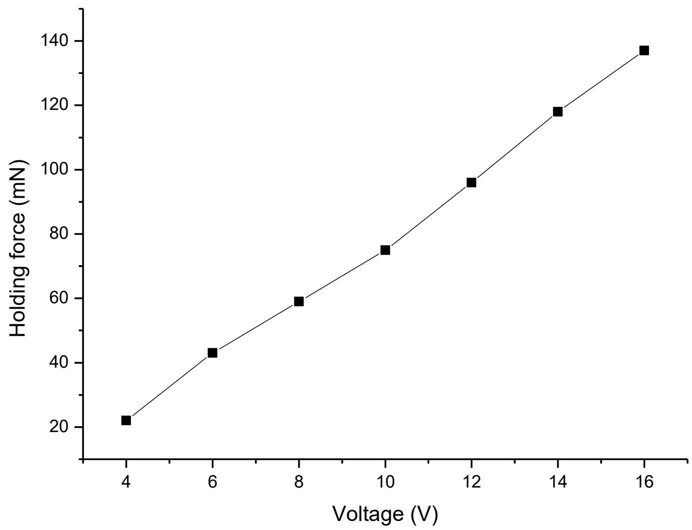

Figure V-19 Holding force test with sinusoidal signal

V.6.3. Vertical force test

This version of DILI was designed for 2D motion. We test the vertical holding force as shown in Figure V-20. Since the size of SEP magnet is small, the holding force of the vertical surface is enough for holding but not enough for moving. When trying to move upward, there is a moment when module falls that corresponds to the smallest vertical holding force (static). In the next generation of DILI robot, we plan to improve the design for permitting modules to have 3D motion.

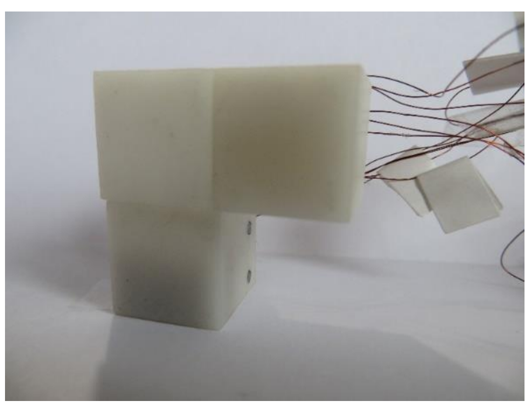

Figure V-20 Static vertical force test

V.7. Conclusion

Based on the research work in Chapter III and Chapter IV, we successfully build the DILI, module of our distributed robot system. Firstly, in order to achieve a quick response, we have analyzed the dead-time in the circuit and designed two circuits, the main circuit, and the bridge circuit. Then we have designed the structure. The DILI module is a cube with 4 work surfaces, which can move in four directions. The principles of motion and connection are also detailed in this chapter. Finally, we have tested the performance of DILI robot through a series of experiments. We have sorted the friction between the surfaces and the DILI from small to large: glass <paper <wood <cement. For each mode, we note that the speed is almost indistinguishable on the different surfaces. About the holding force, we can summarize the following rules:

a) If the voltage is less than 4 V, the circuit cannot produce a holding force.

b) Holding force increases as the voltage rises.

c) Generally, the more the number of pulses, the greater the holding force. Nevertheless, there is a saturation state whereby the holding force does not increase when the number of pulses increases.

d) The greater the voltage, the less the number of pulses required to reach a saturated holding force. For example, when the voltage is 16V, only one pulse is needed to reach the holding force at saturation state.

References in Chapter V

[1] Lin D., et al. A new nonlinear anisotropic model for soft magnetic materials [J]. IEEE transactions on magnetics, 2006, 42(4): 963-966.

[2] Kim P.S., Kim Y. Field and thermal modeling of magnetizing fixture by impulse [C]. Power Electronics and Drive Systems, 2003. PEDS 2003. The Fifth International Conference on. IEEE, 2003, 2: 1301-1306.

[3] Williams A. Microcontroller projects using the Basic Stamp [M]. Gilroy, CA: CMP Books, 2002.

[4] Piranda B., Laurent G. J., Bourgeois J., Clévy, C., Möbes, S., & Le Fort-Piat, N. A new concept of planar self-reconfigurable modular robot for conveying microparts [J]. Mechatronics, 2013, 23(7): 906-915.

[5] DILI experiment video, https://youtu.be/kxlJRraiZQI.

Chapter VI. Distributed Algorithms and Simulation Software for DILI Robot System

VI.1. Introduction

Modular self-reconfigurable robotic systems are usually composed of tens or hundreds of modules. Their control is mainly divided into centralized control and distributed control. Both classes of methods have their own advantages and drawbacks. These classes of methods are suitable for different types of applications.

The structure of centralized control is shown in Figure VI-1 (a). Only one controller is used to control multiple robots. The advantage is that the topology of the control system is simple. But the centralized controller is a single node system. When the control system fails, it will likely cause instability or even paralysis of the global system. In addition, the controller needs to communicate with the modules and dynamically assign them tasks. When the number of modules increases, the traffic and computations in the controller increases rapidly, which puts forward higher requirements for the computation performance of the controller. Thus, this type of control methods is only applicable to small-scale modular robot systems. When the configuration changes, the control method needs to make a corresponding change. This approach is not scalable and difficult to adapt to complex environments.

The structure of distributed control is shown in Figure VI-1 (b). Distributed control methods do not have a hierarchical structure. Modules only carry out task planning according to the local information, which allows scalability and robustness. Modules cooperate with other modules to complete a given task. Obviously, this reduces the data traffic. Distributed control results in higher robustness and stability throughout the system. We note that a single module does not have the global information.

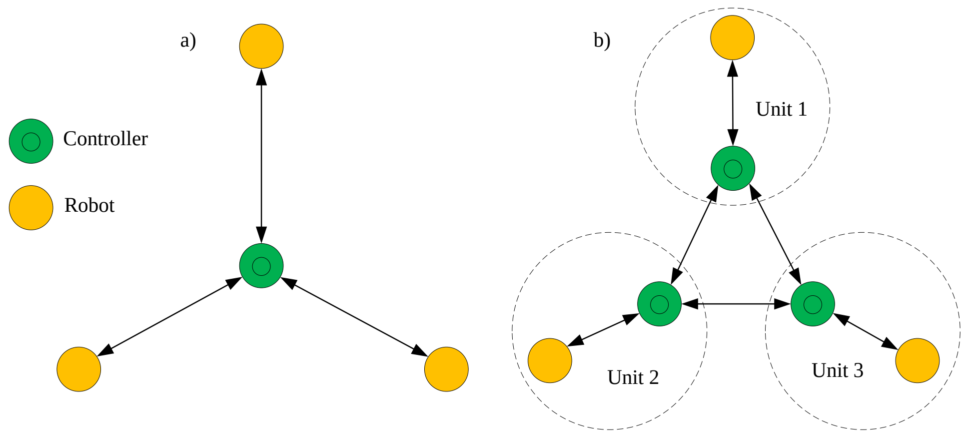

Figure VI-1 Structure of centralized (a) and distributed (b) control

Obviously, distributed control is more suitable for DILI robot since it is designed with multiple modules. This chapter deals with distributed algorithms and the simulation of motion of DILI modules via a simulator that we have designed in order to test and validate distributed algorithms. Firstly, we discuss the capabilities of DILI modules which are presented in Section VI.2. Section VI.3 details the distributed algorithms. A simulator of distributed algorithms for DILI robot system is presented in Section VI.4. The conclusion of this chapter is given in Section VI.5.

VI.2. Capabilities of DILI Module

Chapter V has already presented the motion principle of DILI module. In this subsection, we concentrate on module motion. We begin by a definition of module motion that will be used in the remaining part of this chapter.

Definition: without loss of generality, a module motion will represent a move of one or several modules along the same direction on a distance of one module.

VI.2.1. Elementary motion

Module motion relies on the interactions between modules; that is, one module slides along another module. Furthermore, when a module moves, at least two surfaces / modules are needed. As shown in Figure VI-2 (a), if we want to move module 1 to the right, then we need surface 1 as current support, and surface 2 as future support.

These characteristics make the motion of DILI very simple as compared with other distributed robotic systems. Nevertheless, this leads to some limitations on the motion as well as difficulties to complete complex tasks and even blocking situations. Figure VI-2 (b) displays an example of a blocking situation where modules 1, 2, 3, and 4 do not have another surface as future support of the motion. As a consequence, all modules cannot really carry out a module motion. This kind of situation is common in the motion process of cube-shaped modular robot systems.

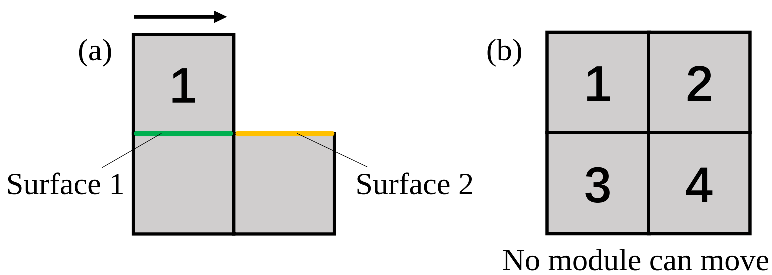

Figure VI-2 Elementary motion of DILI module

Also, we note that elementary motion of DILI module has no expansion capability. Figure VI-3 displays an example whereby, dotted arrows represent possible motion and direction. Module 1 can move one step to the east or module 3 can move one step to the north. After the motion of modules 1 or 3, some other modules can also move; but in any case, *W* (width) and *L* (length) will not change, that is, the change of shape can only happen in their own coverage area, they cannot expand the boundary. Without the possibility of expansion, the motion would be very limited.

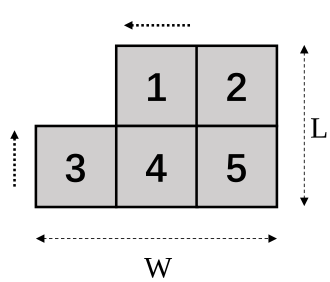

Figure VI-3 Elementary motion of DILI module without expansion capability

VI.2.2. Extended motion capabilities of DILI module

We consider now several types of complex motion mechanisms that are also possible with DILI module, i.e., Push, Pull, and Carry. Figure VI-4 displays examples of extended capabilities of the DILI robot system.

(a) Push, shows module 1 pushes module 2 from left to right;
(b) Pull, shows module 1 pulls module 2 from right to left;
(c) Carry, shows module 1 carries module 2 to right or left. Details of each capability will be given in the sequel.

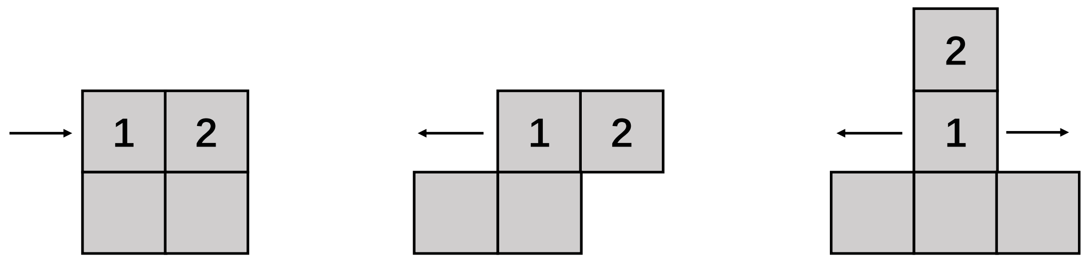

(a)**Push**
Module 1 pushes module 2
from left to right

(b) **Pull**
Module 1 pulls module 2
from right to left

(c)**Carry**
Module 1 carries module 2
to right or left

Figure VI-4 Three extended motion capability of DILI module

VI.2.3. Push capability

Push capability permits a module to push another module (see Figure VI-4 a). In order to ensure that the pushed module does not affect the movement, the SEPs of that module can be demagnetized first.

Push capability is an important capability of DILI module because it can provide expansion capacity. Figure VI-5 (a) is a top view of four DILI modules, in a two-dimensional plane. Initially, the total width is *W,* and total length is *L*. Module 1 can push module 2 to the west, as shown in Figure VI-5 (b), the arrow represents one module motion, the total width of the set of modules becomes $W + 1$, where 1 is the length of a module. If we consider the push capability of module 4, then it can push module 2 to the north, as shown in Figure VI-5 (c), the total length of all modules becomes $L + 1$. Therefore, the push function will permit one to obtain expansion.

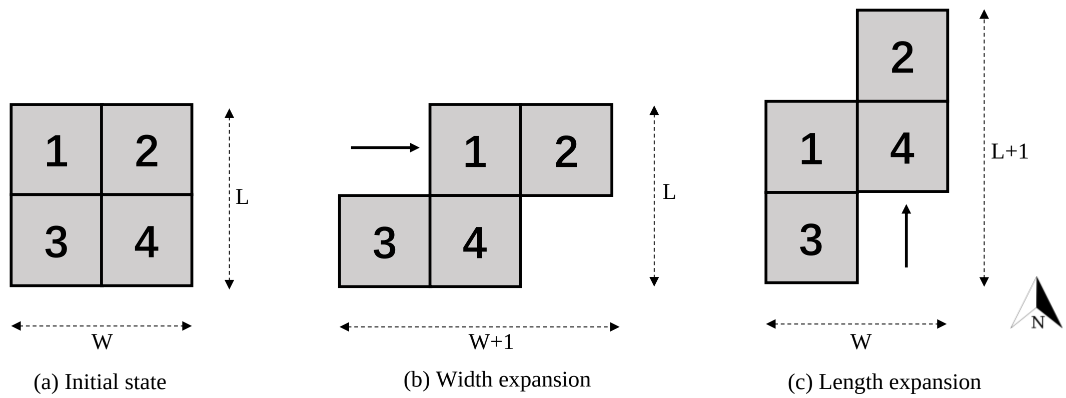

Figure VI-5 Push function providing the possibility of expansion

Another feature of the push capability is to facilitate turning. DILI is a smart system with distributed intelligence, so the turning ability is particularly important. Figure VI-6 gives an example of a module that turns. As presented before, DILI module can slide along another module in two directions. But in the edge of a path, it cannot turn directly. In Figure VI-6, if we want to move module 1 from the initial position to position A, we need to seek the support of another module, i.e. module 2. Module 2 pushes module1 to the edge; then module 1 has two sliding surfaces, then after one step, module 1 arrives at position A.

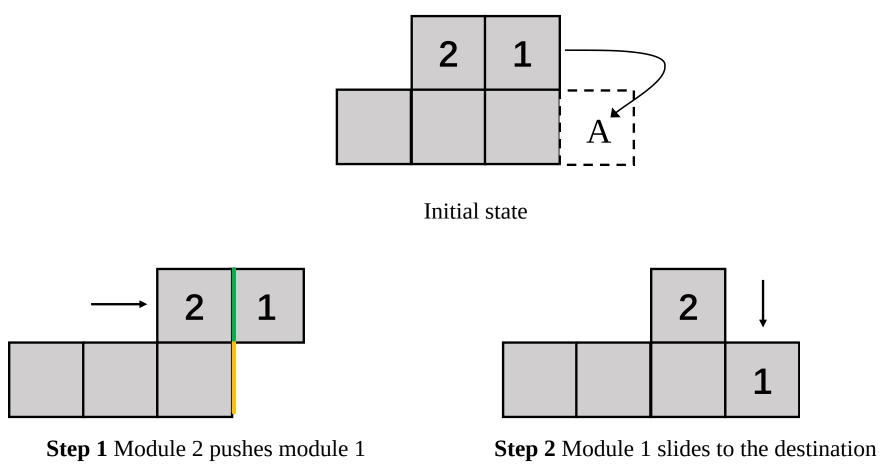

Figure VI-6 Turning strategy

Remark 1, one can encompass easily turns to the left by using a similar principle.

Remark 2, the push function can also be assimilated to the motion of trains of blocks like in [1].

VI.2.4. Pull capability

The deformation of the modular robot is a complex process of expansions and contractions; in particular, the pull capability permits one to contract the modular robot.

With the pull capability, a module pulls another module (see Figure VI-4 b). As shown in Figure VI-7, module 1 pulls module 2 to the west, the total width of all modules changes from W to $W - 1$, where 1 is the length of a module. Thus, the main function of pull capability is to provide a kind of contraction.

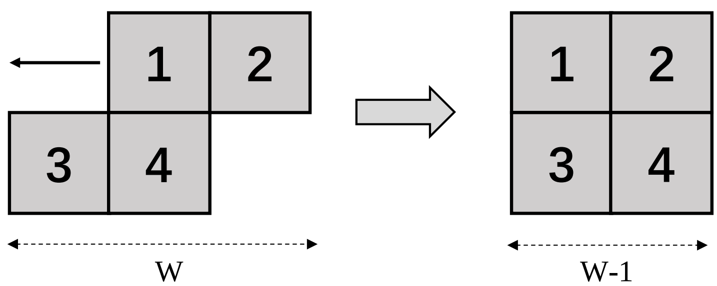

Figure VI-7 Pull capability providing contraction

It should be noted that when considering pull capabilities unless it is on the edge of the path, the module that is driven either can change the states of the internal SPE magnets to fit the movement or can be demagnetized.

VI.2.5. Combined push and pull

There is a special situation that we need to discuss here, which is shown in Figure VI-8. In this case, the module 1 and module 2 share one surface, the arrow shows the direction of motion. At this point, each module does not have a complete surface; the driving force of one module is not enough for pushing or pulling another module. So, a combination of push and pull is needed. Module 1 provides pull force, and module 2 provides push force. This is a cooperative process; we can control module 1 and module 2 as one module. We take a look at the state of the internal magnets in the related modules. There is an attractive force between NdFeB 1 and SEP 1, a repulsive force between NdFeB 1 and SEP 2; and repulsive between NdFeB 2 and SEP 3, SPE 4. The result of several force interactions is that module 1 and module 2 move to the right. It should be noted that the control of this situation is more difficult than only push or pull.

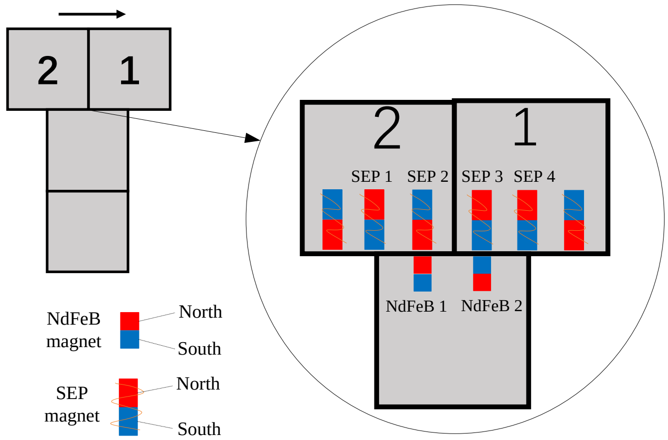

Figure VI-8 Push and pull cooperative capability

VI.2.6. Carry capability

Carry capability corresponds to the case when a module carries another module (see Figure VI-4 c). The module which is carried does not need to have the motion ability. The existence of carry capability can effectively reduce the number of movements. This point will be presented in detail in subsection VI.4.

VI.2.7. Tests of DILI module

Whatever the push, pull or carry capabilities, the key to achieving these capabilities lies in the loading capacity of DILI module. Through experiments, we prove the feasibility and stability of these three capabilities. Figure VI-9 presents our experiments. Modules 1 to 4 support motion of module 5, module 5 provides a driving force, and module 6 is the module that is driven. The arrow shows the direction of motion. An experiment video is shown in [2].

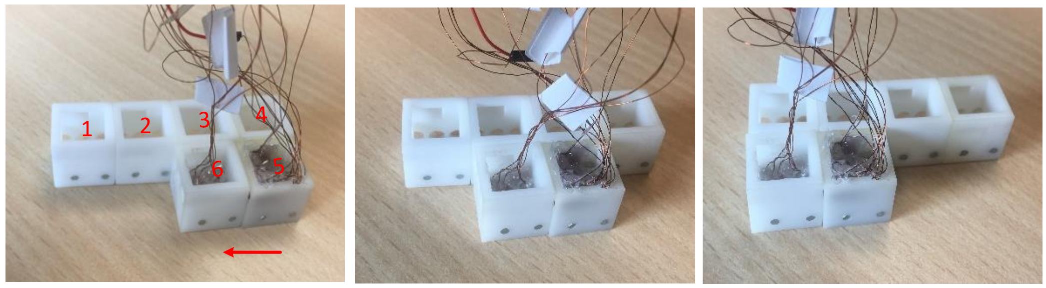

(a) Test on push capability

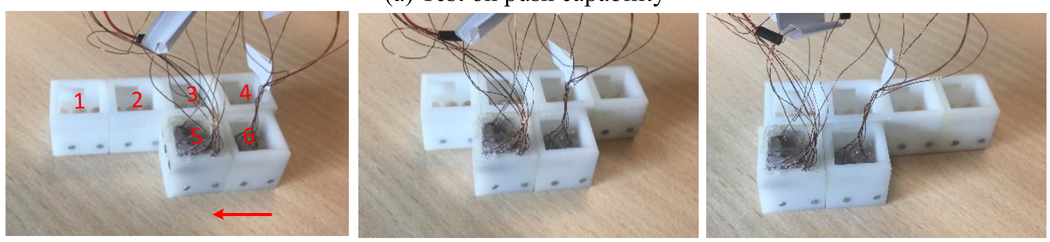

(b) Test on pull capability

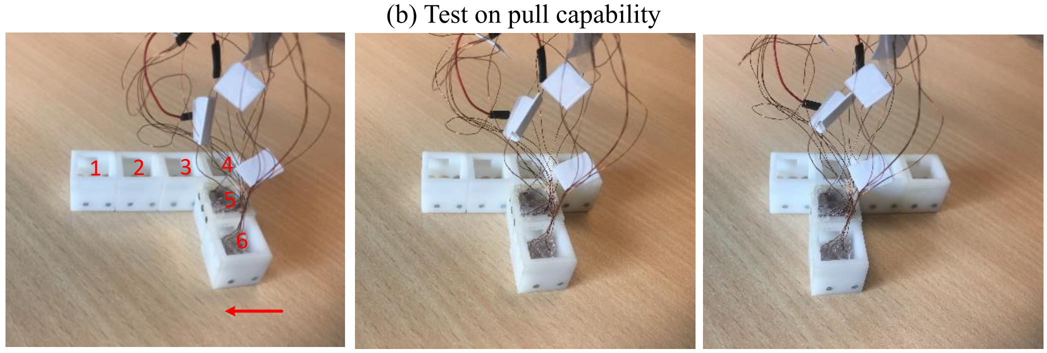

(c) Test on carry capability

Figure VI-9 Tests on the loading capacity of DILI module (arrow shows the motion direction)

We also did tests about driving two modules. The experiments show that one module can push or pull two modules, but the motion is not as good as when driving only one module. When carrying two modules, since the torque is too large, the modules tend to separate from the support. Thus, we only consider the case of driving one module in the sequel.

VI.3. Distributed Algorithm

In this section, we present the distributed algorithm for controlling multiple connected DILI modules so that they form a specific shape via cooperation like for example a smart conveyor from a given origin to a destination (see Figure VI-10).

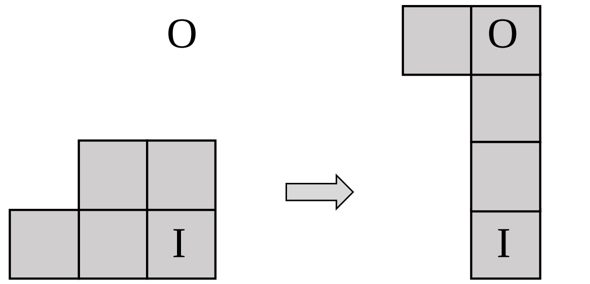

Figure VI-10 Deformation diagram

VI.3.1. Basic principle of the distributed algorithm

A set of DILI modules is available on the surface; we assume that the modules are connected and that one module occupies the cell that corresponds to the beginning of the smart conveyor, i.e. the position of the input I. The end of the smart conveyor is also called the output and is denoted by O.

We propose a distributed iterative algorithm in order to set up a smart conveyor. The distributed iterative algorithm looks for a solution that gives the shortest path between input I and output O; at the same time, it tries to minimize the number of module motion. Our distributed algorithm is an exact method for the shortest path problem and a heuristic for the module motion problem.

The distributed algorithm contains 3 steps (see Figure VI-11).

Step 1: distributed election of a module that could be a good candidate for possible motions to the output O.

Step 2: definition of a square domain centered at the selected module and study of possible motions of modules in this domain.

Step 3: when there is no possible motion in the domain, then go to step 1.

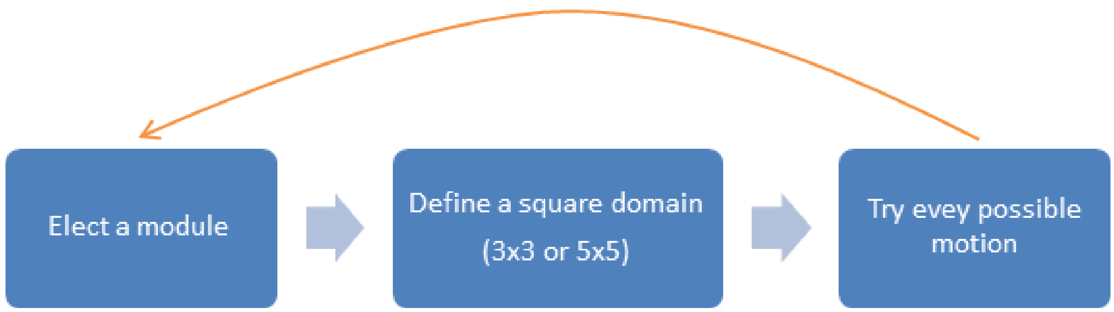

Figure VI-11 Steps of the distributed algorithm

VI.3.2. Details

Our algorithm is based on distributed iterative elections of modules that can be good candidates for possible motions to the output O. From time to time; a module is elected in an asynchronous distributed manner see Figure VI-11. We then define a square domain that is centered at the elected module. Modules within this square will be chosen for possible motion. We have considered implementations of our distributed algorithm with 3×3 or 5×5 squares; each cell within the square domain represents the possible position of a module.

For facility of presentation, we consider here the case when input I and output O are in the same column. We introduce a coordinate system with output as the origin, the line from output to input is the x-axis, the y-axis is perpendicular to the x-axis (see Figure VI-12), and we note that the direction of the y-axis does not affect the calculation done in the sequel.

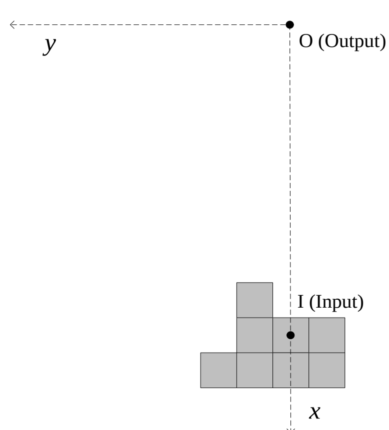

Figure VI-12 Module motion coordinate system

We introduce now a cost function *F* that associates to each position of the cell on the surface a value related to its position relatively to the output O. When the module belongs to the column between input I and output O (x-axis), we assign a value equal to 100,000,000 in order to prevent that the module that occupies this position leaves the shortest path between I and O. The cost function is given as follows.

$$F(x,y)=\begin{cases}100000000 & module \in x\_axis \\ x^4+y^2 & otherwise\end{cases} \tag{6.1}$$

We then compute a value δ which permits one to evaluate the possible gain of the modules when moving towards the output O.

$$\delta = \sum_{matrix \in 3\times 3} (F(x_i, y_i) - F(x_{i+1}, y_{i+1})), \tag{6.2}$$

where *i* denotes the current position, and *i +1* represents the next step. Note that, the module elected via the distributed election algorithm corresponds to the module with maximum value.

VI.3.3. Step 1: distributed election

The procedure of distributed election is based on the distributed procedure of Dijkstra and Scholten [1] that use activity graph and acknowledgment of messages. All the modules store in their registers their position (*x,y*) in the coordinate system. In the beginning, only the module situated at Input I, called the *Root* is active. The *Root* sends messages to its neighbor in order to activate them. We say that the *Root* is the *Father* of its neighbors. Each active module computes the value δ.

Each activation message activates a neighboring module that becomes a *Son*. Typically, activation messages are of the type:

$$Activate\ [Father,\ Son,\ F(x,y),\ \delta,\ ID\delta_{\max}], \tag{6.3}$$

where the different fields of the message are: the ID of the sender (*Father*); the ID of the destination (*Son*), *F(x,y),* δ and $ID\delta_{\max}$, respectively.

As the computation progresses, the activity graph evolves, and more and more modules become active. At some finite time, all modules have been activated and have computed δ. Active modules that cannot activate neighbors anymore since they do not have a neighbor, but their father, or since all their neighbors have been activated by other modules become inactive and send an acknowledgment message to their father. Similarly, active modules that have received acknowledgements from all their sons become inactive and send an acknowledgment message to their father. Acknowledgment messages are of the type:

$$Ack\ [Son,\ Father,\ F(x,y),\ \delta,\ ID\delta_{\max}], \tag{6.4}$$

where the different fields of the message are, the ID of the sender (*Son*), the ID of the destination (*Father*), *F(x,y),* δ and $ID\delta_{\max}$, respectively.

In the end, only the *Root* is active. This ends the first phase of the election algorithm. The *Father* then elects the module with $\delta_{\max}$. If there are several modules with the same $\delta_{\max}$, then the Root elects randomly one module with $\delta_{\max}$ and sends a Select message to the elected module. The selection message is routed to the elected module according to the Father/Son path obtained in the first phase of the election algorithm. The Elected module sends an acknowledgement message to the Root. Upon reception of the acknowledgement message, the Root becomes inactive. The distributed election is then terminated.

VI.3.4. Step 2: definition of square domain centered at the selected module

We define a square domain centered at the module elected at step 1 and consider possible motions of modules within this domain. This domain can be a 3x3 or a 5x5 domain. We can also choose a combination of 3x3 and 5x5 domains. In the cases of 5x5 domain and combination of 3x3 and 5x5 domains, the distributed algorithm will try to carry out at most 20 module motions in the 5x5 area. We emphasize that computations take time when considering large domains like 5x5 domain. In the case of a combination of 3x3 and 5x5 domain, the distributed algorithm works first on the 5x5 domain. If no module motion is possible, then the distributed algorithm concentrates only on a 3x3 domain. Details on this strategy will be presented in the sequel of this subsection.

We consider module motions allowed by the physical system. The area occupied by a module can be seen as a cell. In order to check if a module can move, we examine the initial state of the cell as well as the state of neighbouring cells, i.e., if their positions are initially occupied by modules or not. The approach we consider here is slightly different from the one in [1].

We introduce a local square matrix, i.e., the Presence Matrix. The Presence Matrix shows the corresponding state of a cell and the state of adjacent cells. The entries of the Presence Matrix are equal to 1 if the cell is occupied by a module and equal to 0 if that position is not occupied by a module. For facility of presentation, we consider here only 3x3 matrix.

We display now an example (see Figure VI-13).

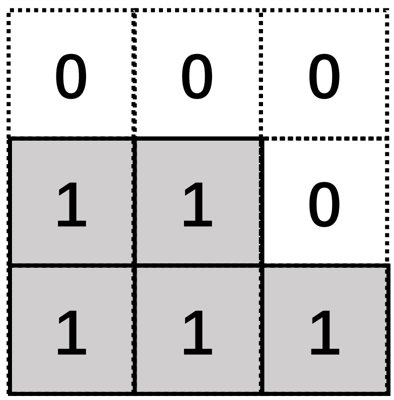

Figure VI-13 Position of modules (in gray) and associated Presence Matrix

We consider the associated 3x3 Presence Matrix M_p.

$$M_p = \begin{bmatrix} 0 & 0 & 0 \\ 1 & 1 & 0 \\ 1 & 1 & 1 \end{bmatrix} \tag{6.5}$$

In step 2, the distributed algorithm computes all possible module motions toward the output O in the considered 3x3 area. More precisely, the distributed algorithm determines what motion can be carried out by the different modules contained in the 3x3 domain. The different modules are considered in sequence. A module motion is carried out if and only if there is support of other modules, i.e. if there is one or several adjacent entries equal to 1 in the 3x3 Presence Matrix, the future position is empty (corresponding entry of the future position in the Presence Matrix is equal to 0) and no module is left alone.

As an example, the module whose position corresponds to the third line and third column in the Presence Matrix M_p can move up (see Figure VI-13).

We detail now the procedure that is used in order to select modules for possible motion in a 3x3 domain. For simplicity of presentation, we consider here only elementary motion (we do not consider push, pull and carry motion). Starting from initial state given by the Presence Matrix, the algorithm computes possible motion as a tree structure (see Figure VI-14). When similar states are obtained like case 5 that is similar to case 4, the computations are stopped on that branch. The algorithm also computes the value of δ for each node of the tree. Finally, the algorithm selects the node with maximum δ value that will correspond to the final situation of a set of module motion. The distributed algorithm then communicates in sequence to the different modules in the square domain, the module motion they have to implement in order to obtain the situation corresponding to the node with maximum δ value.

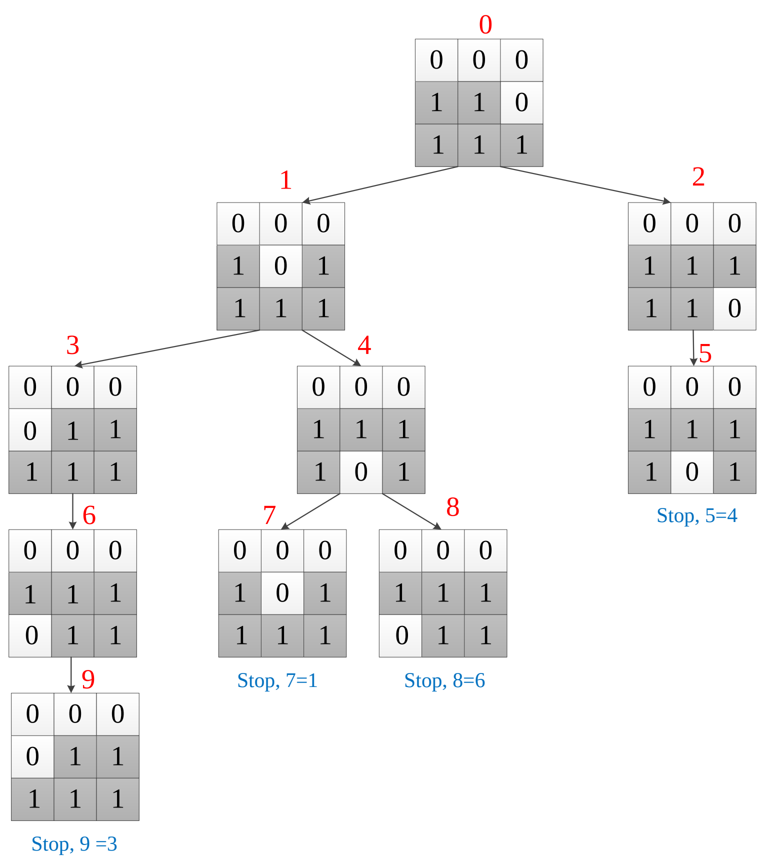

Figure VI-14 Tree of possible motions

Special case with 5x5 domain.

We note that with 3x3 matrix the distributed algorithm may not handle some special cases, like some motions with carry capability, due to the limited neighbourhood. This is the reason why we have also introduced a 5x5 matrix. We recall that the objective of the distributed algorithm is to construct a set of adjacent modules from the input I to output O progressively.

We present now part of the pseudocode that computes module motion in the 5x5 case.

Input: Positions of modules in the 5x5 domain

Procedure:

counter = 0

PriorityQueue = [initial_positions_of_modules_in_5x5_domain]

While counter <= 20:

(1) From the PriorityQueue, pop the position_of_module with the maximum Objective Function Value δ

(2) Insert all possible next-move positions from the popped one to the PriorityQueue, with their corresponding Objective Function Value, as well as the corresponding history to make such movements.

(3) Increase counter by 1

End While

Return: positions_of_modules with the minimum Objective Function Value in the PriorityQueue

----

A complete solution of the shortest path problem via the distributed algorithm presented above is displayed on the Figure VI-19.

VI.4. Simulator of Smart Modules (SSM)

We have designed and developed a Simulator of Smart Modules (SSM) in order to test and validate our distributed algorithm that solves the shortest path problem. This simulator permits one to display the position of modules and their motion when the algorithm is implemented. SSM is a Python-based simulator which can work on Windows, Linux, and IOS.

VI.4.1. Interface

The positions of the modules, the module motions, and modules in the domain resulting from the elections are displayed in real-time.

The simulator interface is divided into four areas (see Figure VI-15), that is Module display area, Parameter setting area, Operating area, Results area. The simulator interacts by clicking the mouse, such as setting the input, selecting the modules, selecting parameters, clicking on the Pause, etc. We detail now the different areas.

Module display area：

This area displays the position and status of the modules in real time, up to 14x20 modules can be displayed here.

Parameter setting area：

a). The domain around elected module can be chosen as 3x3, 5x5, or both of them.

b). Push enable, Pull enable, Carry enable. The three buttons permit one to add or withdraw the three capabilities mentioned in section VI.2. By enabling or disabling these capabilities, the effects of these three capabilities can be directly observed from the module display area and the number of elections and steps.

c). The bottom All connected imposes that all modules are connected during the movement, due to hardware limitations.

d). When the input and output are not in the same horizontal or vertical line, the shortest paths is bounded by two polylines. Both of the two polylines will be displayed if the select button “Two paths” is active; on the other hand, only one randomly chosen polylines will be displayed if the select button “Two paths” is inactive.

Operating area:

This area is related to the operating mode of the simulation, three buttons are shown here, that is Run, Pause, and Reset.

Results area:

This area allows the observation of the total numbers of elections and the number of module motions (steps). These types of data directly reflect the efficiency of program execution under different conditions.

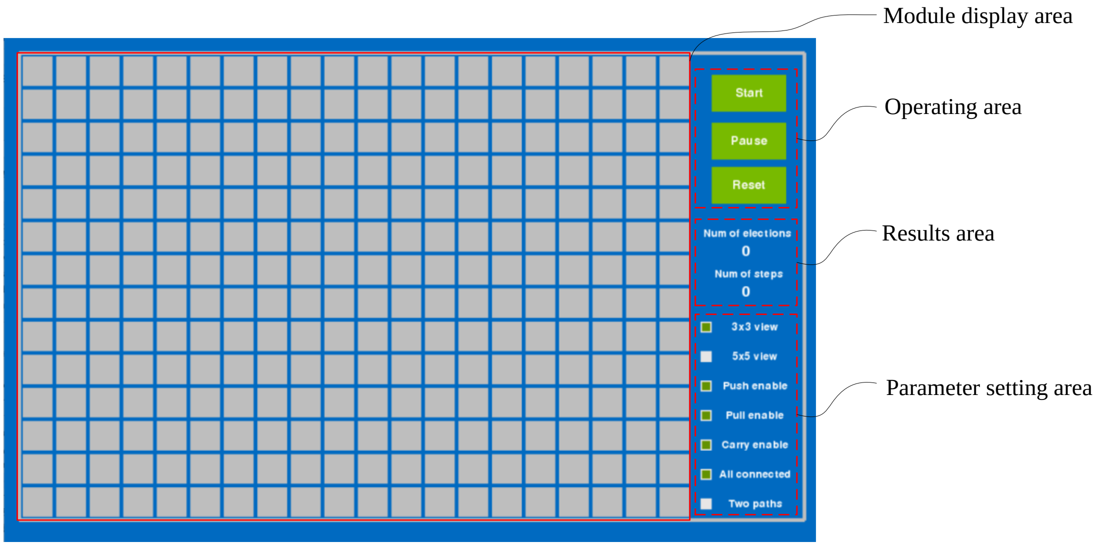

Figure VI-15 Four areas of the graphics interface

VI.4.2. Usage of SSM

Step 1:

Setting the simulation parameter in the setting area.

Step 2:

In the module display area, Input (beginning of the module structure shown as IN) will be set by the first click of mouse, Output (end of the module structure shown as OUT) will be set by the second click, both of them appear in red. After Input and Output, each click will add a module in the corresponding cell in yellow, so that the initial shape can be set. When setting the initial shape, we note that Input must be occupied.

Figure VI-16 shows an example with Input and Output, and initial shape. The Input is occupied by a module; this module will become red when the simulation is running.

Step 3:

Click Start to begin the simulation. If the initial shape is set incorrectly or the simulation is finished, then we have to click Reset to return to the initial state as shown in Figure VI-15. The simulation also can be paused.

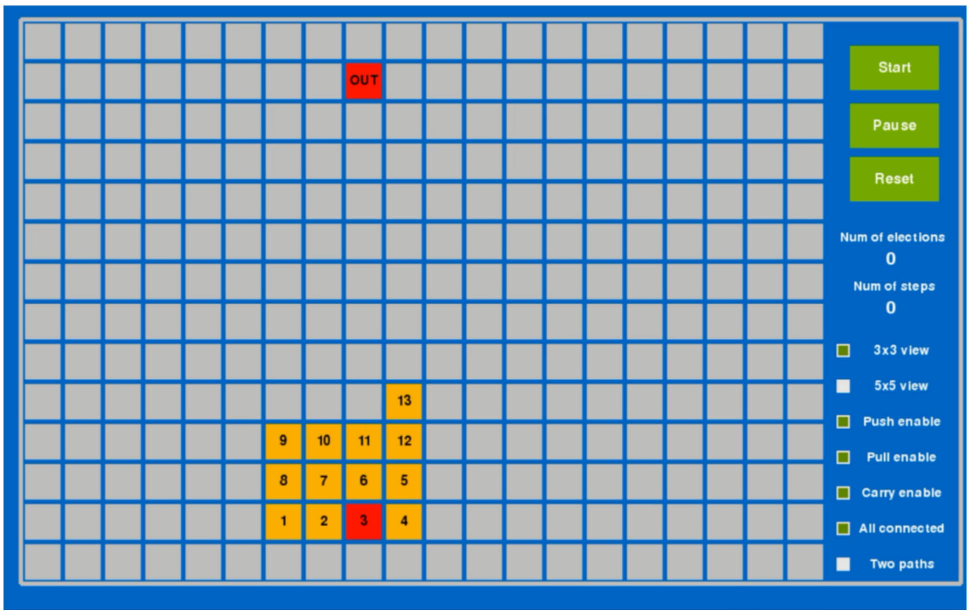

Figure VI-16 Setting the Input (occupied by module 3), Output and initial shape

In order to facilitate the observation of the simulation, each election is also displayed. In particular, all the modules in the area around the elected module are displayed in green (see Figure VI-17). In this example, module 10 at the center of the 3x3 domain is elected.

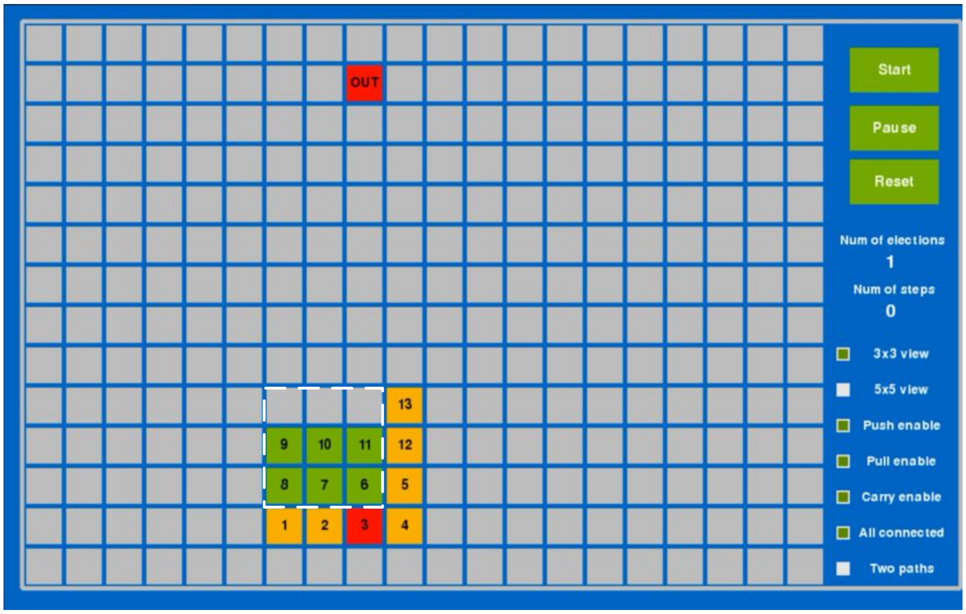

Figure VI-17 Modules (in green) in the domain around the elected module

VI.4.3. Results

This simulator not only allows us to observe the experimental results but also helps to validate the distributed algorithm experimentally. Figure VI-18 gives simulation results for two shortest path problems. Number of elections and steps also displayed. Figure VI-19 displays a complete solution with details on election processes.

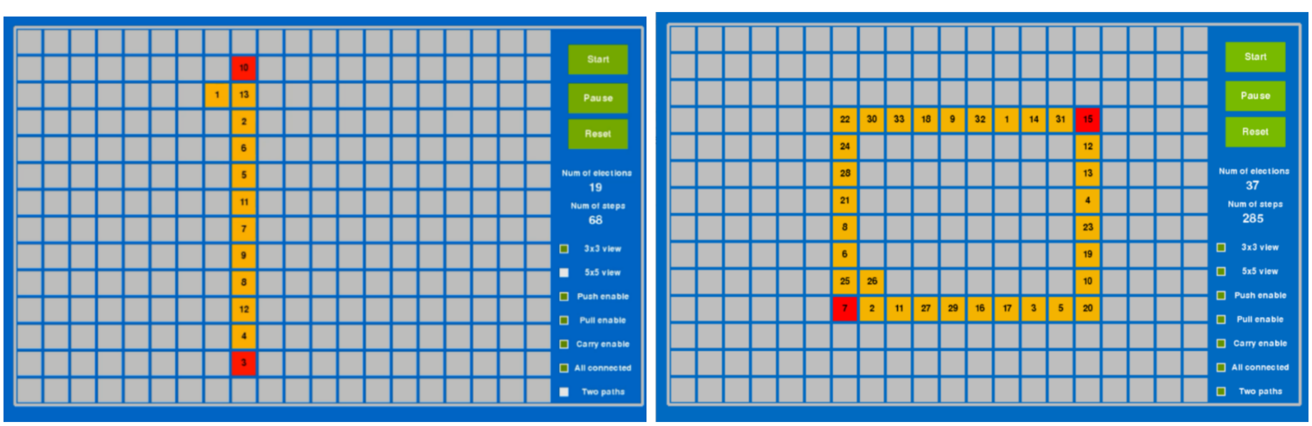

Figure VI-18 Simulation results of the shortest path problem

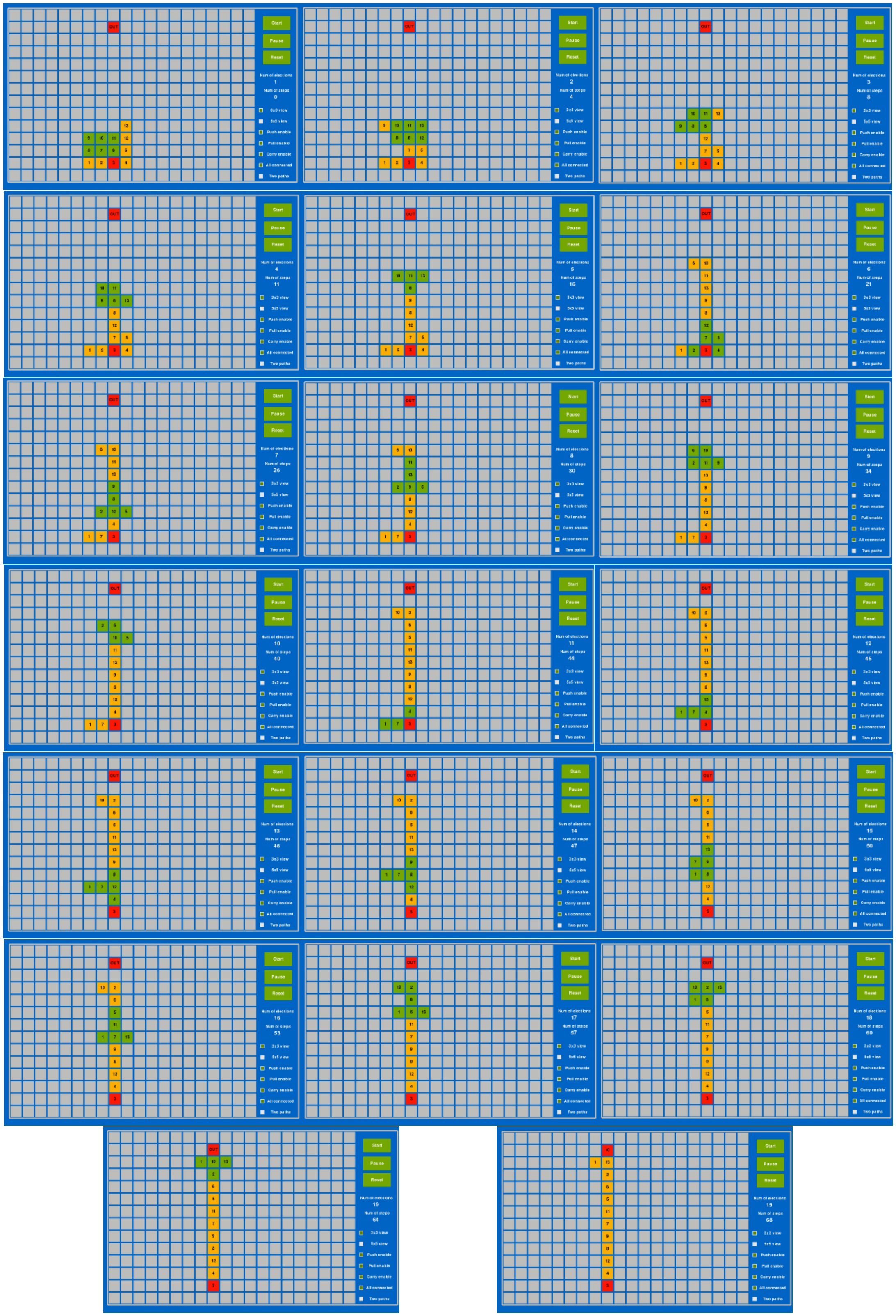

Figure VI-19 Complete solution of the shortest path problem via distributed algorithm displayed with SSM simulator

VI.5. Conclusion

Push and Pull capability are necessary. Without Push or Pull capability, it is generally impossible to find out the shortest path between input I and output O. Without Carry capability, in most cases, it is possible to complete the task, but more elections and steps are needed.

Another conclusion of this chapter is that many trajectory optimization problems between the Input and Output; with shortest path length N−1; can be solved in finite time with at most N modules by the proposed distributed algorithm. The extra module which is called Support is used to provide a support surface for the last module of the path.

Through experiments, we found out also that if we consider 5x5 domain, both the number of elections and steps can be reduced as compared with the situation with the 3x3 domain. Moreover, the more the number of modules, the advantage is more obvious.

Considering a combination of 5x5 and 3x3 domains is generally better than considering only 3x3 domain. As a matter of fact, using 3x3 domain may not permit the distributed algorithm to converge to the solution of the shortest path problem while 5x5 domain permits the algorithm to take into account a larger neighborhood and carry out more sophisticated module motion.

With a larger domain, some initial tricky situations can be considered with success, like shown in Figure IV-20, and video [3]. The line consisting of modules 3, 4, 5 and 6 is out of the range of 3x3 matrix. There is only a line inside the matrix centered on module 5 or module 6, no Support; so, these modules cannot move. On the other hand, one 5x5 matrix can cover module 3, 4, 5, 6 and 7; module 7 can be seen as the Support.

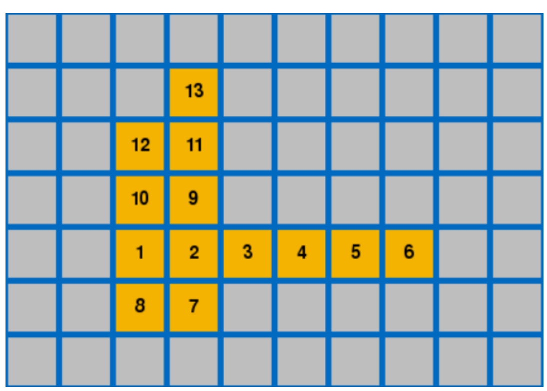

Figure VI-20 Initial shape

References in Chapter VI

[1] El Baz D, Piranda B, Bourgeois J. A distributed algorithm for a reconfigurable modular surface [C]. Parallel & Distributed Processing Symposium Workshops (IPDPSW), 2014 IEEE International. IEEE, 2014: 1591-1598.

[2] https://youtu.be/Xs5-HF0M6JU.

[3] https://youtu.be/Eqg95hqfq60.

Chapter VII. Conclusion and Perspectives

VII.1. Conclusion

For most institutes that make research works on modular self-reconfiguring robotic (MSRR) system, scientific contributions are either on hardware or on software; they seldom focus on both. Also, robotic systems like conveyor may not continue to be efficient when changes in goals or environments and faults occur.

This thesis is an extension of the Smart Surface and Smart Blocks projects which aimed at building smart conveyors. Based on this goal, the research work that been carried out in this thesis proposes a MSRR platform, whose name is DILI. The main work focuses on both hardware and software, which contains actuator design and their numerical simulation, fabrication, tests, design of distributed algorithm, and simulator of our MSRR platform. In the physical composition, actuation and connection systems are two important parts of a modular robot. Typically, actuators occupy more than 50% of the volume and weight of modules and thus are major obstacles in downsizing modules.

In this manuscript, we have presented simplified electro-permanent (SEP) magnets along with a new concept of a linear motor. SEP magnets can change the magnetic field direction. The new linear motor can achieve both motion and connection with only one system and does not require energy consumption while connected. This linear motor provides a miniaturization solution for other modular robots. By using this motor, the complexity of the structure of modular robot systems can be greatly reduced; the size of the robot modules can also be greatly reduced. Moreover, this motor can save energy, which is important for robots at small scale. We have also proposed a model of SEP magnet in COMSOL Multiphysics; the numerical results play a guidance role in designing and validating SEP magnets. We have designed the circuit and structure of DILI and tested its performance via a series of experiments, DILI module can slide along the surface of other modules with three modes: the fastest mode, the stable mode, and the enhanced mode.

Modules of MSRR have limited computing and sensing capabilities. Thus, control algorithm must be able to adapt to the actual compute power and motion ability of the modules, and take into account the coordination of motion of the modules to ensure the regular overall macro motion of the whole system. We have introduced a distributed algorithm for DILI in order to set up a smart conveyor; the distributed iterative algorithm looks for a solution that gives the shortest path between given input I and output O; at the same time, it tries to minimize the number of module motion. The distributed algorithm relies on several steps, like step 1, the distributed election of a module that could be a good candidate for possible motion to the output O; step 2, definition of a square domain centered at the selected module and consider the possible motions of modules in that domain. Our distributed algorithm is an exact method for the shortest path problem and a heuristic for the module motion problem.

Finally, in order to test and validate the distributed algorithms, we have developed a Simulator of Smart Modules (SSM) for DILI robot system. The simulator SSM is a Python-based simulator which can work on Windows, Linux, and IOS. This simulator permits one to display the position of modules and their motion when the algorithm is implemented.

We note that DILI modules may have a lot of applications. For example, they can be used in smart manufacturing (like smart conveyors for drug manufacturing or tiny systems, e.g. clockwork manufacturing). They can be produced for educational purpose or smart robots that evolve on difficult terrain. The concept behind DILI robot may also be used for programmable matter, e.g. furniture, tools, sculpture (art).

VII.2. Perspectives

Until now, we have built a MSRR platform which contains both hardware and software. Based on the current work, a number of research directions should be investigated in the future.

- Since the beginning of our project, the circuit of DILI module is apart from the frame; This limits the test with a large number of modules. In the next step, we plan to replace the 3D printed frame with a flexible circuit that will be placed in the frame, just like the Pebbles robot system.

- Sensing capabilities and communication capabilities should be included in order to detect adjacent modules and communicate with them respectively.

• A type of actuator should be selected; These actuators will be placed on the top of DILI module to build a device like a smart conveyor.

• Using SSM simulator of DILI robot will permit us to address the issue related to the 3D motion of modules. Each DILI module is a cube; in the future, we plan to work on the design of modules having 3D motion capability. This will certainly lead to rearranging the SEP magnets and NdFeB magnets.

• Comparing with the connection mechanism, the connectivity of SEP magnet is relatively weak. We can add a mechanical connection structure to DILI, such as a gripper, but the gripper is used only for the final fixation, and the gripper is not needed during module movement. Comparing with the robotic system with only mechanical connection system inside, this hybrid design can not only provide a stable connectivity but also can save energy, save action time and reduce the complexity of the algorithm.

• Distributed algorithm that permits one to reconfigure the set of modules when a fault occurs in the system should be proposed.

• Also, the scalability of distributed algorithms should be studied in order to deal with a large set of modules.

List of publications and demos

- **Li Zhu**, Didier El Baz, Huangsheng Ning. Survey on Air Levitation Conveyors with possible scalability properties [C]. The 15th IEEE International Conference on Scalable Computing and Communications, 2015, Beijing, China, August 2015, 802-807.

- **Li Zhu**, Didier El Baz, Huangsheng Ning. Design of a new fasten-able linear motor for smart distributed robot system [C]. (UIC/ATC/ScalCom/CBDCom/IoP/SmartWorld 2016) International IEEE Conferences. 2016, Toulouse, France, July 2016, 874-879.

- Didier El Baz, **Li Zhu**. Smart systems, the fourth industrial revolution and new challenges in distributed computing [C]. Parallel Computing Conference 2017 (ParCo 2017), keynote speech, to appear in the proceedings of the conference, Bologna, Italy September 2017.

- **Li Zhu**, Didier El Baz. DILI, a distributed modular robot with one system combining locomotion and connection. In preparation for submission to a journal.

- Video of DILI module carrying out the rectilinear motion: https://youtu.be/kxlJRraiZQI.

- Video of DILI module carrying out the push, pull, carry and load functions: https://youtu.be/Xs5-HF0M6JU.
- Video of SSM simulator: https://youtu.be/Eqg95hqfq60.